Active Network Management for Electrical Distribution Systems

PhD Dissertation

Quentin Gemine

Advisor: Prof. Damien Ernst

Department of Electrical Engineering and Computer Science
Faculty of Applied Sciences
University of Liège
Belgium

October 2016

Abstract

With the increasing share of renewable and distributed generation in electrical distribution systems, Active Network Management (ANM) has become a valuable option for a distribution system operator to operate his system in a secure and cost-effective way without relying solely on network reinforcement. ANM strategies are short-term policies that control the power injected by generators and/or taken off by loads in order to avoid congestion or voltage issues. While simple ANM strategies consist of curtailing temporary excess generation, more advanced strategies instead attempt to move the consumption of loads to anticipated periods of high renewable generation.

Such advanced strategies mean that the system operator has to solve large-scale optimal sequential decision-making problems under uncertainty. The problems are sequential for several reasons. For example, decisions taken at a given moment constrain the future decisions that can be taken, and decisions should be communicated to the system's actors sufficiently in advance to give them enough time for implementation. Uncertainty must be explicitly accounted for because neither demand nor generation can be accurately forecasted.

This dissertation presents various research contributions about ANM for distribution systems. These contributions range from the motivation of using a framework of sequential decision-making under uncertainty to the study of computational methods that implement ANM strategies. A particular emphasis is placed on the formulation of the problem, which ultimately falls within the class of Markov decision processes. The modeling of stochasticity is explored and a novel approach that relies on a Gaussian Mixture Model is presented. Computational methods including several relaxations and approximations of multi-period and multi-scenario extensions of the optimal power flow problem with discrete decision variables were considered.

Résumé

Avec la part croissante de production renouvelable et distribuée dans les réseaux électriques de distribution, la gestion active des réseaux de distribution devient une option crédible pour permettre aux gestionnaires de réseaux de distribution d'opérer leurs systèmes électriques. Les stratégies de gestion active sont des politiques de contrôle à court terme qui modulent la puissance injectée par les générateurs et/ou consommée par les charges afin d'éviter des problèmes de congestion ou de tension. Si les stratégies les plus simples se contentent de réduire les excès temporaires de production, d'autres plus complexes visent plutôt à anticiper les périodes de forte production renouvelable pour y déplacer la consommation des charges.

De telles stratégies signifient que le gestionnaire de réseau doit résoudre des problèmes de prise de décisions séquentielles sous incertitude et de grande taille. Ces problèmes sont séquentiels pour plusieurs raisons. Par exemple, certaines décisions prises à un instant donné contraignent les décisions qui peuvent être prises dans le futur. Les décisions doivent également être communiquées suffisamment à l'avance aux acteurs du système pour leur laisser le temps de les implémenter. L'incertitude doit être explicitement prise en compte à cause de l'imprécision des prévisions de consommation et de production.

Cette dissertation présente des contributions de recherche en gestion active des réseaux électriques de distribution. Ces contributions abordent notamment la motivation du cadre de décisions séquentielles sous incertitude et l'étude des méthodes de calcul qui implémentent les stratégies de gestion active. Une attention particulière est portée sur la formulation du problème, qui est finalement présenté comme un processus de décision markovien. Une approche originale reposant sur un modèle de mélange gaussien est décrite pour représenter l'incertitude. Des méthodes de calcul sont également considérées, en particuliers différentes relaxations et approximations d'extensions multi-périodes et multi-scénarios du problème d'écoulement de puissance optimal avec des variables entières.

Contents

1

Overview

The first chapter introduces and motivates the active network management problem. It also details and summarizes the main contributions contained in this dissertation.

Contents

1.1 Introduction

In Europe, the 20/20/20 objectives of the European Commission and the consequent financial incentives established by local governments are currently driving the growth of electricity generation from renewable energy sources [1]. A substantial part of the investments is made at the distribution networks (DN) level and consists of the installation of wind turbines or photovoltaic panels. The significant increase of the number of these distributed generators (DGs) undermines the *fit and forget* doctrine, which has dominated the planning and operation of DNs until now. This doctrine was developed when energy was transmitted from the transmission network (TN) to consumers, through the distribution network (DN). With this approach, adequate investments in network components (i.e., lines, cables, transformers, etc.) are made to avoid congestion and voltage issues, without requiring continuous monitoring and control of the power flows or voltages. To that end, network planning is done with respect to a set of critical scenarios in which information is gathered about production and demand levels, in order to always ensure sufficient operational margins. Nevertheless, with the rapid growth of DGs, the preservation of such conservative margins implies significant network reinforcement costs[i], because the net energy flow may be reversed, from the distribution network to the transmission network, and flows within the distribution network may be very different from those observed historically.

In order to host a larger share of distributed generation [2] and avoid potentially prohibitive reinforcement costs [3], *active network management* (ANM) strategies have recently been proposed as alternatives to the *fit and forget* approach. The principle of ANM is to address congestion and voltage issues via short-term decision-making policies [4]. Frequently, ANM schemes maintain the system within operational limits in quasi real-time by relying on the curtailment of wind or solar generation [5, 6, 7]. Curtailment of renewable energy may, however, be very controversial from an environmental point of view and should probably be considered as a last resort. With that mindset, it is worth investigating ANM schemes that could also exploit the flexibility of the loads, so as to decrease the reliance on generation curtailment. Exploiting flexible loads within an ANM scheme comes with several challenges. One such challenge is that modulating a flexible load at one instant will often influence its modulation range at subsequent instants. This is because flexible loads (e.g. heat pumps)

[i] Network reinforcement is the process of upgrading the transmission capacity of lines, cables, transformers, and other devices. As distribution systems of interest in this paper mostly comprise underground cables, upgrading them implies a lot of infrastructure work.

are often constrained to consume a specific amount of energy over a certain duration. In this context, it is therefore important for a distribution system operator (DSO) to take decisions by planning operations over a sufficiently long time horizon [8, 9, 10]. The uncertainty of future power injections from DGs relying on natural energy sources (wind, sun, *etc.*), as well as the uncertainty of the power consumption of the loads, should also be explicitly accounted for in the ANM strategy. An accurate model of this uncertain dynamical system is critical in order to take adequate control actions. Moreover, and contrary to wider power systems, the uncertainty about stochastic quantities (e.g. wind speed, solar irradiance, load consumption) is not softened by an averaging effect because of the local nature of distribution systems.

In this work we consider the operation of the medium-voltage (MV) network of the DSO, i.e. low voltage subnetworks are aggregated, since in general current DSOs' dispatching centers only monitor the MV part, and ANM in low voltage distribution systems is generally performed using distributed algorithms [11].

1.2 Main contributions

This dissertation is mainly a collection of research publications. This section describes the contributions contained in the dissertation and the publications from which the content is derived.

1.2.1 Planning under uncertainty

Chapter 2 introduces the problem faced by a DSO when planning the operation of a network in the short-term and in the context of high penetration of distributed generation. A small test system is designed and serves a case study that highlights the importance of explicitly taking the uncertainty into account to efficiently operate demand-side flexibility.

This chapter is based on the following publication:

- Gemine, Q., Karangelos, E., Ernst, D., & Cornélusse, B. (2013). Active network management: planning under uncertainty for exploiting load modulation. In *Proceedings of the 2013 IREP Symposium - Bulk Power Systems Dynamics and Control - IX. IEEE.*

1.2.2 Multi-period optimal power flow problems

Chapter 3 presents a novel relaxation for mixed-integer nonlinear programs (MINLP) resulting from a class of OPF applications where some loads offer a modulation service in exchange for an activation fee. This relaxation is based on a network-flow reformulation and, while it produces lower bounds that are comparable with a Lagrangian relaxation, it reduces the infeasibility of the relaxed solution with respect to the original problem.

This chapter is based on the following publication:

- Gemine, Q., Ernst, D., Louveaux, Q., & Cornélusse, B. (2014). Relaxations for multi-period optimal power flow problems with discrete decision variables. In *Proceedings of the 18th Power Systems Computation Conference (PSCC'14)*.

1.2.3 Stochastic modeling

Chapter 4 exposes a novel algorithm that models a stochastic process as a Markov process from a set of time series of observations and using a multivariate Gaussian Mixture Model (GMM). The hyper parameters of the model, i.e. the Markov order and the number of mixture components, are determined using a multi-armed bandit technique, while the mixture parameters are learned from the data using an Expectation-Maximization (EM) algorithm. Empirical results show that the proposed approach outperforms an autoregressive moving-average (ARMA) approach for the considered application of lookahead security analysis, for datasets of residential power consumption and of wind speed.

This chapter is based on the following publication:

- Gemine, Q., Cornélusse, B., Glavic, M., Fonteneau, R., & Ernst, D. (2016). A Gaussian mixture approach to model stochastic processes in power systems. In *Proceedings of the 19th Power Systems Computation Conference (PSCC'16)*.

1.2.4 Formulation, benchmark, and approximate solution

In Chapter 5, the ANM problem is formulated as a Markov Decision Process (MDP) and then casted as a stochastic mixed-integer nonlinear program, as well as second-order cone and linear counterparts. Three test beds of different complexity are presented for which we provide quantitative results using state-of-the-art solvers and perform a sensitivity analysis over the size of the system, the amount of available flexibility, and the number of scenarios considered in the deterministic equivalent of the stochastic program. To foster further research on this problem, we have made the systems available at `http://www.montefiore.ulg.ac.be/~anm/` as Python code. This code contains a simulator of the distribution system, with stochastic models for the generation and consumption devices, and eases the implementation and testing of various ANM strategies.

This chapter is based on the following publications:

- Gemine, Q., Ernst, D., & Cornélusse, B. (2014). Gestion active d'un réseau de distribution d'électricité : formulation du problème et benchmark. In *Proceedings des 9èmes Journées Francophones de Planification, Dècision et Apprentissage*.

- Gemine, Q., Ernst, D., & Cornélusse, B. (2016). Active network management for electrical distribution systems: problem formulation, benchmark, and approximate solution. To appear in *Optimization and Engineering*.

1.2.5 Realistic test system

Chapter 6 confronts the tools studied in this thesis with a test system designed based on a real distribution system. We evaluate the performance of the lookahead policy described in Chapter 5 in operating the realistic test system. In addition, the GMM approach presented in Chapter 4 is used to model the stochastic processes from actual measurement data. The obtained numerical results highlight the sensitivity of a policy's performance to the quality of the lookahead model and thus to the adequacy of the historical data from which stochastic models are learned.

1.2.6 Appendix: the microgrid case

The material presented in Appendix A falls within the context of the optimization of the levelized energy cost of microgrids featuring photovoltaic panels associated with both long-term (hydrogen) and short-term (batteries) storage devices. I contributed to this research as a *secondary author* and mainly focused on the problem formulation. This formulation encompasses the state and action spaces, the exogenous variables, as well as the discrete-time dynamics of the system.

This chapter is based on the following publication:

- François-Lavet, V., Gemine, Q., Ernst, D., & Fonteneau, R. (2016). Towards the minimization of the levelized energy costs of microgrids using both long-term and short-term storage devices. *Smart Grid: Networking, Data Management, and Business Models*, 295-319.

2

Planning under uncertainty for exploiting load modulation

This chapter addresses the problem faced by a distribution system operator (DSO) when planning the operation of a network in the short-term. The problem is formulated in the context of high penetration of renewable energy sources (RES) and distributed generation (DG), and when flexible demand is available. The problem is expressed as a sequential decision-making problem under uncertainty, where, in the first stage, the DSO has to decide whether or not to reserve the availability of flexible demand, and, in the subsequent stages, can curtail the generation and modulate the available flexible loads. We analyze the relevance of this formulation on a small test system, discuss the assumptions made, compare our approach to related work, and indicate further research directions.

Contents

2.1 Introduction

The principle of *active network management* (ANM) is to address congestion and voltage issues via short-term decision-making policies [4], developed on the basis of the *optimal power flow* (OPF) problem formulation [12]. Liew and Strbac [5] considered a deterministic problem formulation with the objective of minimizing the market value of the curtailed DG energy production. Dolan *et al.* [7] developed a deterministic, OPF-based adaptation of the *'last-in, first-off'* operating practice. A multi-period framework has been considered to account for the effects of the variability of renewable DG resources [6, 13, 14]. In this context, the problem of maximizing the utilization of the available DG inflow has been addressed [6], as well as the minimization of the energy losses in the electrical network [13]. The integration of advanced network constraints, including fault levels and N-1 security, has been established within this multi-period framework [14].

In these references, ANM schemes maintain the system within operational limits in a quasi real-time by relying on the curtailment of wind or solar generation. Curtailment of renewable energy may, however, be very controversial on an environmental point of view and should probably be considered as a last resort. In that mindset, it would be worth investigating ANM schemes that could also exploit the flexibility of the load, so as to decrease the reliance on generation curtailment. Let us consider a typical case where, due to a high production of renewable energy, the distribution network sends an amount of power to the transmission network that creates congestion at the MV/HV transformer. By asking flexible loads of the distribution network (DN) to increase their consumption at that time, the congestion could potentially be relieved without having to rely on renewable generation curtailment. Well-known examples of flexible loads are electric heaters, boilers, and electric car batteries. It is worth noting that exploiting flexible loads within an ANM scheme comes with several challenges. One such challenge is that modulating a flexible load at one time is often going to influence its modulation range at subsequent times. This is because flexible loads are often constrained to consume a specific amount of energy over a certain duration. In the above example, this would imply that after increasing the consumption of the flexible loads during a certain time period, the DSO would be constrained to later decrease their consumption, which may significantly aggravate congestion. In this context, it is therefore important for a DSO not to take myopic decisions, but to make decisions by planning over a relevant time horizon. Due to the uncertainty of the future power injections from renewable sources relying on natural phenomena (wind,

sun, *etc.*) and of the power consumption of the loads, this would necessarily imply for the DSO to implement ANM scheme able to plan adequately control actions *under uncertainty*, which may be very challenging.

In this chapter, we consider that the DSO can rely on both generation curtailment and load modulation for the active management of the network. We focus on a specific setting where the DSO can procure the right to control the demand pattern of the flexible loads, in exchange for an availability fee. We also assume that the DSO has to pay a fee per MWh of energy curtailed, and that the fee depends on the market price of electricity at the time of curtailment. In this context, we discuss the way the DSO should plan the control actions to operate safely the network at minimal cost. In the following section, we describe the main characteristics of the ANM problem. Following this, we formalize the problem as an optimal sequential decision-making problem under uncertainty, and discuss resolution strategies. The chapter concludes with simulation results obtained on a six bus test system. These results show that proper management of the uncertainty can be very beneficial.

2.2 Problem description

We focus on the problem faced by a DSO that aims at maintaining the network infrastructure within operational limits over a one day horizon. We consider the possibility that the DSO can impose power curtailment instructions on the DG resources, in exchange for financial compensation. From the alternative payment structures outlined in [15], we adopt a scheme where the per unit compensation is defined as the electricity market price for the curtailment period.

In addition, we account for the possibility for the DSO to procure the right to control the demand pattern of the flexible loads in exchange for an availability fee. Unlike non flexible loads, we consider that a load participating in this flexibility market must be able to precisely follow both the instructed modulations if the flexibility offer is selected by the DSO, or the baseline demand profile, if this option is not selected. There is therefore no uncertainty introduced by these loads. In summary, we characterize the flexible operating region of such loads through the following features:

- A baseline demand profile, to be followed with certainty unless instructed by the DSO.
- Upward and downward demand modification limits per period.

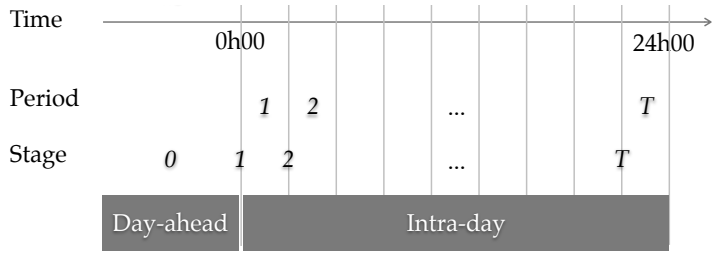

Figure 2.1: Decision framework.

- A net energy balance requirement, so that any instruction by the DSO should not modify the net energy volume consumed by a flexible load over the optimization horizon, with respect to the baseline profile.

The time horizon covered in this problem is accounted by optimizing the operation of the system over a set of $t \in [1, T]$ discrete periods. The decision framework illustrated in Figure 2.1 consists of:

- An *ex-ante* stage, in which the provision of load flexibility is settled, which can coincide with the termination of the usual day-ahead trading process.
- A series of recourse opportunities, at the start of every market period, during which the DSO can rely to submit curtailment orders.

Finally, we have a set of $k \in [0, T]$ decision stages. At the *ex-ante* decision stage ($k = 0$), the energy inflow from the DG units and the demand of non-flexible loads are uncertain for all the periods within the optimization horizon $t \in [1, T]$. Moreover, at each recourse stage $k \in [1, T]$, these quantities are assumed to be known with certainty for periods $t \in [1, k]$ but are uncertain for the subsequent time interval $t \in [k + 1, T]$. Within each period, the behavior of the network is modeled by steady-state AC power flow equations, to allow us to state operational limits on voltage, current, and power.

2.3 Sequential decision-making under uncertainty

We gradually define the elements of an optimal sequential decision-making problem, and then enrich the problem by modeling the uncertainty explicitly, to allow us to state the detailed formulation of the targeted application in the next section.

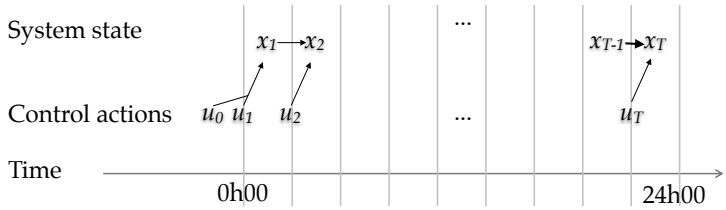

Figure 2.2: States and control actions.

2.3.1 Optimal sequential decision-making

We place ourselves in a setting where we want to control the evolution of a system over a time horizon discretized in T time steps. Sequential decision-making problems arise when the decisions taken before the time $t < T$ influence the decisions available between times t and T. Therefore, the problem cannot be decomposed into a sequence of T independent problems.

Let $x \in \mathcal{X}$ be the *state variable*, that is the vector describing the system, and $u \in \mathcal{U}(x) \subset \mathcal{U}$ the vector describing a decision, or *control action*, which can be taken to modify the state x. By definition, the state contains enough information so that knowing the control action at time t and the state at the previous period, respectively u_t and x_{t-1}, it is always possible to compute x_t, $\forall t \in \{1, 2, ..., T\}$. In other words, the evolution of the system is guided by the function

$$f : \mathcal{X} \times \mathcal{U} \to \mathcal{X}$$

such that

$$x_t = f(x_{t-1}, u_t).$$

This is illustrated schematically in Figure 2.2. In our specific framework, given that the initial decision stage does not coincide with a specific period, we adapt the previous notation for x_1 and introduce $f_1 : \mathcal{U}_0 \times \mathcal{U} \to \mathcal{X}$, to obtain

$$\begin{aligned} x_1 &= f_1(u_0, u_1) \\ x_t &= f(x_{t-1}, u_t), \forall t \in \{2, ..., T\} \end{aligned}$$

A sequence of control actions $(u_0, u_1, u_2, ..., u_T)$ is *admissible* if x stays within $\mathcal{X}$ for $t \in \{1, 2, ..., T\}$. To ease notations, we denote $(u_0, u_1, u_2, ..., u_t)$ by $\mathbf{u}_{[t]}$ and $(x_1, x_2, ..., x_t)$ by $\mathbf{x}_{[t]}$ and pose $\mathcal{T} = \{2, 3, ..., T\}$, $\mathbf{x} = \mathbf{x}_{[T]}$, $\mathbf{u} = \mathbf{u}_{[T]}$. To guide the choice of a sequence of control actions from all the admissible sequences,

we need to define an objective function

$$J : \mathcal{X}^T \times \mathcal{U}_0 \times \mathcal{U}^T \to \mathbb{R}.$$

The optimal sequential decision-making problem can then be summarized as

$$\begin{aligned}
\min_{\mathbf{x},\mathbf{u}} \quad & J(\mathbf{x}, \mathbf{u}) && (2.1)\\
s.t. \quad & x_1 = f(u_0, u_1) && (2.2)\\
& x_t = f_1(x_{t-1}, u_t), \quad \forall t \in \mathcal{T} && (2.3)\\
& x_t \in \mathcal{X}_t, \quad \forall t \in \{1\} \cup \mathcal{T} && (2.4)\\
& u_t \in \mathcal{U}_t(x_{t-1}), \quad \forall t \in \mathcal{T} && (2.5)\\
& u_1 \in \mathcal{U}_t(u_0) && (2.6)\\
& u_0 \in \mathcal{U}_0 && (2.7)
\end{aligned}$$

In this work, we consider that u contains generation curtailment and flexible load modulation decisions and that x contains the flexibility availability indicator and the energy already supplied to each flexible load. One exception is that u_0 only contains flexibility provision decisions. All the variables describing the electrical state of the system are also included in x. As we consider steady state operation of the electrical system, these variables are time independent knowing the energy already supplied to each flexible load. Hence, the transition function f propagates the flexibility availability indicator and accumulates the energy supplied to each flexible load, whereas $x \in \mathcal{X}$ ensures that the power flow equations and operational limits are satisfied. Finally, $J(\mathbf{x}, \mathbf{u})$ is the sum of curtailment and flexibility provision costs, and is decomposable by period.

2.3.2 Handling uncertainty

Many problems can be formulated as computing an optimal sequence of decisions over a time horizon tarnished with uncertainty, and allowing a series of recourse opportunities to adapt the sequence of decisions to the outcome of the random process representing the uncertainty. One of the first power system applications where uncertainty was explicitly considered was the unit commitment problem [16]. In the mathematical programming community, this type of problem is referred to as a multi-stage stochastic program (MSP). A classical way to formulate a MSP is to optimize the expectation of an objective function of several variables over an uncertainty set of the parameters, the variables being required to satisfy constraints for all possible realizations of the uncertain

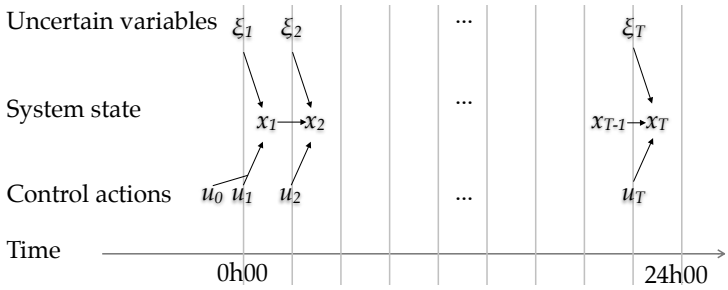

Figure 2.3: States, control actions and uncertainty.

parameters, and to impose the structure of the recourse opportunities. In doing so, control actions are taken so as to hedge against the possible evolutions of the exogenous variables of the system.

Let ξ be a stochastic process defined on the probability space $(\mathbf{\Omega}, \mathbf{F}, \mathbf{P})$. ξ_t is a realization of ξ at time $t \in \{1, 2, ..., T\}$ and the notation $\xi_{[t]}$ represents the sequence $(\xi_1, ..., \xi_t)$. We now consider that the evolution of the system as well as the control actions are functions of those exogenous variables. This is expressed by $x_t(\xi_{[t]})$ and $u_t(\xi_{[t]})$, and is illustrated schematically in Figure 2.3. The optimal sequential decision-making problem (2.1)–(2.7) can be adapted to handle uncertainty as follows:

$$\min_{\substack{\mathbf{x}(\xi_{[T]}) \\ \mathbf{u}(\xi_{[T]})}} \quad \mathbb{E}_{\xi_{[T]}} \left\{ J(\mathbf{x}(\xi_{[T]}), \mathbf{u}(\xi_{[T]}), \xi_{[T]}) \right\} \tag{2.8}$$

$$s.t. \quad x_1(\xi_1) = f_1(u_0, u_1(\xi_1), \xi_1) \tag{2.9}$$

$$u_0 \in \mathcal{U}_0 \tag{2.10}$$

$$u_1(\xi_1) \in \mathcal{U}_t(u_0, \xi_1) \tag{2.11}$$

$$\forall t \in \mathcal{T},$$

$$x_t(\xi_{[t]}) = f(x_{t-1}(\xi_{[t-1]}), u_t(\xi_{[t]}), \xi_t) \tag{2.12}$$

$$u_t(\xi_{[t]}) \in \mathcal{U}_t(x_{t-1}(\xi_{[t-1]})) \tag{2.13}$$

$$\forall t \in \{1\} \cup \mathcal{T},$$

$$x_t(\xi_{[t]}) \in \mathcal{X}_t \tag{2.14}$$

As the process $\xi_{[T]}$ does not have a finite number of realizations in the applications that we target, this formulation leads to an infinite dimensional optimization problem [17]. We now present a common method of approximating this problem.

2.3.3 Scenario tree based approximation

We approximate the random process with a discrete distribution and a finite support in order to build scenarios (Figure 2.4a) of possible realizations of the random process, and to optimize the objective function only for the realizations of the random process represented by these scenarios. *Non-anticipativity constraints* are imposed to enforce the structure of the recourse opportunities: for a given recourse opportunity, all decisions related to scenarios with a common past must be equal. Each recourse opportunity is called a *stage*. To facilitate the representation of these constraints, the scenarios are often clustered in a *scenario tree* as shown in Figure 2.4b. The depth of the tree

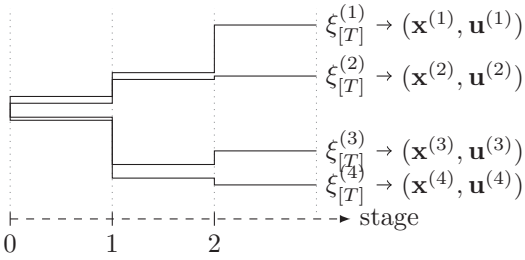

(a) Hierarchical clustering into a scenario tree. A unique decision corresponds to each node of the tree.

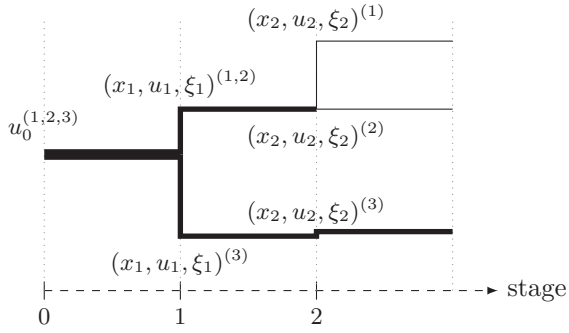

(b) Scenarios and stages.

Figure 2.4: Representation of different possible sequences of realizations thanks to scenarios. A sequence of decisions corresponds to each scenario.

constructed by this approach is equal to T. With the exception of the root node, which corresponds to the day-ahead, each node of the tree corresponds to a realization of the random process at a given stage and has at least one son for $t = 1, ..., T-1$. A *scenario* contains successive realizations of the random variable, and is represented in the tree by going from the root node and taking

one son at each subsequent level down to the final level. Scenario k is denoted by $\xi_{[T]}^{(k)}$ with $k \in \{1, 2, ..., K\}$ where K is the number of leaves in the tree. Each node $n \in \{1, 2, ..., N\}$, where N is the total number of nodes in the tree truncated at the root node, has an associated occurrence probability w_n and stage t. The node $n = 0$ corresponds to the root node. We use subscript n to reference state, control actions and exogenous variables at node n of the tree, and use subscript $[n]$ to refer to the sequence of states, control actions and exogenous variables from the root of the scenario tree to node n. Using this notation, the scenario tree based approximation of problem (2.8)–(2.14) is

$$\min_{\mathbf{x},\mathbf{u}} \quad \sum_{k=1}^{K} w_k J(\mathbf{x}^{(k)}, \mathbf{u}^{(k)}, \xi_{[T]}^{(k)}) \tag{2.15}$$

$$s.t. \quad x_n = f(u_0, u_n), \forall n \in \mathcal{C}(0) \tag{2.16}$$

$$u_0 \in \mathcal{U}_0 \tag{2.17}$$

$$x_{n'} = f(x_n, u_{n'}, \xi_{[n']}) \ \forall n' \in \mathcal{C}(n), \forall n \in \mathcal{N} \tag{2.18}$$

$$x_n \in \mathcal{X}_n, \forall n \in \mathcal{N} \tag{2.19}$$

$$u_{n'} \in \mathcal{U}_{n'}(x_n), \forall n' \in \mathcal{C}(n), \forall n \in \mathcal{N} \tag{2.20}$$

where w_k is the probability of the terminal node in scenario k, $\mathcal{C}(n)$ is the set of successors of node n, and $\mathcal{N} = \{1, 2, ..., N\}$ is the set of nodes of the scenario tree truncated at its root node.

2.4 Detailed optimization model

This section details the components of the compact formulation presented in problem (2.15)–(2.20).

2.4.1 Network topology

The network is represented by a graph, where the set of vertices $\mathcal{B}$ represents the electrical buses and the set of edges $\mathcal{L}$ contains the links connecting buses. A nominal voltage level is associated with each bus. In this work we focus on the MV level network. Several devices can be connected to each bus. We distinguish three types of devices: generators, static loads, and flexible loads. These devices represent either a single physical element, such as a wind turbine, or the aggregation of elements of the same type connected to an individual bus,

such as residential loads at the low voltage (LV) level. $\mathcal{G}$, $\mathcal{S}$ and $\mathcal{F}$ represent the set of generators, static loads, and flexible loads, respectively. $\mathcal{G}(b)$, $\mathcal{S}(b)$ and $\mathcal{F}(b)$ represent the devices of each type connected to bus b, respectively. Links are transformers, lines or cables. No special notation is required to distinguish different types of links, as these are directly translated into the values of the admittance matrix.

2.4.2 Parameters

Let $P_{g,n} \geq 0$ be the injection of generator g and $P_{s,n} \geq 0$ and $P_{f,n} \geq 0$ the off-takes of the static and flexible loads, respectively. Off-takes of each flexible load are known with certainty and are characterized by the time-dependent minimum, $\underline{P}_{f,t}$, and maximum, $\overline{P}_{f,t}$, power levels[i]. On the other hand, wind and solar power injections and off-takes of static loads are considered uncertain. In addition, we consider that all devices operate at constant power factor $\cos\phi_d$ and their reactive power injections are thus defined by:

$$Q_{d,n} = \tan\phi_d P_{d,n}, \forall d \in \mathcal{G} \cup \mathcal{S} \cup \mathcal{F}.$$

All electrical parameters are gathered in the admittance matrix[ii] $Y \in \mathbb{C}^{|\mathcal{B}|\times|\mathcal{B}|}$. Operational limits are $\underline{V}_b$ and $\overline{V}_b$, the minimum and maximum voltage magnitude, respectively, and $\overline{I}_l$, the maximum current.

The cost of flexibility availability and curtailment are C_f^{flex}, and $C_{g,t}^{curt}$, respectively. At any decision stage $k \in [1, T]$, the cost would be uncertain, given that the curtailed energy would have to be compensated at the real-time market price.

2.4.3 State variables

The state variable is

$$x = \left(\mathbf{e}^\top, \mathbf{y}^\top, \mathbf{p}^\top, \mathbf{q}^\top, \mathbf{V}^\top\right)$$

where

- $\mathbf{e} \in \mathbb{R}^{|\mathcal{F}|}$ is the vector of the energy status of flexible loads,

[i] For simplicity, flexibility bids cover the whole time horizon. Removing this restriction does not change the nature of the optimization problem.

[ii] The operator $|\cdot|$ applied to a set returns its cardinality.

- $\mathbf{y} \in \{0,1\}^{|\mathcal{F}|}$ is the vector of availability indicators of flexible loads,
- $\mathbf{p} \in \mathbb{R}^{|\mathcal{B}|}$ is the active power injection vector,
- $\mathbf{q} \in \mathbb{R}^{|\mathcal{B}|}$ is the reactive power injection vector,
- $\mathbf{V} \in \mathbb{C}^{|\mathcal{B}|}$ is the bus voltage vector ($V_b = v_b e^{j\phi_b}$).

The slack bus is fixed at the high voltage level side of the transformer connecting the distribution network to the transmission network. By convention we refer to this bus as bus 0, and impose $v_0 = 1$ *p.u.* and $\phi_0 = 0$.

2.4.4 Feasible states

To be feasible the state x_n must reside within the set $\mathcal{X}_n$ defined by:

- $\forall b \in \mathcal{B}$, the active and reactive power definition

$$p_{b,n} + jq_{b,n} = V_{b,n} \sum_{b' \in \mathcal{B}} Y^*_{b,b'} V^*_{b',n}$$

- $\forall b \in \mathcal{B}$, the voltage limits

$$\underline{V}_b \leq v_{b,n} \leq \overline{V}_b$$

- $\forall l \in \mathcal{L}$, the current limits ($l$ connects buses b and b')

$$|Y_{bb'}(V_{b,n} - V_{b',n})| \leq \overline{I}_l,$$

- if n is a leaf of the tree, the energy constraint of flexible orders

$$e_{f,n} = \sum_{k \in scenario(n)} P_{f,k} \Delta t, \ \forall f \in \mathcal{F}.$$

2.4.5 Control actions

The first stage decision u_0 encompasses the flexibility procurement decisions, $u_{f,0}$, $\forall f \in \mathcal{F}$. For stages 1 to T the control variable is $u = (\mathbf{c}, \mathbf{m})$, where $\mathbf{c} \in \mathbb{R}^{|\mathcal{G}|}$ is the vector of curtailment instructions for the generation units and $\mathbf{m} \in \mathbb{R}^{|\mathcal{F}|}$ is the vector of flexible load power modulations.

2.4.6 Feasible control actions

The control actions $u_{n'}$ are restricted to the set $\mathcal{U}_{n'}(x_n)$, where n is the parent node of n'. This set is defined by

- $\forall g \in \mathcal{G}$, the generator curtailment limits

$$c_{g,n'} \in [0,1]$$

- $\forall f \in \mathcal{F}$, the modulation limits of the flexible loads

$$m_{f,n'} \in \left[\frac{\underline{P}_{f,n'} - P_{f,n'}}{P_{f,n'}} y_{f,n}, \frac{\overline{P}_{f,n'} - P_{f,n'}}{P_{f,n'}} y_{f,n}\right].$$

For the first stage control action u_0, the flexibility provision variables are binary: $u_{0,f} \in \{0,1\}$, $\forall f \in \mathcal{F}$.

2.4.7 Transition function

The transitions $x_{n'} = f(x_n, u_{n'})$ are defined by, $\forall n' \in \mathcal{C}(n)$ and $\forall n \in \mathcal{N} \setminus \{0\}$,

- the evolution of the energy provided to flexible loads

$$e_{f,n'} = e_{f,n} + (1 + m_{f,n'}) P_{f,n'} \Delta t, \ \forall f \in \mathcal{F}$$

  where Δt is the period duration

- the propagation of the load flexibility availability indicator

$$y_{f,n'} = y_{f,n}, \ \forall f \in \mathcal{F}$$

- the net active and reactive power injections, $\forall b \in \mathcal{B}$

$$p_{b,n'} = \sum_{g \in \mathcal{G}(b)} c_{g,n'} P_{g,n'} - \sum_{s \in \mathcal{S}(b)} P_{s,n'} - \sum_{f \in \mathcal{F}(b)} (1 + m_{f,n'}) P_{f,n'} \quad (2.21)$$

$$q_{b,n'} = \sum_{g \in \mathcal{G}(b)} c_{g,n'} Q_{g,n'} - \sum_{s \in \mathcal{S}(b)} Q_{s,n'} - \sum_{f \in \mathcal{F}(b)} (1 + m_{f,n'}) Q_{f,n'} \quad (2.22)$$

Finally, $\forall n \in \mathcal{C}(0)$, we have simply $y_{f,n} = u_{f,0}$.

2.4.8 Objective function

The first term of the objective function corresponds to the cost of procuring the availability of flexible loads in advance. The second term expresses the cost of the forthcoming energy curtailment decisions.

$$J(\mathbf{x}, \mathbf{u}) = \sum_{f \in \mathcal{F}} y_f C_f^{flex} + \sum_{n \in \mathcal{N}} w_n \sum_{g \in \mathcal{G}} (1 - c_{g,n}) P_{g,n} C_{g,t}^{curt}.$$

2.4.9 Nature of the optimization problem

The presence of flexibility procurement decisions and AC power flow equations result in a mixed integer and non-linear program (MINLP). Furthermore, the dependency between periods and the explicit modeling of uncertainty dramatically increase the dimensions of the problem. In the following sections, we describe results obtained on a small test system, with a short time horizon and a moderate number of scenarios. In the concluding section, we discuss pitfalls and avenues for solving realistic scale instances.

2.5 Case Study

We analyze issues arising at the MV level in some Belgian distribution systems (Figure 2.5). Often, wind-farms are directly connected to the HV/MV transformer, as modeled in our test system by the generator connected to *bus 2*. Power off-takes and injections induced by residential consumers are aggregated at *bus 4* by a load and a generator representing the total production of PV panels. Finally, the load connected to *bus 5* represents an industrial consumer.

The cumulative capacity of DG units exceeds the capacity of the HV/MV transformer. This leads to congestion issues when, within the distribution network, high generation and low consumption arise simultaneously. Voltage rises can also be induced in the downstream nodes because the power flow is mainly directed towards the transformer. On the other hand, when the local generation level is low and loads consumption is high, the power flow is inverted, and this can lead to undervoltage problems.

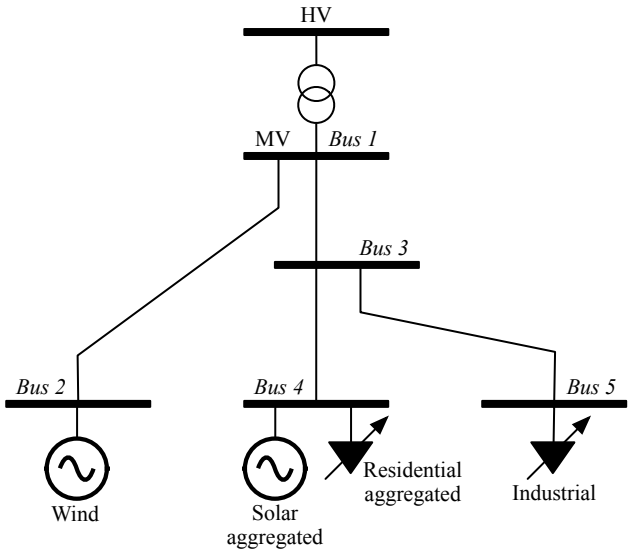

Figure 2.5: Model of distribution network used for the case study.

The optimization horizon covers three periods. The procurement of load flexibility occurs before the first period. The stochastic process associated with this time horizon relates to the uncertainty on the production of renewable generators. It is modeled through two random variables $\mathcal{W}$ and $\mathcal{S}$ which define the efficiency factors of wind and PV generators, respectively (cf. Figure 2.6). The actual output level of a DG unit is thus its maximum capacity scaled by the associated efficiency factor. Figure 2.6 shows the scenario tree used for this case study, comprising eight possible scenarios. As both random variables model natural phenomena (wind level and sunshine), we expect uncertainty to increase as we move away from real-time. This is modeled by an increase in the standard deviation associated with the random process, as shown on Figure 2.7. Unlike renewable generators, the two loads have peak consumption during the first two periods. However, both can provide flexibility. The baseline demand profile and the upward and downward modulation limits are shown in Figure 2.8. We define the *flexibility price*, p_f, such that the flexibility fees at buses 4 (aggregated residential load) and 5 (industrial load) equal p_f and $1.5p_f$, respectively.

We compare two sequential decision-making policies:

- the *mean scenario approach* (MSA): the procurement of flexibility is first determined by optimizing over the mean scenario. The mean scenario is updated at each recourse stage, and we solve an optimization problem for each stage while following the nodes defining the scenario in the tree

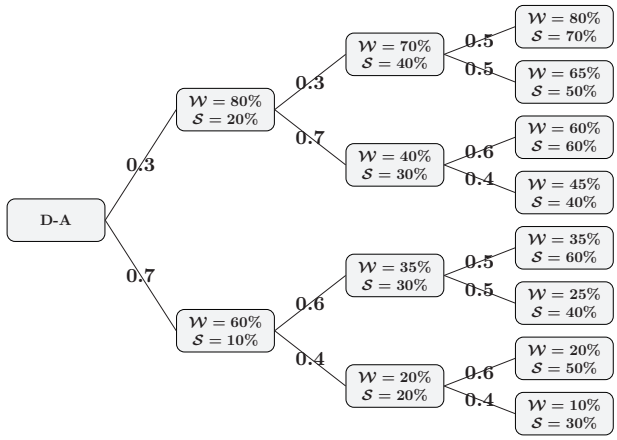

Figure 2.6: Scenario tree used for the case study. The nodes show the values of the random variables and the label on the edges define the transition probabilities between nodes.

and fixing the variables related to former periods (*i.e.*, ancestor nodes). This method is evaluated for each scenario of the case study.

- the *scenario tree approach* (STA): this policy solves the problem by optimizing over the whole scenario tree, as described in formulation (2.15)–(2.20). Load flexibility is also evaluated using this stochastic formulation.

2.6 Experimental results

We first illustrate for one scenario the control actions taken by both approaches. The approaches are then compared in terms of expected cost and variability of cost. Finally, we show the sensitivity of the first stage and of curtailment decisions to the price of flexibility.

2.6.1 Scenario analysis

The selected scenario is presented in Figure 2.9. Without any action from the DSO, two operational limits would be violated during the third period (Figure 2.10):

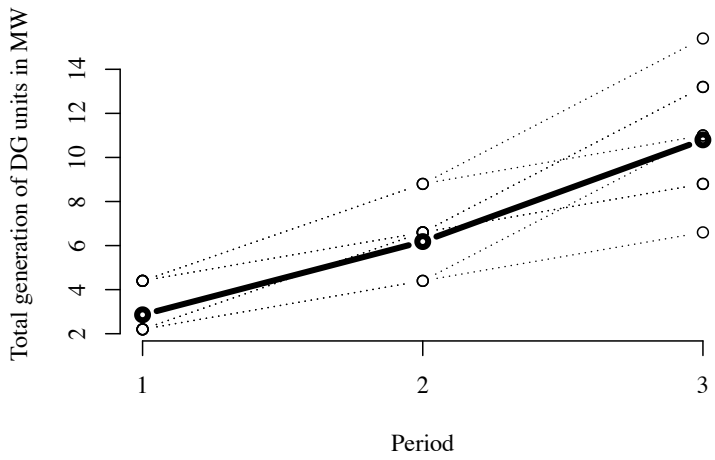

Figure 2.7: Cumulative level of power injected by the DG vs. time. Dotted lines represent scenarios and the solid line corresponds to the mean scenario.

- the magnitude of the current in the transformer would exceed the 10 *p.u.* limit (11.53 *p.u.*);
- an over-voltage would appear at *bus 4* (1.054 *p.u.* for a maximum of 1.05 *p.u.*).

The MSA does not procure flexibility while the STA only procures the flexibility of the residential load. Thus, for the MSA, maintaining the system within the operational margins can only be ensured through curtailment orders: power from *bus 2* is curtailed, at a cost of \$224. On the other hand, as the STA procures flexibility from the load at *bus 4* at a cost of \$30, curtailment is not required to keep the system within acceptable bounds for this scenario. The consumption of the load instructed by the DSO is presented in Figure 2.11.

2.6.2 Features of the stochastic model

The expected cost of operation achieved over all the scenarios for both the MSA and the STA, as well as the maximum and minimum costs among possible scenarios, are presented in Table 2.1. The smallest expected cost of operation was achieved by the STA. In addition, the STA also ensures a smaller variability of the cost over the set of scenarios. On the contrary, as the MSA overfits its decisions to the mean scenario, it achieves zero cost on scenarios close to the mean scenario, but this is at the expense of large curtailment costs on several possible scenarios far from the mean.

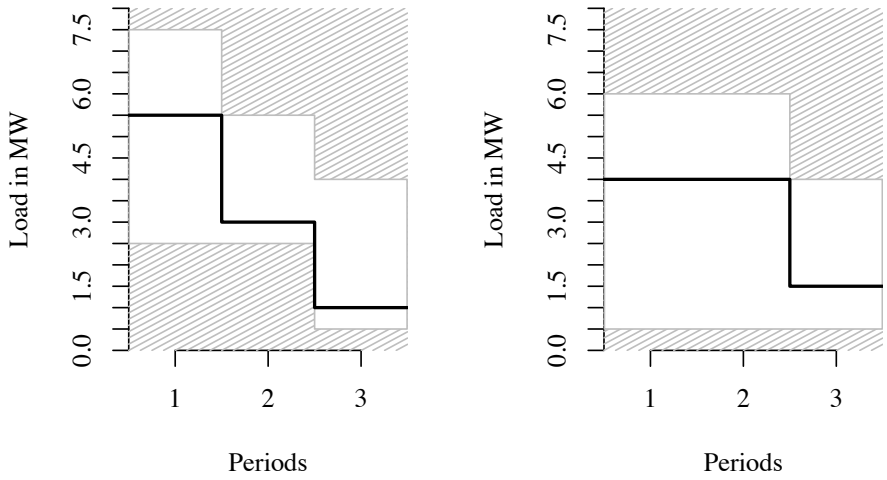

Figure 2.8: Flexible loads. The white area is delimited by $\underline{P}$ and $\overline{P}$, and the black line is the baseline consumption P.

	$\mathbb{E}\{cost\}$	*max cost*	*min cost*	*std. dev.*
MSA	73$	770$	**0$**	174$
STA	**46$**	**379$**	30$	**72$**

Table 2.1: Results for the MSA and the STA over all the scenarios (best value in bold, column-wise).

2.6.3 Features of load flexibility

We now analyze the impact of load flexibility in terms of curtailed power from DG units and cost of operation. Figure 2.12 shows the evolution of the expected percentage of curtailed power, the number of activated flexible loads and the expected cost of operation, when the flexibility price p_f increases and the curtailment prices remain constant. We observe that a very low flexibility price induces the activation of both loads, and the DSO can avoid issuing curtailment orders. At a given threshold, the flexibility fee of the industrial load (*bus 5*) becomes too high and only one load is activated. With only one flexible load, the DSO may have to curtail power, depending on the scenario, which thus increases the expected cost. When the price of flexibility becomes too high, the only action taken by the DSO is generation curtailment.

Hence, if the load flexibility price and curtailment prices are competitive, a DSO can reduce both the cost of operation and the amount of power curtailed from the distributed generators.

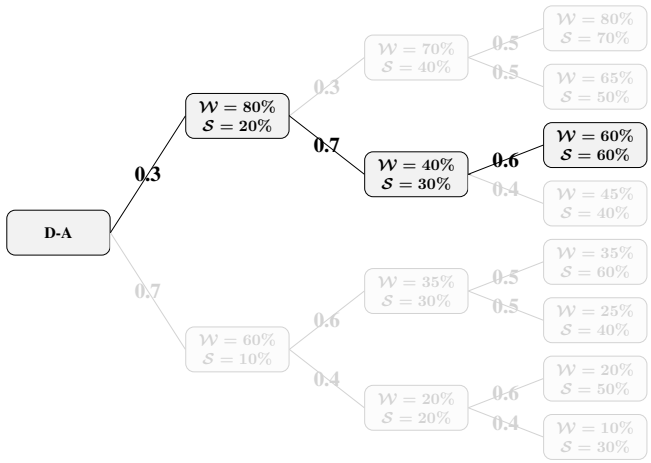

Figure 2.9: Selected scenario.

2.7 Implementation and algorithmic details

It is not easy to find off-the-shelf solvers that can manage this MINLP, even on such a small test system. We conducted several experiments with SCIP [18] (with and without IPOPT [19] to solve node relaxations) and Knitro [20]. Finally, we decided to implement a custom branch-and-bound algorithm that can use both IPOPT and Knitro to solve the NLP node relaxations. We observed that solutions of the optimization programs were insensitive to the choice of the NLP solver.

2.8 Conclusions and future work

This chapter proposes a novel formulation of the ANM problem that allows utilization of the demand-side operational flexibility. We highlighted both the sequential and the uncertain nature of this ANM problem and addressed it as an optimal sequential decision-making problem under uncertainty. As the scope of this chapter is to serve as a proof-of-concept, we benchmarked the proposed approach on a small case study, and showed that it is critical to explicitly take into account the uncertainty to efficiently operate demand-side flexibility.

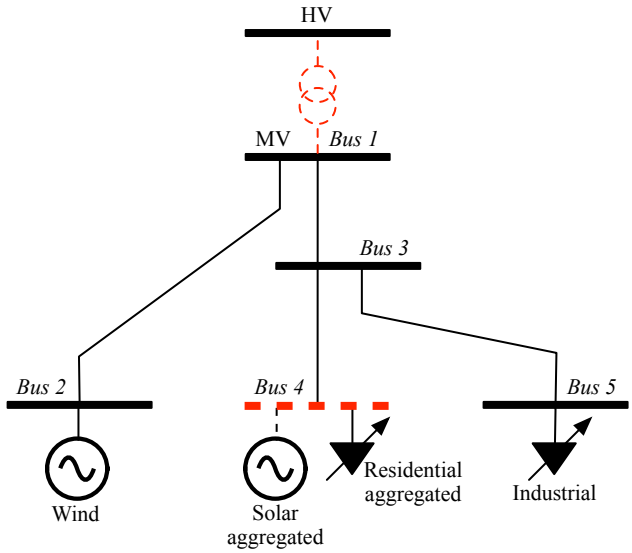

Figure 2.10: Operational limit violations are located at the red-dashed elements.

The model governing the interactions between the stakeholders of the distribution system must be carefully considered. We have presented one particular flexibility model, where availability is procured one day ahead in exchange for an availability fee, and curtailed power is remunerated at the market price. In the next steps of this work, it would be worth analyzing alternative models to identify the ones that offer incentives to foster demand-side flexibility and increase the share of renewable energy. The flexibility product that we proposed may fit a subset of the loads, but other products may be required to satisfy the technical constraints of other consumers. For example, this work could be easily extended to tank-like models, such as the one proposed in [21]. Furthermore, existing configurations could already enable activation of the demand flexibility through ON/OFF signals that actuate a relay in some domestic meters (such as day and night meters). However, these models may necessitate more specific information on the consumption side, and introduce more integer variables to the optimization problem.

More or less independently of the interaction model implemented, computational challenges are a barrier to the application of this formulation to real size systems. Indeed, the complexity of the optimization problem is simultaneously increased by the integer variables, the non-linearity of the power flow equations, and the high dimensionality caused jointly by the multi-period aspect and the explicit treatment of uncertainty. It is certainly worth considering the recent works that propose new approaches for efficiently solving single period OPF problems [22, 23]. Another interesting research direction would be to develop

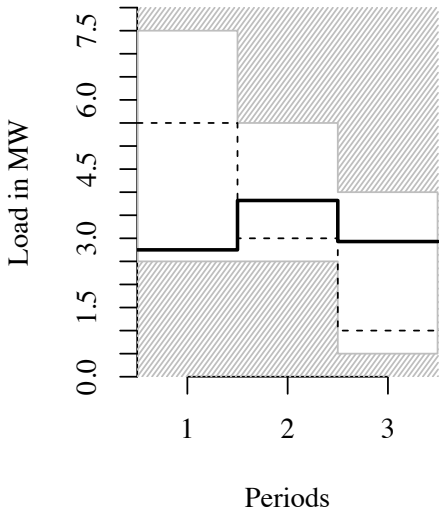

Figure 2.11: Consumption pattern instructed by the DSO (line), and baseline consumption (dashed line).

optimization algorithms specifically designed to tackle the complexity induced by the scenario-tree based approach [24, 25].

In the long-term, it will also be necessary to find investment strategies that reach the best possible trade-off between the *fit-and-forget* and full ANM approaches. Assessing such a trade-off may not be an easy task, especially since it would require the evaluation of the cost of an ANM scheme, which may be a difficult task. Note that this cost depends not only on the price paid for modulating the load and the generation over a long period of time, but also on the cost required for the evolution of the infrastructure. Indeed, deploying these types of approaches would require non-negligible ICT, metering and control investments, amongst others.

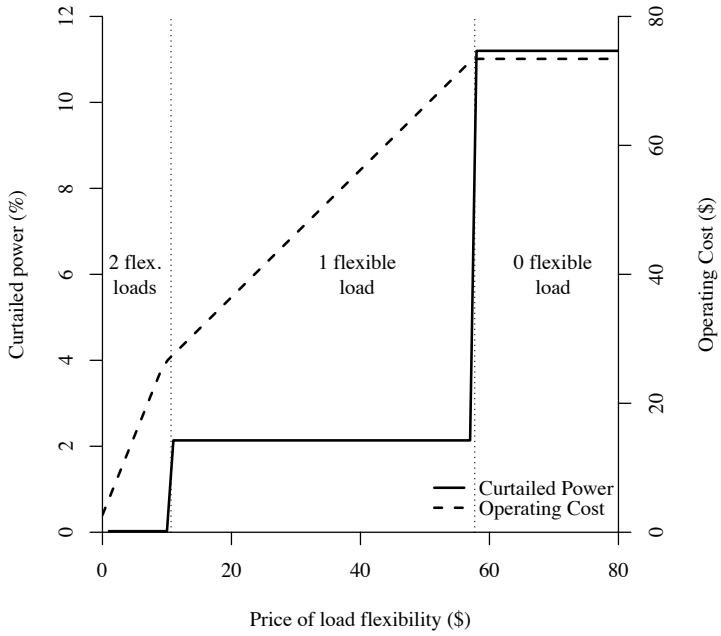

Figure 2.12: Load flexibility cost analysis.

3

Relaxations for multi-period optimal power flow problems

We consider a class of optimal power flow (OPF) applications where some loads offer a modulation service in exchange for an activation fee. These applications can be modeled as multi-period formulations of the OPF with discrete variables that define mixed-integer non-convex mathematical programs. We propose two types of relaxations to tackle these problems. One is based on a Lagrangian relaxation and the other is based on a network flow relaxation. Both relaxations are tested on several benchmarks and, although they provide a comparable dual bound, it appears that the constraints in the solutions derived from the network flow relaxation are significantly less violated.

Contents

3.1 Introduction

Many power system applications that require solving an optimal power flow (OPF) problem share two features. Firstly, these applications are multi-period because of the evolution of market prices, of the ramping limits of generation units and of the behavior of static and flexible loads. Secondly, they contain integer decision variables to model the acceptance or the rejection of bids, or the start up of some generation units. As a first example, the day-ahead energy market in Europe computes spot prices based on supply and demand offers. This application has a multi-period and discrete nature because of the "block bids", and because of some ramping constraints. Active power flows are constrained by a simple network flow model. Operational constraints on reactive power, voltage and current are aggregated in the arc capacities of the network flows. More realistic (so called "flow based" [26]) network models are emerging, but they are still a linear approximation of the set of feasible flows around a foreseen operation point. As a second example, new applications arising in distribution networks such as operational planning aim at avoiding the congestion of network elements and minimizing the curtailment of renewable energy sources. To benefit from the flexibility of customers, it is necessary to account for the time-coupled nature of the problem, and integer variables can be used to model the reservation of that flexibility. Because the physical characteristics of distribution networks are different from those of transmission systems, DC power flow approximations can hardly be used.

Hence depending on the complexity of the primary goal of the application and its scale, it is often mandatory to resort to a relaxation of the non-convex network constraints so as to devise a robust and fast algorithm. Also, a common characteristic of these applications is that the main decision variables are the power injections, and especially active power flows as they underlie most of the financial transactions. The other variables (voltage, current) can be viewed as consequences of the power flows in the network, and we must ensure that they stay within the operational limits. These observations motivate the relaxation algorithms studied in this chapter. We focus on relaxations that decompose the problem into one subproblem that works exclusively with active and reactive power flows but encompasses the multi-period and discrete aspects, and subproblems that assert that for each time step those flows do not violate voltage and other technical limits. After the precise statement of the discrete multi-period optimal power flow we are targeting in Section 3.2 and a review of the recent literature on these topics in Section 3.3, we propose two relaxations achieving these goals in Section 3.4. The first relaxation is a

straightforward generalization of the Lagrangian relaxation (LR) of [23] to this problem. The downside of this LR scheme is that the power related subproblem lacks information on the network topology. The second relaxation builds on a network flow reformulation of the original problem by introducing link-flow variables. It is then relaxed into a convex problem by substituting non-linear terms with their convex envelopes. Small semidefinite programming (SDP) relaxations are used to translate operational limits into bounds of voltage and link-flow variables. Section 3.5 compares the two proposed approaches on several test systems, whereas Section 3.6 concludes and gives directions of further research.

3.2 General problem statement

We consider the problem of finding the optimal operation of a set $\mathcal{D}$ of devices (i.e. loads and generators) over a certain time horizon while maintaining the network and the devices within operational limits. The network is defined as a set $\mathcal{L}$ of links, that is lines, cables or transformers that define pairwise connections between elements of the set $\mathcal{B}$ of buses. Several devices can be connected to a single bus. The time horizon is modeled by a set $\mathcal{T}$ of periods. We denote by $\mathcal{F} \subset \mathcal{D}$ the flexible loads. The consumption of a flexible load can be modulated around a baseline profile. In particular, we use the flexibility model presented in [8], where the right to modulate a flexible load is conditioned to the payment of an availability fee. The operational constraints associated to these loads are upward and downward modulation limits as well as an energy constraint, stating that any modulation should consume the same amount of energy than the baseline profile. We use the following notations throughout this chapter, where the superscript (t) refers to period t:

- $\boldsymbol{P}^{(t)} \in \mathbb{R}^{|\mathcal{D}|}$, the active power injections of devices (positive when power flows from the device to the network);
- $\boldsymbol{Q}^{(t)} \in \mathbb{R}^{|\mathcal{D}|}$, the reactive power injections of devices (same sign convention as $\boldsymbol{P}^{(t)}$);
- $\boldsymbol{d} \in \{0,1\}^{|\mathcal{F}|}$, the availability indicators of flexible loads;
- $\boldsymbol{c}_f \in \mathbb{R}_+^{|\mathcal{F}|}$, the availability costs of the flexible loads;
- $\boldsymbol{P}^{bl(t)} \in \mathbb{R}^{|\mathcal{F}|}$, the active power injections of flexible loads when operating at their baseline;
- $\overline{\boldsymbol{P}}^{(t)}$ and $\underline{\boldsymbol{P}}^{(t)} \in \mathbb{R}^{|\mathcal{B}|}$, the bounds on active power injection of devices;

- $\mathbb{A} \in \mathbb{R}^{N_c \times 2|\mathcal{D}|}$ and $\boldsymbol{a} \in \mathbb{R}^{N_c}$, matrix and vector modeling the P-Q capability of the devices (with N_c the total number of linear constraints between $\boldsymbol{P}^{(t)}$ and $\boldsymbol{Q}^{(t)}$);

- $\mathbb{M} \in \{0,1\}^{\mathcal{B} \times \mathcal{D}}$, mapping from devices to buses ($M_{i,j} = 1$ if device j is connected to bus i and 0 otherwise);

- $\boldsymbol{e}^{(t)} \in \mathbb{R}^{|\mathcal{B}|}$, the real part of the voltage at buses;

- $\boldsymbol{f}^{(t)} \in \mathbb{R}^{|\mathcal{B}|}$, the imaginary part of the voltage at buses;

- $\overline{\boldsymbol{V}}$ and $\underline{\boldsymbol{V}} \in \mathbb{R}^{|\mathcal{B}|}$, the limits on the voltage magnitudes;

- g_{ij} the conductance of link $(i,j) \in \mathcal{L}$;

- b_{ij} the susceptance of link $(i,j) \in \mathcal{L}$.

The decision variables are the subset of the active and reactive power injections for which the bounds $\overline{P}_k^{(t)}$ and $\underline{P}_k^{(t)}$ are not equal ($k \in \mathcal{D}$), the voltage at all buses, and the discrete decision variables $\boldsymbol{d}$. The notion of optimal operation is defined by a generic cost function $f(\boldsymbol{P})$ (linear or a convex quadratic) that we want to minimize together with $\boldsymbol{c}_f \cdot \boldsymbol{d}$, the availability fees of flexible loads. The whole problem is modeled in (3.1-3.10) where we use the notation $\boldsymbol{P}$, $\boldsymbol{Q}$, $\boldsymbol{e}$ and $\boldsymbol{f}$ to denote the concatenation of, respectively, the vectors $\boldsymbol{P}_t$, $\boldsymbol{Q}_t$, $\boldsymbol{e}_t$ and $\boldsymbol{f}_t$ for all $t \in \mathcal{T}$.

$$\min_{\substack{\boldsymbol{P},\boldsymbol{Q} \\ \boldsymbol{d},\boldsymbol{e},\boldsymbol{f}}} \quad f(\boldsymbol{P}) + \boldsymbol{c}_f \cdot \boldsymbol{d} \tag{3.1}$$

$$\text{s.t.} \quad \mathbf{d} \in \{0,1\}^{|\mathcal{F}|} \tag{3.2}$$

$$\forall\, t \in \mathcal{T}:$$

$$\underline{\boldsymbol{P}}^{(t)} \leq \boldsymbol{P}^{(t)} \leq \overline{\boldsymbol{P}}^{(t)} \tag{3.3}$$

$$\mathbb{A} \begin{pmatrix} \boldsymbol{P}^{(t)} \\ \boldsymbol{Q}^{(t)} \end{pmatrix} \leq \boldsymbol{a} \tag{3.4}$$

$$\forall k \in \mathcal{F}:$$

$$\sum_{t \in \mathcal{T}} \left(P_k^{(t)} - P_k^{bl\,(t)} \right) = 0 \tag{3.5}$$

$$\forall (t,k) \in \mathcal{T} \times \mathcal{F}:$$

$$P_k^{(t)} \geq (1 - d_k) P_k^{bl\,(t)} + d_k \underline{P}_k^{(t)} \tag{3.6}$$

$$P_k^{(t)} \leq (1 - d_k) P_k^{bl\,(t)} + d_k \overline{P}_k^{(t)} \tag{3.7}$$

$$\forall (t,i) \in \mathcal{T} \times \mathcal{B} :$$

$$(\mathbb{M}\ \boldsymbol{P}^{(t)})_i = \sum_{j \in \mathcal{N}(i)} \Big(g_{ij}({e_i^{(t)}}^2 + {f_i^{(t)}}^2 - e_i^{(t)} e_j^{(t)} - f_i^{(t)} f_j^{(t)}) + b_{ij}(e_i^{(t)} f_j^{(t)} - f_i^{(t)} e_j^{(t)}) \Big) \tag{3.8}$$

$$(\mathbb{M}\ \boldsymbol{Q}^{(t)})_i = \sum_{j \in \mathcal{N}(i)} \Big(b_{ij}(e_i^{(t)} e_j^{(t)} + f_i^{(t)} f_j^{(t)} - {e_i^{(t)}}^2 - {f_i^{(t)}}^2) + g_{ij}(e_i^{(t)} f_j^{(t)} - f_i^{(t)} e_j^{(t)}) \Big) \tag{3.9}$$

$$\underline{V_i}^2 \leq {e_i^{(t)}}^2 + {f_i^{(t)}}^2 \leq \overline{V}_i^2 \tag{3.10}$$

This is a mixed-integer non-convex mathematical program where the non-convexity comes from constraints (3.8)-(3.10) and from integer variables (3.2). In addition, the electrical variables (i.e. powers and voltages) are coupled over the set $\mathcal{T}$ of periods because of the time-coupling constraints (3.5)-(3.7) that model the flexible loads.

3.3 Literature review

We first review the methods designed to solve "static" OPF problems, in the sense that the problem has no temporal aspect. We then review the literature on multi-period OPF, which is a scale up of a static problem caused by time coupling constraints on power variables. Finally, we review the literature on works where some discrete variables have been introduced in the OPF problem to model the ability to act on power injections or withdrawals, that is, problems comparable to the problem introduced in Section 3.2.

Optimal power flow problems, although non-convex, have been for long solved using local non-linear optimization methods. Interior-point methods are probably the most widespread class of methods dedicated to this problem [27]. If the solution they provide has no guarantee to be globally optimal, they have been made popular by their convergence speed and their ability to solve fairly efficiently problems of large dimension.

Recently, SDP was successfully applied as a convex relaxation to the OPF problem [22]. The OPF is formulated over all the degree 2 monomials of the real and imaginary parts of the voltage variables. Dropping the rank 1 constraint of the corresponding matrix yields the SDP relaxation. For technical reasons, the dual of this SDP relaxation is solved (strong duality holds). When the duality gap is zero, a primal feasible optimal solution to the original OPF

problem can be recovered from the solution of the dual SDP. The authors report no duality gap on some standard meshed test systems and randomized versions of these test systems. The zero duality gap property was thus observed experimentally on standard test systems, and further research resulted in sufficient conditions. This is the case, for example, if the objective function is convex and monotonically increasing with the active power generation, and the network has a radial topology [28, 29]. Another approach aiming at global optimality relies on LR [23], which is further explained in Section 3.4.1. The author also describes a spatial branch and bound (B&B) algorithm to close the gap, should it exist one. The ability of both SDP and LR to decrease the optimality gap within a B&B framework was evaluated in [30]. If SDP appeared to be computationally more attractive, it showed that it could be very challenging to reach a significant gap reduction within reasonable time limits, even for small test systems.

Multi-period applications related to energy storage are investigated in [31], where the SDP relaxation of [22] is successfully applied, as their particular application met the conditions for having no duality gap. The authors of [32] argue that extending [30] to a multi-period setting yields a SDP too large for current solvers to be solved efficiently and suggest to relax the time-coupling constraints using LR. However, it ended up being computationally too heavy to make the B&B approach worthwhile.

Many papers consider the unit commitment problem over an AC network, which is an instance of a multi-period OPF with discrete variables. For instance in [33], a generalized Benders decomposition divides the problem in a linear master problem with discrete variables and non-linear multi-period subproblems. Benders cut are generated from the subproblems to tighten the MIP master problem.

3.4 Relaxations description

We are looking for a computationally affordable relaxation of the problem stated in Section 3.2 that would offer both a narrow optimality gap and a solution close to be feasible. The main complexity sources of problem (3.1)-(3.10) are the discrete decision variables (3.2) and the non-convexity of (3.8)-(3.10). Furthermore the problem is large scale because of the time-coupling constraints (3.5)-(3.7). If the set of constraints (3.8)-(3.10) could be addressed independently, finding an optimal solution of (3.1)-(3.10) would

result in solving less complex subproblems. This decomposition is particularly attractive because:

- the large time-coupled problem is now a mixed-integer quadratic program (MIQP) or a mixed-integer linear program (MILP) which are much easier to solve than a MINLP of comparable size;

- every constraint of (3.8)-(3.10) only involves period-specific variables and this non-convex program (NLP) can thus be split in $|\mathcal{T}|$ smaller independent problems.

However, these two sets of constraints share the power injection variables appearing in (3.5)-(3.7) and in the left-hand sides of (3.8)-(3.9). Thus some coordination between those subproblems is required to obtain a solution to (3.1)-(3.10).

Such a decomposition has already been proposed in [23] for single-period continuous OPFs, where the coordination between the power and voltage subproblems was performed using LR. The extension of this work to the considered problem statement is presented in Section 3.4.1. In addition, we introduce in Section 3.4.2 a novel flow-based relaxation for this class of multi-period mixed-integer OPFs. The main idea behind this relaxation is that the power flow equations (3.8)-(3.9) can be formulated as a network flow with losses.

3.4.1 Lagrangian relaxation

As previously discussed, the author of [23] proposes a Lagrangian Relaxation (LR) scheme in which the constraints (3.8)-(3.10) are dualized. He proves that this leads to two independent subproblems: a problem involving the active and reactive power injections, and a quadratic problem involving the voltage variables. If we apply the same idea to the problem presented in Section 3.2,

we obtain the Lagrangian L as

$$
\begin{aligned}
&L(\boldsymbol{P},\boldsymbol{Q},\boldsymbol{d},\boldsymbol{e},\boldsymbol{f},\boldsymbol{\lambda},\boldsymbol{\gamma},\boldsymbol{\alpha},\boldsymbol{\beta}) \\
&\quad = f(\boldsymbol{P}) + \boldsymbol{c}_f \cdot \boldsymbol{d} \\
&\quad + \sum_{(t,i)\in\mathcal{N}\times\mathcal{T}} \boldsymbol{\lambda}_i^{(t)} \Bigg((\mathbb{M}\boldsymbol{P}^{(t)})_i - \sum_{j\in\mathcal{N}(i)} \Big(g_{ij}({e_i^{(t)}}^2 + {f_i^{(t)}}^2 \\
&\qquad - e_i^{(t)} e_j^{(t)} - f_i^{(t)} f_j^{(t)}) + b_{ij}(e_i^{(t)} f_j^{(t)} - f_i^{(t)} e_j^{(t)}) \Big) \Bigg) \\
&\quad + \sum_{(t,i)\in\mathcal{N}\times\mathcal{T}} \boldsymbol{\gamma}_i^{(t)} \Bigg((\mathbb{M}\boldsymbol{Q}^{(t)})_i - \sum_{j\in\mathcal{N}(i)} \Big(b_{ij}(e_i^{(t)} e_j^{(t)} \\
&\qquad + f_i^{(t)} f_j^{(t)} - {e_i^{(t)}}^2 - {f_i^{(t)}}^2) + g_{ij}(e_i^{(t)} f_j^{(t)} - f_i^{(t)} e_j^{(t)}) \Big) \Bigg) \\
&\quad + \sum_{(t,i)\in\mathcal{N}\times\mathcal{T}} \boldsymbol{\alpha}_i^{(t)} \big(\underline{V}_i^2 - {e_i^{(t)}}^2 - {f_i^{(t)}}^2 \big) \\
&\quad + \sum_{(t,i)\in\mathcal{N}\times\mathcal{T}} \boldsymbol{\beta}_i^{(t)} \big({e_i^{(t)}}^2 + {f_i^{(t)}}^2 - \overline{V}_i^2 \big)
\end{aligned}
$$

where $\boldsymbol{\lambda}$, $\boldsymbol{\gamma} \in \mathbb{R}^{|\mathcal{T}||\mathcal{N}|}$ and $\boldsymbol{\alpha}$, $\boldsymbol{\beta} \in \mathbb{R}_+^{|\mathcal{T}||\mathcal{N}|}$ are the Lagrange multipliers for the relaxed constraints.

Any value of the dual function g defined as

$$
\begin{aligned}
g(\boldsymbol{\lambda},\boldsymbol{\gamma},\boldsymbol{\alpha},\boldsymbol{\beta}) = \min_{\substack{\boldsymbol{P},\boldsymbol{Q} \\ \boldsymbol{d},\boldsymbol{e},\boldsymbol{f}}} \quad & L(\boldsymbol{P},\boldsymbol{Q},\boldsymbol{d},\boldsymbol{e},\boldsymbol{f},\boldsymbol{\lambda},\boldsymbol{\gamma},\boldsymbol{\alpha},\boldsymbol{\beta}) && (3.11) \\
\text{s.t.} \quad & \text{(3.2)-(3.7)} && (3.12)
\end{aligned}
$$

provides a lower bound on the optimal value of the original problem. The Lagrangian dual bound is obtained by maximizing g, which is known to be a concave function. Still following the approach of [23], the relaxation is tightened by introducing, $\forall t \in \mathcal{T}$, the constraints

$$
\sum_{i\in\mathcal{N}} \underline{V}_i^2 \le \sum_{i\in\mathcal{N}} ({e_i^{(t)}}^2 + {f_i^{(t)}}^2) \le \sum_{i\in\mathcal{N}} \overline{V}_i^2 \tag{3.13}
$$

If they are redundant in the original problem, they are not in (3.11)-(3.12) because (3.10) has been relaxed.

More specifically we can rewrite the problem as

$$\begin{aligned}\max_{\substack{\boldsymbol{\lambda},\boldsymbol{\gamma}\\ \boldsymbol{\alpha},\boldsymbol{\beta}}} & g(\boldsymbol{\lambda},\boldsymbol{\gamma},\boldsymbol{\alpha},\boldsymbol{\beta}) \\ &= \max_{\substack{\boldsymbol{\lambda},\boldsymbol{\gamma}\\ \boldsymbol{\alpha},\boldsymbol{\beta}}} \Big\{ L_P^*(\boldsymbol{\lambda},\boldsymbol{\gamma}) + L_V^*(\boldsymbol{\lambda},\boldsymbol{\gamma},\boldsymbol{\alpha},\boldsymbol{\beta}) \\ &\qquad + \sum_{(t,i)\in\mathcal{N}\times\mathcal{T}} (\boldsymbol{\alpha}_i^{(t)}\underline{V}_i^2 - \boldsymbol{\beta}_i^{(t)}\overline{V}_i^2) \Big\}\end{aligned} \tag{3.14}$$

where the power subproblem $L_P(\boldsymbol{\lambda},\boldsymbol{\gamma})$ is defined as

$$\begin{aligned}L_P^*(\boldsymbol{\lambda},\boldsymbol{\gamma}) = \min_{\substack{\boldsymbol{P},\boldsymbol{Q}\\ \boldsymbol{d}}} \quad & f(\boldsymbol{P}) + \boldsymbol{c}_f \cdot \boldsymbol{d} + \sum_{(t,i)\in\mathcal{N}\times\mathcal{T}} \boldsymbol{\lambda}_i^{(t)} (\mathbb{M}\boldsymbol{P}^{(t)})_i \\ & \qquad + \sum_{(t,i)\in\mathcal{N}\times\mathcal{T}} \boldsymbol{\gamma}_i^{(t)} (\mathbb{M}\boldsymbol{Q}^{(t)})_i \\ \text{s.t.} \quad & (3.2)\text{-}(3.7)\end{aligned}$$

and requires solving a MIQP (or MILP). The voltage subproblem $L_V(\boldsymbol{\lambda},\boldsymbol{\gamma},\boldsymbol{\alpha},\boldsymbol{\beta})$ is on the other hand defined as

$$\begin{aligned}&L_V^*(\boldsymbol{\lambda},\boldsymbol{\gamma},\boldsymbol{\alpha},\ \boldsymbol{\beta}) \\ &= \sum_{t\in\mathcal{T}} \Big\{ \min_{\boldsymbol{e}^{(t)},\boldsymbol{f}^{(t)}} \quad - \sum_{i\in\mathcal{N}} \boldsymbol{\lambda}_i^{(t)} \sum_{j\in\mathcal{N}(i)} \Big(b_{ij}(e_i^{(t)} f_j^{(t)} - f_i^{(t)} e_j^{(t)}) \\ &\qquad + g_{ij}({e_i^{(t)}}^2 + {f_i^{(t)}}^2 - e_i^{(t)} e_j^{(t)} - f_i^{(t)} f_j^{(t)}) \Big) \\ &\qquad - \sum_{i\in\mathcal{N}} \boldsymbol{\gamma}_i^{(t)} \sum_{j\in\mathcal{N}(i)} \Big(b_{ij}(e_i^{(t)} e_j^{(t)} + f_i^{(t)} f_j^{(t)} \\ &\qquad - {e_i^{(t)}}^2 - {f_i^{(t)}}^2) + g_{ij}(e_i^{(t)} f_j^{(t)} - f_i^{(t)} e_j^{(t)}) \Big) \\ &\qquad + \sum_{i\in\mathcal{N}} (\boldsymbol{\beta}_i^{(t)} - \boldsymbol{\alpha}_i^{(t)})({e_i^{(t)}}^2 + {f_i^{(t)}}^2) \\ &\qquad \text{s.t.} \quad (3.13) \ \Big\}\end{aligned}$$

and consists in solving $|\mathcal{T}|$ independent problems that, even though they are non-convex, can be reformulated as trust-region subproblems and solved efficiently in polynomial time.

The convex problem (3.14) belongs to the class of non-smooth (i.e. non-differentiable) optimization. If subgradient algorithms [34] are frequently use to solve these problems, they have shown serious convergence issues for our particular application in the presence of a nonzero duality gap [30]. For this reason, we suggest to use a bundle method algorithm [35] to solve (3.14).

3.4.2 Network flow relaxation

In the LR scheme presented in Section 3.4.1, no information on the topology of the network is used in the power subproblem L_P. Here we present a relaxation that uses the topological information by coupling the original problem with a network flow. As the network flow formulation is a linear relaxation of the power flow equations, it does not account for their non-convexities. In particular it can be observed that in a linear network flow, the total amount of power produced is equal to the total amount of power consumed, which is rarely the case in our application. It is therefore important to tighten the formulation by adding some new constraints that account for these losses in the lines. In particular, we rely on a reformulation-linearization technique (RLT) approach [36] that relaxes quadratic constraints (3.8)-(3.9) by convexifying the set of values that each bilinear and quadratic term can take. As a prerequisite for the network flow formulation, we first introduce some notations:

- $P_{ij}^{(t)}$ is the active power injected in link $(i,j) \in \mathcal{L}$ at bus i, positive when power is withdrawn from bus i;
- $Q_{ij}^{(t)}$ is the reactive power injected in link $(i,j) \in \mathcal{L}$ at bus i, positive when power is withdrawn from bus i;
- $P_{ij}^{loss^{(t)}}$ is the active power losses in link $(i,j) \in \mathcal{L}$.

Using these variables, the conservation of the power flows through links, taking the losses into account, can be written as, $\forall (i,j) \in \mathcal{L}$:

$$P_{ij}^{(t)} + P_{ji}^{(t)} = P_{ij}^{loss^{(t)}} \tag{3.15}$$

$$Q_{ij}^{(t)} + Q_{ji}^{(t)} = -\frac{b_{ij}}{g_{ij}} P_{ij}^{loss^{(t)}} \big(= Q_{ij}^{loss^{(t)}} \big) \tag{3.16}$$

and the flow conservation at bus $i \in \mathcal{B}$ as:

$$(\mathbb{M}\, \boldsymbol{P}^{(t)})_i = \sum_{j \in \mathcal{N}(i)} P_{ij}^{(t)} \tag{3.17}$$

$$(\mathbb{M}\, \boldsymbol{Q}^{(t)})_i = \sum_{j \in \mathcal{N}(i)} Q_{ij}^{(t)} \tag{3.18}$$

A connection between these flow variables and the voltage variables $\boldsymbol{e}$ and $\boldsymbol{f}$ is achieved through the following equations:

$$\begin{aligned} P_{ij}^{(t)} &= g_{ij}({e_i^{(t)}}^2 + {f_i^{(t)}}^2 - e_i^{(t)}e_j^{(t)} - f_i^{(t)}f_j^{(t)}) \\ &\quad + b_{ij}(e_i^{(t)}f_j^{(t)} - f_i^{(t)}e_j^{(t)}) \end{aligned} \tag{3.19}$$

$$\begin{aligned} Q_{ij}^{(t)} &= b_{ij}(e_i^{(t)}e_j^{(t)} + f_i^{(t)}f_j^{(t)} - {e_i^{(t)}}^2 - {f_i^{(t)}}^2) \\ &\quad + g_{ij}(e_i^{(t)}f_j^{(t)} - f_i^{(t)}e_j^{(t)}) \end{aligned} \tag{3.20}$$

$$\begin{aligned} {P_{ij}^{loss}}^{(t)} &= g_{ij}({e_i^{(t)}}^2 + {e_j^{(t)}}^2 + {f_i^{(t)}}^2 + {f_j^{(t)}}^2 \\ &\quad - 2e_i^{(t)}e_j^{(t)} - 2f_i^{(t)}f_j^{(t)}) \end{aligned} \tag{3.21}$$

which are used together with (3.15)-(3.18) to obtain a reformulation of the original problem:

$$\begin{aligned} \min_{\substack{\boldsymbol{P},\boldsymbol{Q} \\ \boldsymbol{d},\boldsymbol{e},\boldsymbol{f}}} \quad & f(\boldsymbol{P}) + \boldsymbol{c}_f \cdot \boldsymbol{d} \\ \text{s.t.} \quad & (3.2)\text{-}(3.7) \\ & \forall (t,i) \in \mathcal{T} \times \mathcal{B} : \\ & \quad (3.10), (3.17)\text{-}(3.18) \\ & \forall (t,(i,j)) \in \mathcal{T} \times \mathcal{L} : \\ & \quad (3.15)\text{-}(3.16), (3.19)\text{-}(3.21) \end{aligned} \tag{3.22}$$

This problem is a mixed-integer quadratically constrained quadratic program (MIQCP), which is non-convex just as the original problem. It is important to note that there are redundant constraints in this formulation. For example, removing (3.15)-(3.16) and (3.21) would produce an equivalent mathematical program. However, it does not mean that the relaxed counterparts of these constraints will also be redundant. It has indeed been shown in [37] that such redundancy helps generating tighter relaxations.

Such a problem can be relaxed by replacing bilinear (i.e $x_i x_j$) and quadratic (i.e. x_i^2) terms by their McCormick envelopes, which can be generated by following the procedure:

$$\begin{aligned} &\text{Let } x_i \in [l_i, u_i] \text{ and } x_j \in [l_j, u_j] \\ &\text{then} \quad x_i x_j \rightarrow w_{ij} \\ &\text{with} \quad w_{ij} \geq u_i x_j + u_j x_i - u_i u_j \\ &\qquad w_{ij} \geq l_i x_j + l_j x_i - l_i l_j \\ &\qquad w_{ij} \leq u_i x_j + l_j x_i - u_i l_j \\ &\qquad w_{ij} \leq l_i x_j + u_j x_i - l_i u_j \end{aligned}$$

However, before doing so, it is important to observe that such a relaxation converges towards the original problem as the variable domain is getting smaller, i.e. max $(x_i x_j - w_{ij})$ converges to zero as $(\overline{x}_i - \underline{x}_i)$ and $(\overline{x}_j - \underline{x}_j)$ tends to zero too. In other words, the closer the bounds are, the tighter is the relaxation. Unfortunately, the bounds of $\boldsymbol{e}$ and $\boldsymbol{f}$ are initially quite loose: $e_i^{(t)}$ and $f_i^{(t)}$ belong to $[-\sqrt{\overline{V}_i}, +\sqrt{\overline{V}_i}]$, $\forall (i,t) \in \mathcal{T} \times \mathcal{B}$. In order to tighten the relaxed problem, it would be interesting to refine these bounds given the set $\mathcal{S}$ of feasible solutions of (3.1)-(3.10). Because computing such bounds in the original problem would result in the same time-complexity as the original problem, we rely on a subset of period-specific constraints of (3.2)-(3.10) to approximate $\mathcal{S}$. For each time period $t \in \mathcal{T}$, some constraints are removed from the original problem to obtain an approximated set $\tilde{\mathcal{S}}_t$ such that $\mathcal{S}_t \subset \tilde{\mathcal{S}}_t$ with $\mathcal{S}_t$ the projection of the original set of feasible solutions to the set of period-t-specific variables. In other words, the resulting bounds of $\boldsymbol{e}$ and $\boldsymbol{f}$ deduced from sets $\tilde{\mathcal{S}}_t$ are guaranteed not to remove any feasible solution from the original problem. In particular, the set $\tilde{\mathcal{S}}_t$ is defined as:

$$\{\ (\boldsymbol{P}^{(t)}, \boldsymbol{Q}^{(t)}, \boldsymbol{e}^{(t)}, \boldsymbol{f}^{(t)}) \mid \text{(3.3)-(3.4),(3.8)-(3.10) are not violated } \}$$

and finding the upper and lower bounds of a voltage variable v (i.e. $e_i^{(t)}$ or $f_i^{(t)}$, $\forall (i,t) \in \mathcal{B} \times \mathcal{T}$) is equivalent to solving the following problem:

$$\overline{v}/\underline{v} = \max_{\substack{\boldsymbol{P}^{(t)}, \boldsymbol{Q}^{(t)} \\ \boldsymbol{e}^{(t)}, \boldsymbol{f}^{(t)}}} / \min \quad v \tag{3.23}$$

$$\text{s.t.} \quad (\boldsymbol{P}^{(t)}, \boldsymbol{Q}^{(t)}, \boldsymbol{e}^{(t)}, \boldsymbol{f}^{(t)}) \in \tilde{\mathcal{S}}_t \tag{3.24}$$

Even if this problem is much smaller than the original one, it is still non-convex. For this reason, the bounds on $\boldsymbol{e}$ and $\boldsymbol{f}$ are finally computed by solving an SDP relaxation [38] of (3.23)-(3.24). These are the bounds used to build the RLT relaxation of (3.22).

The last tightening step that we perform is to bound the variables $P_{ij}^{(t)}$, $P_{ji}^{(t)}$, $Q_{ij}^{(t)}$, $Q_{ji}^{(t)}$ and $P_{ij}^{loss\,(t)}$ by solving the SDP relaxation of (3.23)-(3.24) with as objective function their expression in equations (3.19)-(3.21).

3.5 Quantitative analysis

3.5.1 OPF applications

In order to benchmark the relaxations presented in Section 3.4, we focus on two applications of the OPF. The first one is the common minimization of generation costs, where we define the cost function $f(\boldsymbol{P})$ as

$$f_{\text{gen}}(\boldsymbol{P}) = \sum_{t\in\mathcal{T}}\sum_{g\in\mathcal{G}}\left(a_g^{(t)}{P_g^{(t)}}^2 + b_g^{(t)}P_g^{(t)} + c_g^{(t)}\right)$$

with $\mathcal{G}$ the set of generators. In particular, we consider that the generation costs can vary over time. This is modeled by using time-varying parameters $\{a_g^{(t)}, b_g^{(t)}, c_g^{(t)}\}$. In this context, flexible load can be worthwhile to shift the demand when generation costs are low.

The second application is a curtailment minimization and is an extension of the deterministic version of [8]. In this case, the cost function $f(\boldsymbol{P})$ is defined as

$$f_{\text{curt}}(\boldsymbol{P}) = \sum_{t\in\mathcal{T}}\left[c_{\text{curt}}\sum_{g\in\mathcal{G}}\left(\overline{P}_g^{(t)} - P_g^{(t)}\right) + c_{\text{losses}}\sum_{d\in\mathcal{D}}P_d^{(t)}\right]$$

where the first term represents the curtailment costs and the second term expresses the cost of network losses. Such a cost function is representative of the objective of a distribution system operator that operates a network with distributed generators. Flexible loads can be profitable if their consumption is shifted when production from distributed generators is high, e.g. to avoid congestions or over-voltages without relying too much on curtailment. For both applications, the term $\boldsymbol{c_f}\cdot\boldsymbol{d}$ must be added to the cost function in order to account for availability fees.

3.5.2 Implementation details

The test program is written in C++ and uses several solver libraries. For LR, a continuous relaxation of the original problem is first solved using IPOPT [19] to initialize Lagrange multipliers and solving the non-smooth problem is done

with ConicBundle [39]. The subproblem L_P is solved with MOSEK [40] while L_V, after being casted into a minimal eigenvalue problem, is addressed using Eigen [41]. For the network flow relaxation (NFR), all SDP relaxations as well as the final convex relaxation are solved with MOSEK.

The primal solutions, computed to evaluate the optimality gap of the relaxed solutions, were obtained using SCIP [18] configured with IPOPT as NLP solver.

3.5.3 Instances

An instance is defined by a cost function, a network and a number of periods. Table 3.1 presents the different networks used in the test case (if the original test contains shunt admittances, they are ignored).

Name	Number of			Source
	buses $\|\mathcal{B}\|$	generators $\|\mathcal{G}\|$	flexible loads $\|\mathcal{F}\|$	
ww6	6	3	3	[42]
ch9	9	3	3	[43]
ieee14	14	5	4	[44]
anm6	6	2	2	[8]

Table 3.1: Networks used for the benchmark.

The cost function f_{gen} is tested on (A)-(C) and f_{curt} on (A)-(D). For the curtailment application on networks (A)-(C), one of the generator (the slack bus) is modified to model a connection with another network. The power injection at the corresponding bus can, within some limits, be either positive or negative.

The test instances are finally generated by considering these 7 (network, cost function) pairs over 4 and 8 periods to obtain a total of 14 instances.

3.5.4 Numerical results

Numerical results on the 14 instances are presented in Table 3.2-a and Table 3.2-b. The relative optimality gap is computed as follow:

$$\text{gap} = \frac{ub^* - lb}{lb}$$

where lb is the optimal solution of the relaxed problem (i.e. a lower bound) which can vary for every relaxation used and ub^* is the best primal solution known, and is a fixed number. For each instance, the reported time is the duration of the program before termination, running on a 2.6 GHz processor and limited to a single core. We observe that both relaxations have similar performances for the optimality gap, in the sense that they are always within the same order of magnitude. Concerning the running time performance, there is not an approach that outperforms the other as both relaxations show very diverse results.

We are also interested in evaluating another feature of these relaxations: the level of infeasibility of their solutions in the original problem. This feature can indeed affect the efficiency of a relaxation within a spatial B&B framework [45] when seeking for a globally optimal solution of Problem (3.1)-(3.10). Relaxed solutions that are closer to feasibility can speed up the discovery of feasible solutions and at the same time provide upper bounds to the objective function earlier in the space exploration procedure. Obtaining upper bounds is critical for these approaches as it helps pruning nodes and reduces the computational budget required before termination. Table 3.2-c presents the sum of squared infeasibilities for the set of constraints (3.8)-(3.10) (i.e. those relaxed in LR and NFR). We observe that NFR shows less infeasibility than LR on 9 out of 14 instances. For some cases, NFR produces solutions that are very close to be feasible (e.g. $(\text{A})_{\text{gen}}$ and $(\text{D})_{\text{curt}}$) while LR does not exhibit similar performances even when it is able to close the gap (e.g. $(\text{B})_{\text{gen}}$). In addition, some of the solutions of LR are affected with a very high level of infeasibility (e.g. $(\text{C})_{\text{curt}}$ and $(\text{D})_{\text{curt}}$), which is orders of magnitude worse than NFR.

3.6 Conclusion

In this chapter, we presented a novel relaxation for multi-period OPF with discrete variables that is based on a network-flow reformulation. While the lower bounds it produces are comparable with the Lagrangian relaxation, the infeasibility of the relaxed solutions is reduced. This feature suggests that it is worthwhile to evaluate NFR beside the current state-of-the-art relaxations (i.e. [23] and [22]) within a B&B framework.

On the other hand, this relaxation should still be improved on two aspects. The first one is the quality of lower bounds, especially for curtailment applications. We believe that a special care should be taken concerning the upper bounds of the active losses in links. We observed that the SDP relaxation used to

compute these bounds is not very informative and it penalizes the tightness of the overall relaxation. The second aspect to improve is on the computational side. For this purpose, we would like to consider subnetworks instead of the whole network to infer the bounds on the voltage and link-flow variables. If it would reduce the size of SDP problems and speed up their convergence, it could also reduce the value of the resulting bounds. For this reason, an iterative approach that would increase the size of specific subproblems to narrow the most useful bounds is not to put aside.

Following the observations of this work, we think that another interesting

	Lagrangian relax.		Network flow relax.	
Case	gap (%)	time (s)	gap (%)	time (s)
$ww6_{gen}$	2.37	203.7	4.27	11.1
$ch9_{gen}$	0.00	1.2	2.24	12.7
$ieee14_{gen}$	0.11	143.0	5.16	84.2
$ww6_{curt}$	79.69	45.0	225.72	16.0
$ch9_{curt}$	9.07	20.1	12.53	23.5
$ieee14_{curt}$	648.64	140.1	593.58	163.3
$anm6_{curt}$	60.90	40.9	60.99	11.3

(a) Numerical results for 4 periods ($|\mathcal{T}| = 4$).

	Lagrangian relax.		Network flow relax.	
Case	gap (%)	time (s)	gap (%)	time (s)
$ww6_{gen}$	2.51	2905.2	4.50	38.7
$ch9_{gen}$	0.00	4.1	2.20	40.7
$ieee14_{gen}$	0.24	780.5	5.07	254.7
$ww6_{curt}$	124.86	83.9	255.16	82.7
$ch9_{curt}$	11.90	60.9	13.22	111.0
$ieee14_{curt}$	879.68	414.8	649.43	1207.9
$anm6_{curt}$	65.10	112.5	60.09	64.1

(b) Numerical results for 8 periods ($|\mathcal{T}| = 8$).

	Nb. of periods $\|\mathcal{T}\| = 4$		Nb. of periods $\|\mathcal{T}\| = 8$	
Case	LR	NFR	LR	NFR
$ww6_{gen}$	6.02	0.02	8.72	0.05
$ch9_{gen}$	70.87	99.33	141.50	196.21
$ieee14_{gen}$	1.24	1.72	1.86	3.58
$ww6_{curt}$	86.75	6.78	163.28	13.46
$ch9_{curt}$	179.86	152.51	142.72	162.40
$ieee14_{curt}$	456.88	6.91	57.57	16.35
$anm6_{curt}$	854.16	0.10	1564.37	0.19

(c) Sum of squared infeasibilities of relaxed solutions for constraints (3.8)-(3.10).

Table 3.2: Results for the 14 instances.

research direction would be to merge the two relaxations considered in this chapter. Tightening the power subproblem of a Lagrangian relaxation with a network-flow relaxation could both improve the convergence of the non-smooth problem of LR thanks to a tighter subproblem and reduce the infeasibility of produced solutions.

4

A Gaussian mixture approach to model stochastic processes

We present in this chapter an algorithm that models a stochastic process as a Markov process using a multivariate Gaussian Mixture Model, as well as a model selection technique to search for the adequate Markov order and number of components. The main motivation is to sample future trajectories of these processes from their last available observations (i.e. measurements). An accurate model that can generate these synthetic trajectories is critical for applications such as security analysis or decision making based on lookahead models. The proposed approach is evaluated in a lookahead security analysis framework, i.e. by estimating the probability of future system states to respect operational constraints. The evaluation is performed using a 33-bus distribution test system, for power consumption and wind speed processes. Empirical results show that the GMM approach slightly outperforms an ARMA approach.

Contents

4.1 Introduction

The recent massive integration of renewable generation has increased the level of uncertainty in power systems, to the extent that probabilistic methods are emerging for operating electrical networks [46]. This is particularly true for the operation of distribution systems, which is progressively migrating from a fit-and-forget doctrine to Active Network Management (ANM) strategies [47]. An accurate model of this uncertain dynamical system is critical in order to take adequate control actions. Moreover, and contrary to wider power systems, the uncertainty about stochastic quantities (e.g. wind speed, solar irradiance, load consumption) is not softened by an averaging effect because of the local nature of distribution systems.

In this chapter, we present an algorithm that models a stochastic process as a Markov process using a multivariate Gaussian Mixture Model (GMM). Such a parametric model learns the transition density of the process from time series of observations. For a given order of the Markov process (i.e. the length of the process history that is used to model the density of the next realization) and a given number of components in the mixture, the parameters of the GMM are learned from the data using a maximum likelihood approach. A model selection technique that relies on a multi-armed bandit framework [48] is used to search for the adequate order and number of components of the GMM.

We focus in this chapter on the ability of stochastic models to perform reliable security analyses, i.e. lookahead security estimates of the operational state of a grid. It leads to the definition of a quality measure that compares the actual security state of a grid to the Monte Carlo simulations of a model. This measure is used both for the model section phase and for comparison purposes with other modeling approaches.

4.1.1 Related works

Existing approaches in the context of power system dynamic modeling and decision making include forecasting random variables (loads, PV and wind generation) based on the use of numerical weather prediction and time series models [49, 50, 51]. Reference [50] surveys existing approaches for wind power forecasting while [52] provides insight to short-term PV generation forecast. Numerical weather prediction uses meteorological data and models to forecast relevant variables such as wind, irradiance, etc, and further uses physical

models or statistical techniques to forecast generation productions [49, 50, 52]. Artificial neural networks or fuzzy neural networks [49] were also considered for improved forecasting. Time series models use observed data values (historical data) to forecast future values of random variables. Auto-Regressive Moving Average (ARMA) models and its variants - auto regressive integrated moving average (ARIMA), ARMA with exogenous input (ARMAX/ARX) - are the most popular type in the time-series-based approaches for both load and generation forecasting [52, 51]. Neural networks and fuzzy neural networks were also considered in the context of the use of historical data [49, 51, 50].

In the context of power system problems, GMMs were only considered within static decision making where probabilistic power flow is a common tool to handle uncertainties [53]. GMM is used to approximate non-Gaussian probability density functions (Beta, Gamma, Weibull, Rayleigh) of loads [54] and generation [53]. One of the problems related to the use of GMM in this context is the choice of the number of Gaussian mixture components to accurately approximate the original non-Gaussian probability density function. The work presented in [53] compares three pair-merging methods to reduce the number of Gaussian mixture components and proposes a fine-tuning algorithm of integral square difference criterion for further improvements. On the other hand, a Markov process modeling approach was considered as an option to forecast load and wind generation. A Markov-based sensitivity model was proposed in [55] as a look-ahead capability approach for load and wind generation short-term forecasting.

To the best knowledge of the authors no work exist that uses GMMs combined with Markov process modeling for dynamic modeling and decision making in power systems. In a wider context, some developments on the use of GMMs for time series forecasting exist. Reference [56] reports on the initial results of the use of GMMs for time series but focuses exclusively on the forecasting abilities of the approach though the computation of conditional expectations.

4.2 Problem description

We aim at building models of stochastic processes that arise within power systems with the main motivation of sampling future trajectories of these processes from their last available observations (i.e. measurements). An accurate model that can generate these synthetic trajectories is critical for applications such as security analysis or decision making based on lookahead models.

4.2.1 Problem statement

Let $\mathcal{S}^*$ be a real-valued stochastic process and let

$$\mathcal{S} = \left\{ \begin{matrix} (o_1^1, \ldots, o_T^1) \\ \vdots \\ (o_1^{n_\mathcal{S}}, \ldots, o_T^{n_\mathcal{S}}) \end{matrix} \right\}$$

be a set of $n_\mathcal{S}$ real-valued time series of length T that correspond to observations of $\mathcal{S}^*$. Given this set $\mathcal{S}$, we want to learn a Markov model $\mathcal{M}$ that approximates the probability density function $p : \mathbb{R}^L \to \mathbb{R}^+$ of the next realization x_t, conditional to the previous L realizations of the process, i.e. $p_\mathcal{M}(x_t | x_{t-1}, \ldots, x_{t-L})$.

4.2.2 Model evaluation

We do not focus on the forecast performance but instead aim at a model that is relevant to generate synthetic trajectories in a lookahead context. Models are discriminated based on their ability at producing good lookahead security estimates. Such an estimate corresponds to the probability, according to a model $\mathcal{M}$, that an electrical system $\mathcal{D}$ is secure (i.e. its operational constraints are respected) for some lookahead time horizon Δt and given an history $\boldsymbol{x}^{(\text{hist})} = (x_{t-1}, \ldots, x_{t-L})$. We consider that $\mathcal{S}^*$ is the only stochastic process that influences the electrical system $\mathcal{D}$ and that its state is fully determined (e.g. through a power flow simulation) given a time step $t \in \{1, \ldots, T\}$ and the realization x_t or an estimate $\hat{x}_t$ of $\mathcal{S}^*$. We denote thereafter this state $\mathcal{D}(t, x_t)$ or $\mathcal{D}(t, \hat{x}_t)$.

We introduce a score function $\eta_{\mathcal{D},\Delta t,M}(\mathcal{M}, \mathcal{S}) \in [0, 1]$ to assess the quality of lookahead security estimates produced through Monte-Carlo simulations of $\mathcal{M}$, when $\boldsymbol{x}^{(\text{hist})}$ takes as value every sequence of L successive observations in the set $\mathcal{S}$ of time series, and where M is the number of sampled trajectories for every Monte-Carlo simulation. The score function relies on a weighted Brier score [57] (i.e. the mean of squared differences), which is reversed and scaled so that the value of $\eta_{M,\Delta t}(\mathcal{M}, \mathcal{S})$ has the following interpretations:

- 0 means that $\mathcal{M}$'s security estimates are non-informative (i.e. the probability of every state to be secure is 0.5) at best;

- 1 means that $\mathcal{M}$'s security estimates match perfectly the actual security states observed in the set $\mathcal{S}$.

The following pseudo-code details how to compute this score function:

▷ *Overall procedure*
function GET_SCORE($\mathcal{D}, \mathcal{M}, \mathcal{S}, M, \Delta t$)
  $\text{dist}_{\text{ok}}, \text{dist}_{\text{ko}}, n_{\text{ok}}, n_{\text{ko}} \leftarrow 0$
  for $i \leftarrow 1, n_{\mathcal{S}}$ **do**
    for $t \leftarrow L, T - \Delta t$ **do**
      $\boldsymbol{x}^{\text{hist}} \leftarrow (o_t^{(\text{i})}, \ldots, o_{t-L+1}^{(\text{i})})$
      $\hat{p}_{\text{ok}} \leftarrow 0$
      for $m \leftarrow 1, M$ **do**
        $\hat{p}_{\text{ok}} \leftarrow \hat{p}_{\text{ok}} + \frac{\text{IS\_SECURE}(\mathcal{D},\mathcal{M},\boldsymbol{x}^{\text{hist}},t,\Delta t)}{M}$
      if $\mathcal{D}(t + \Delta t, o_{t+\Delta t}^{(i)})$ is secure **then**
        $\text{dist}_{\text{ok}} \leftarrow \text{dist}_{\text{ok}} + (1 - \hat{p}_{\text{ok}})^2$
        $n_{\text{ok}} \leftarrow n_{\text{ok}} + 1$
      else
        $\text{dist}_{\text{ko}} \leftarrow \text{dist}_{\text{ko}} + (\hat{p}_{\text{ok}})^2$
        $n_{\text{ko}} \leftarrow n_{\text{ko}} + 1$
  $\text{score} \leftarrow 1 - \left(\frac{\text{dist}_{\text{ok}}}{n_{\text{ok}}} + \frac{\text{dist}_{\text{ko}}}{n_{\text{ko}}}\right)$
  return $\max(0, \text{score})$

▷ *Single security simulation*
function IS_SECURE($\mathcal{D}, \mathcal{M}, \boldsymbol{x}^{(\text{hist})}, t_0, \Delta t$)
  $t \leftarrow t_0$
  repeat
    $\hat{x} \leftarrow$ sample $p_{\mathcal{M}}(\cdot\,|\boldsymbol{x}^{(\text{hist})})$
    $\boldsymbol{x}^{(\text{hist})} \leftarrow (\hat{x}, x_1^{(\text{hist})}, \ldots, x_{L-1}^{(\text{hist})})$
    $t \leftarrow t + 1$
  until $t = t_0 + \Delta t$
  if $\mathcal{D}(t, \hat{x})$ is secure **then**
    return 1
  else
    return 0

4.3 Gaussian Mixture Model

We consider models $\mathcal{M}_{\boldsymbol{\omega}}(\boldsymbol{\theta})$, $\forall \boldsymbol{\omega} \in \Omega$ and $\forall \boldsymbol{\theta} \in \Theta$, that rely on a mixture of N Gaussian components to build the density function $p_{\mathcal{M}_{\boldsymbol{\omega}}}$, where $\boldsymbol{\omega} = (L, N)$ are the hyper parameters of the model and where $\boldsymbol{\theta}$ denotes the parameters of the Gaussian mixture. These latter parameters are the weight, mean, and covariance matrix of every component $i \in \{1, \ldots, N\}$ of the mixture, they are further denoted by ϕ_i, $\boldsymbol{\mu}_i$, and $\boldsymbol{\Sigma}_i$, respectively. In particular, we have:

$$p_{\mathcal{M}_{\boldsymbol{\omega},\mathcal{L}}(\boldsymbol{\theta})}(x_t|x_{t-1},\ldots,x_{t-L}) = \frac{p^{\cap}_{\mathcal{M}_{\boldsymbol{\omega},\mathcal{L}}(\boldsymbol{\theta})}(x_t,\ldots,x_{t-L})}{\int\limits_{\mathbb{R}} p^{\cap}_{\mathcal{M}_{\boldsymbol{\omega},\mathcal{L}}(\boldsymbol{\theta})}(x_t,\ldots,x_{t-L})dx_t}\,, \tag{4.1}$$

where

$$p^{\cap}_{\mathcal{M}_{\boldsymbol{\omega},\mathcal{L}}(\boldsymbol{\theta})}(x_t,\ldots,x_{t-L}) = \sum_{i=1}^{N} \phi_i \mathcal{N}(x_t,\ldots,x_{t-L};\boldsymbol{\mu}_i,\boldsymbol{\Sigma}_i) \tag{4.2}$$

is the approximation, by model $\mathcal{M}_{\boldsymbol{\omega},\mathcal{L}}(\boldsymbol{\theta})$, of the joint density function of $L+1$ successive realizations. One of the advantages of using Gaussian components is that the conditional density function in (4.1) can be easily determined given the values of the L previous realizations $\boldsymbol{x}_{\text{past}} = (x_{t-1},\ldots,x_{t-L}) \in \mathbb{R}^L$ of the process. The resulting density is also a Gaussian mixture [58] and each component $i \in \{1,\ldots,N\}$ has the following parameters:

$$\phi_i^{t|L} = \frac{\phi_i \mathcal{N}(\boldsymbol{x}_{\text{past}};\boldsymbol{\mu}_i^L,\boldsymbol{\Sigma}_i^{LL})}{\sum_{j=1}^{N} \phi_j \mathcal{N}(\boldsymbol{x}_{\text{past}};\boldsymbol{\mu}_j^L,\boldsymbol{\Sigma}_j^{LL})}\,, \tag{4.3}$$

$$\mu_i^{t|L} = \mu_i^t - (\Lambda_i^{tt})^{-1}\boldsymbol{\Lambda}_i^{tL}\left(\boldsymbol{x}_{\text{past}} - \boldsymbol{\mu}_i^L\right)\,, \tag{4.4}$$

$$\Sigma_i^{t|L} = (\Lambda_i^{tt})^{-1}\,, \tag{4.5}$$

with

$$\boldsymbol{\mu}_i = (\mu_i^t, \boldsymbol{\mu}_i^L)\,,$$
$$\boldsymbol{\Sigma}_i = \begin{pmatrix} \Sigma_i^{tt} & \boldsymbol{\Sigma}_i^{tL} \\ \boldsymbol{\Sigma}_i^{Lt} & \boldsymbol{\Sigma}_i^{LL} \end{pmatrix}, \boldsymbol{\Sigma}_i^{-1} = \begin{pmatrix} \Lambda_i^{tt} & \boldsymbol{\Lambda}_i^{tL} \\ \boldsymbol{\Lambda}_i^{Lt} & \boldsymbol{\Lambda}_i^{LL} \end{pmatrix}.$$

For a given hyper parameter $\boldsymbol{\omega} = (L, N)$, learning model $\mathcal{M}_{\boldsymbol{\omega},\mathcal{L}}(\boldsymbol{\theta})$ consists in determining the mixture's parameters $\boldsymbol{\theta}^*$ that approximate at best the density function $p^{\cap}_{\mathcal{M}_{\boldsymbol{\omega},\mathcal{L}}(\boldsymbol{\theta})}(\,\cdot\,)$ of the set $\mathcal{L}$ of $n_{\mathcal{S}}$ time series, The following procedure allows to compute $\boldsymbol{\theta}^*$ as the maximum likelihood estimate (MLE) of $\mathcal{L}$:

1. build a set $\mathcal{L}'$ of L+1-length tuples:

$$\mathcal{L}' = \left\{(o_{t-L}^l, \ldots, o_{t-1}^l, o_t^l),\ (l,t) \in \{1, \ldots, n_{\mathcal{L}'}\} \times \{L, \ldots, T-1\}\right\} ;$$

2. produce the MLE $\boldsymbol{\theta}^*$ by solving:

$$\boldsymbol{\theta}^* = \arg\max_{\boldsymbol{\theta} \in \Theta} \sum_{\boldsymbol{x} \in \mathcal{L}'} \log p^{\cap}_{\mathcal{M}_{\omega,\mathcal{L}}(\boldsymbol{\theta})}(\boldsymbol{x}) \,,$$

which is the classical MLE equation that can be solved using an expectation-maximization (EM) algorithm [59].

4.4 Model selection

In this section, we describe our sampling-based procedure to navigate within the space of hyper parameters $\Omega = \{\omega_1, \ldots, \omega_K\}$, $K \in \mathbb{N}$, using a multi-armed bandit approach. Our approach relies on the following assumptions: first, we assume that, for a given hyper parameter $\omega \in \Omega$, and a given set of learning data $\mathcal{L}$, we have access to a procedure, which may not be deterministic, that allows to generate a model $\mathcal{M}_{\omega,\mathcal{L}}$ (e.g. see Section 4.3). Then, we assume that we have access to a score function η (e.g. see Section 4.2.2) to compute noisy empirical evaluations of any model. Finally, we also assume that we have access to a selection strategy which allows us to iteratively select which hyper parameter to sample from based on noisy evaluations observed so far, and progressively converge towards an optimal hyper parameter. In the following, a standard UCB-1 algorithm [48] plays the role of this selection strategy.

Our procedure works as follows. Initially, all index values are set to $+\infty$:

$$\forall k \in \{1, \ldots, K\}, B_k^{(0)} = +\infty$$

Then, at every iteration $i \in \{1, \ldots, N\}$,

1. Select a hyper parameter $\omega^{(i)} \in \Omega$ according to a UCB-1 strategy; let $k^{(i)}$ be the index of $\omega^{(i)}$ in the set Ω:

$$k^{(i)} = \arg\max_{k \in \{1,\ldots,K\}} B_k^{(i-1)}$$

2. Perform a random partition of the set of trajectories into two subsets of

trajectories, a learning set $\mathcal{L}^{(i)}$ and a test set $\mathcal{T}^{(i)}$, formalized as follows:

$$\mathcal{L}^{(i)} = \left\{ \begin{array}{c} \left(o_0^{(i),1}, \ldots, o_{T-1}^{(i),1}\right) \\ \vdots \\ \left(o_0^{(i),n_{\mathcal{L}}}, \ldots, o_{T-1}^{(i),n_{\mathcal{L}}}\right) \end{array} \right\}$$

$$\mathcal{T}^{(i)} = \left\{ \begin{array}{c} (\mathfrak{o}_0^{(i),1}, \ldots, \mathfrak{o}_{T-1}^{(i),1}) \\ \vdots \\ (\mathfrak{o}_0^{(i),n_{\mathcal{T}}}, \ldots, \mathfrak{o}_{T-1}^{(i),n_{\mathcal{T}}}) \end{array} \right\}$$

3. Using the learning set $\mathcal{L}^{(i)}$ and the hyper parameter $\omega^{(i)}$, compute a model $\mathcal{M}_{\omega^{(i)},\mathcal{L}^{(i)}}$;

4. Compute a new noisy evaluation $\eta_k^{(i)}$ of model $\mathcal{M}_{\omega^{(i)},\mathcal{L}^{(i)}}$ as:

$$\eta_k^{(i)} = \eta(\mathcal{M}_{\omega^{(i)},\mathcal{L}^{(i)}}, \mathcal{T}^{(i)}),$$

and update the UCB-1 index values as follows:

$$\forall k \in \{1, \ldots, K\}, B_k^{(i)} = \bar{\eta_k} + \sqrt{\frac{2\ln(i)}{n_k^{(i)}}}$$

where $\bar{\eta_k}$ denotes the empirical average of evaluations of hyper parameter ω_k observed so far and $n_k^{(i)}$ denotes the number of times the hyper parameter ω_k has been evaluated so far.

4.5 Numerical results

We present the results obtained for two different datasets, with the GMM approach presented in Section 4.3 and compared with ARMA models, which were also fitted using a MLE algorithm. For both approaches, the hyper parameters were selected using the model selection technique presented in Section 4.4. These hyper parameters are:

GMM: the Markov order L and the number of components N;

ARMA: the autoregressive order L_{ar} and the moving-average order L_{ma}.

Both datasets consist in observations acquired every quarter of hour, and every time serie spans a period of six weeks (i.e. 576 observations). The first dataset has 14 time series (i.e. 8064 observations) of the aggregated power consumption of 200 residential consumers, while the second dataset has 182 time series (i.e. 104832 observations) of wind speed measurements[i]. The electrical system $\mathcal{D}$ used for security analyses is the IEEE 33-bus distribution test system with three additional wind farms, as illustrated in Figure 4.1. The considered operational constraints are the voltage limits at the buses and the thermal limits of the links. Note that the consumption was assumed to be deterministic when evaluating the wind speed models, and conversely. When the stochastic process is the load consumption, the consumption at each bus is defined as a scaling factor times the consumption process. For the wind speed process, the production of wind farms is determined from the wind speed through a usual cubic power curve.

The performance estimations of the different models for the wind speed dataset, a lookahead time horizon of 4h (i.e. 16 time steps), and $M = 50$, are presented in Figure 4.2 for the GMM approach and in Figure 4.3 for the ARMA approach. The performance of these two sets of models was estimated by UCB-1 runs of 40h and 20h for the GMM and ARMA approaches, respectively. Several observations can be made from these results:

- the best GMM outperforms the best ARMA model;
- the performance of the GMMs is less sensitive to the choice of the hyper parameters than for the ARMA models;
- the computational budget (i.e. the average time required to make one evaluation) is higher for the GMM approach than for the ARMA approach.

We also report the performance estimations for the consumption dataset and a lookahead time horizon of half an hour (i.e. 2 time steps). The performance of the two sets of models was estimated by UCB-1 runs of 3h and 2h for the GMM and ARMA approaches, respectively. The results are presented in Figure 4.4 for the GMM approach and in Figure 4.5 for the ARMA one. We now observe that the performance of the best GMM and best ARMA model is very close. However, the sensitivity of the expected score to the hyper parameters is again higher for the ARMA models.

We report in Figures 4.6 and 4.7 the expected performance of every candidate model for both approaches, both datasets, and for lookahead time horizons of 15min, 30min, 1h, 2h, and 4h. The gray scales are defined column-wise and the darkest cell of a column indicates the best expected score for the associated

[i]Both datasets were standardized (i.e. $\mu = 0$ and $\sigma = 1$) and diurnal seasonality was remove.

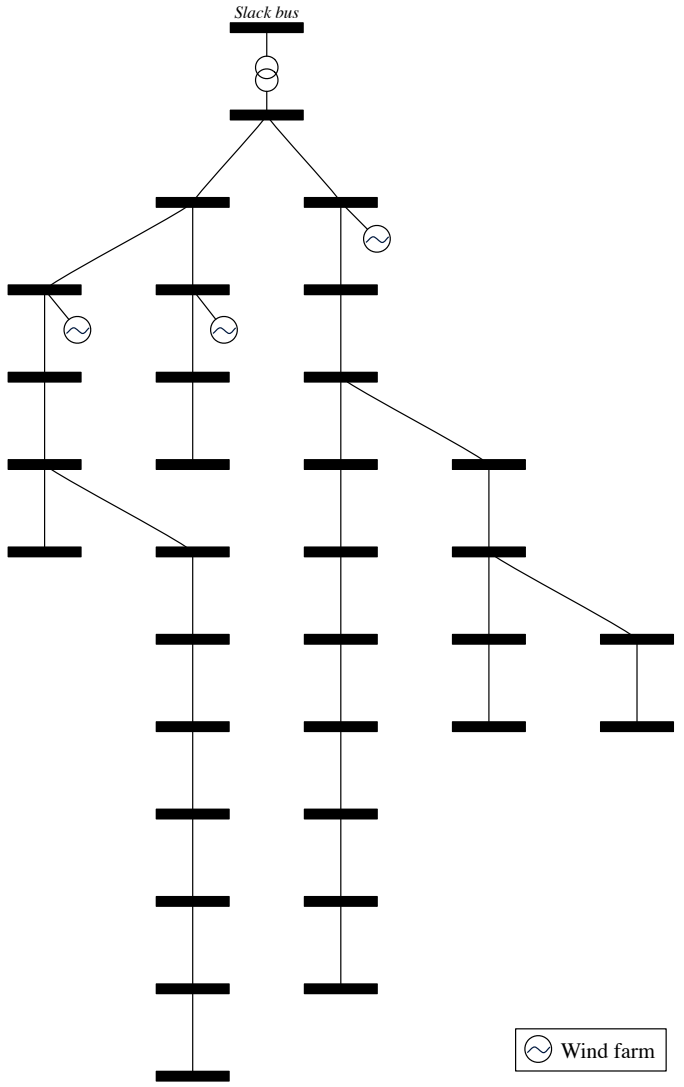

Figure 4.1: Electrical system $\mathcal{D}$, the IEEE 33-bus test system with three additional wind farms.

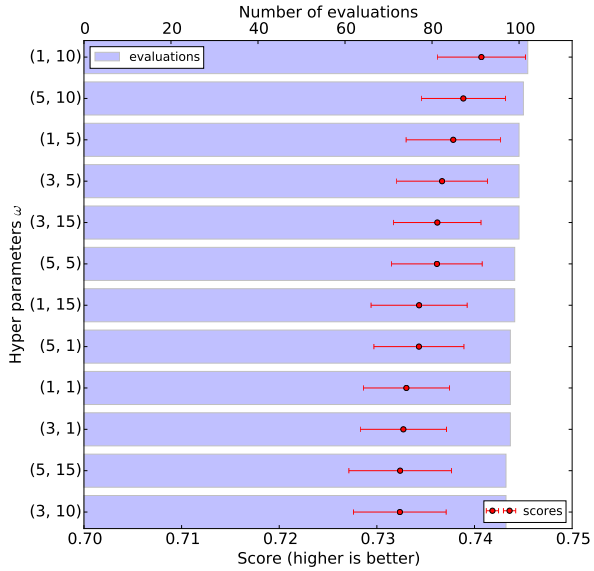

Figure 4.2: Performance estimations for GMMs for the wind speed dataset, a lookahead time horizon of 4h (i.e. 16 time steps), and $M = 50$, after a UCB-1 run of 40h.

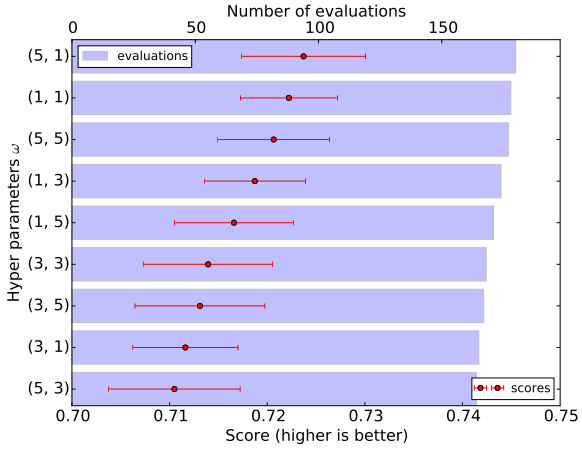

Figure 4.3: Performance estimations for ARMA models for the wind speed dataset, a lookahead time horizon of 4h (i.e. 16 time steps), and $M = 50$, after a UCB-1 run of 20h.

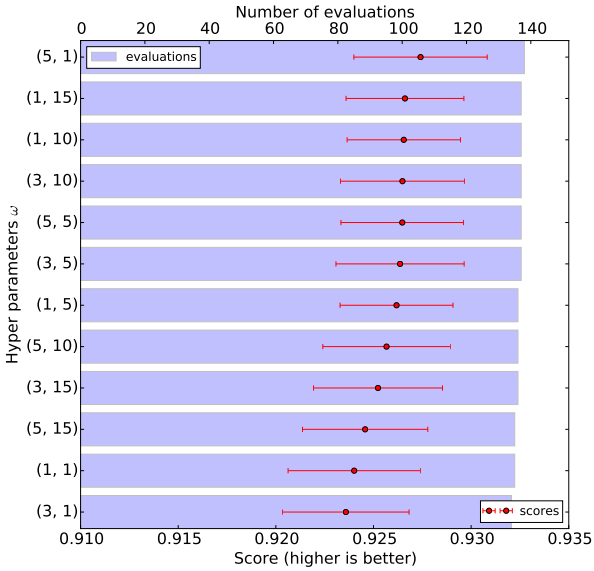

Figure 4.4: Performance estimations for GMMs for the consumption dataset, a lookahead time horizon of half an hour (i.e. 2 time steps), and $M = 50$, after a UCB-1 run of 3h.

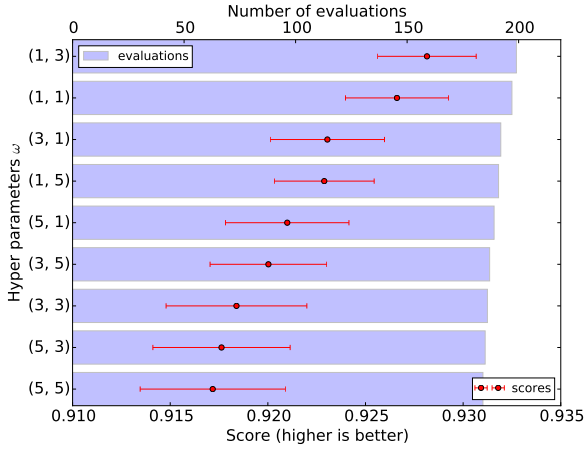

Figure 4.5: Performance estimations for ARMA models for the consumption dataset, a lookahead time horizon of half an hour (i.e. 2 time steps), and $M = 50$, after a UCB-1 run of 2h.

lookahead time horizon. We also illustrate in Figures 4.8 and 4.9 how the best model of the GMM approach performs comparing the best model of the ARMA approach, for the wind speed dataset and consumption dataset, respectively. We observe that, with the exception of the lookahead time horizons up to half an hour, the GMM approach outperforms the ARMA one. In addition, the lead of the GMM approach seems to get larger as the lookahead time horizon increases.

Finally, the values of the parameters that were used for the simulations are reported in Table 4.1.

Table 4.1: Parameters used for the simulations.

	$n_{\mathcal{L}}$	$n_{\mathcal{T}}$	M
$\mathcal{S}_{\text{cons}}$	$0.8\, n_{\mathcal{S}_{\text{cons}}}$	$0.2\, n_{\mathcal{S}_{\text{cons}}}$	50
$\mathcal{S}_{\text{wind}}$	$0.9\, n_{\mathcal{S}_{\text{wind}}}$	$0.1\, n_{\mathcal{S}_{\text{wind}}}$	50

4.6 Implementation details

We benefited from the parallelization abilities of Monte-Carlo methods by running the model selection algorithm in a HPC environment. A distinct computing core was dedicated for every trajectory $m \in \{1, \ldots, M\}$ of the Monte-Carlo simulations. The program is written in Python and relies on the Scikit-Learn library [60] to learn Gaussian mixtures, while ARMA models where fitted to data using R's arima function through a R-to-Python interface.

4.7 Conclusion and Future Work

We presented a novel approach that relies on Gaussian mixtures to model a stochastic process from a set of time series of observations. The hyper parameters of the model, i.e. the Markov order and the number of mixture components, are determined using a multi-armed bandit technique while the mixture parameters are learned from the data using an EM algorithm. Empirical results show that the proposed approach outperforms an ARMA approach for the considered application of lookahead security analysis, for datasets of residential power consumption and of wind speed.

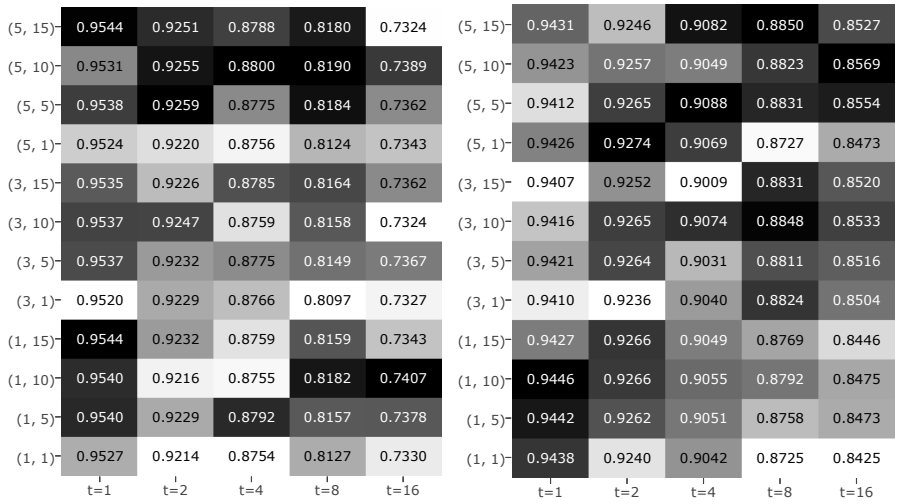

(a) Wind speed dataset **(b)** Consumption dataset

Figure 4.6: Expected score of every candidate GMM for the both dataset, as a function of the lookahead time horizon (in time steps).

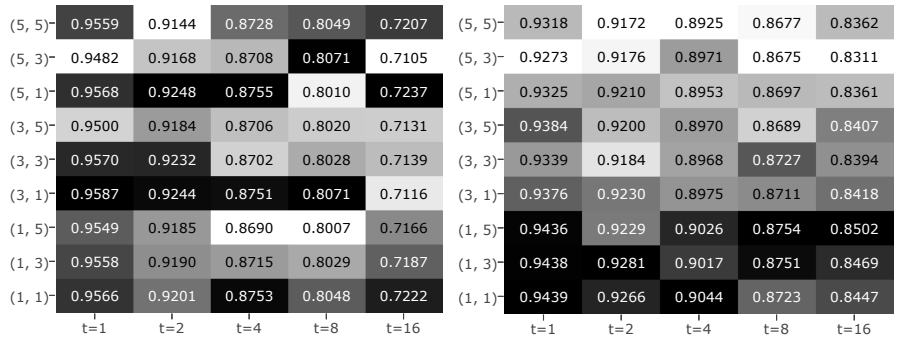

(a) Wind speed dataset **(b)** Consumption dataset

Figure 4.7: Expected score of every candidate ARMA model for the both dataset, as a function of the lookahead time horizon (in time steps).

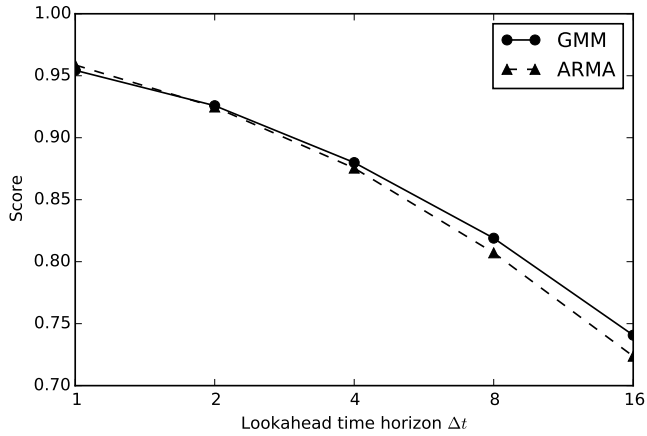

Figure 4.8: Performance comparison of each approach for the wind speed dataset, as a function of the lookahead time horizon (in time steps).

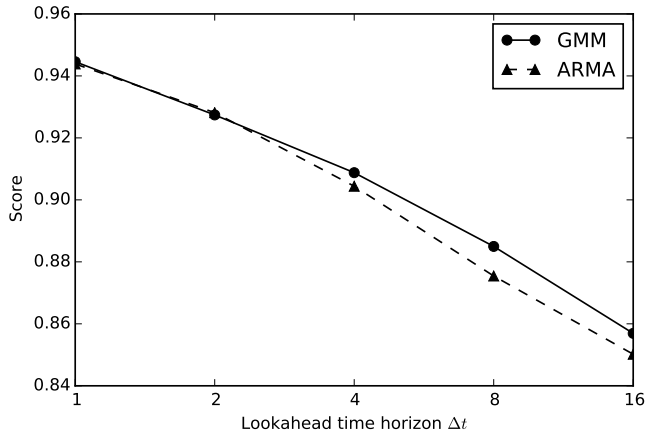

Figure 4.9: Performance comparison of each approach for the consumption dataset, as a function of the lookahead time horizon (in time steps).

As future work we consider several extensions of the present work, including simulations for other processes (e.g. solar irradiance), comparison with alternative modeling approaches (e.g. ARIMA and GARCH), as well as different test systems.

5

Problem formulation, benchmark, and approximate solution

In this chapter, we first formulate the ANM problem, which in addition to be sequential and uncertain, has a nonlinear nature stemming from the power flow equations and a discrete nature arising from the activation of power modulation signals. This ANM problem is then cast as a stochastic mixed-integer nonlinear program, as well as second-order cone and linear counterparts, for which we provide quantitative results using state of the art solvers and perform a sensitivity analysis over the size of the system, the amount of available flexibility, and the number of scenarios considered in the deterministic equivalent of the stochastic program. To foster further research on this problem, we make available at `http://www.montefiore.ulg.ac.be/~anm/` *three test beds based on distribution networks of 5, 33, and 77 buses. These test beds contain a simulator of the distribution system, with stochastic models for the generation and consumption devices, and callbacks to implement and test various ANM strategies.*

Contents

5.1 Notation

We present here the main elements of notation used throughout the text. Some locally defined notation may not be covered in this section.

Indices:

d	Device connected to a node.
m or n	Node of the electrical system.
mn	Link of the electrical system between nodes m and n.
t	Time period.

Sets:

$\mathcal{D}$	Set of electrical devices.
$\mathcal{G}$	Subset of $\mathcal{D}$ containing distributed generators.
$\mathcal{C}$	Subset of $\mathcal{D}$ that are electrical loads.
$\mathcal{F}$	Subset of $\mathcal{C}$ that can be controlled by the DSO.
$\mathcal{T}$	Set of time periods.
$\mathcal{N}$	Set of nodes of the electrical system.
$\mathcal{L}$	Set of links of the electrical system.
$\mathcal{S}_t^{(i)}$	Space of state vector $\boldsymbol{s}_t^{(i)}$ (see the variables below for $i \in \{1,2,3\}$).
$\mathcal{S}$	Global state space of the system.
$\mathcal{A}_{\boldsymbol{s}}$	Feasible action (or control) space in state $s \in \mathcal{S}$.
$\mathcal{A}_{d,\boldsymbol{s}}$	Feasible set of $act_{d,t}$ (see variables).
$\mathcal{W}$	Set of possible realizations of random processes.

Parameters:

$Y_{mn}^{(br)}$	Branch admittance of link (m,n).
$Y_{mn}^{(sh)}$	Shunt admittance of link (m,n) on the side of node m.
t_{mn}	Transformation ratio of link (m,n) on the side of node m.
$\boldsymbol{Y}$	Nodal admittance matrix.
$\boldsymbol{Y}_{n\cdot}$	n^{th} row of $\boldsymbol{Y}$.
Y_{mn}	Element (m,n) of $\boldsymbol{Y}$.
$\underline{V_n}$ and $\overline{V_n}$	Lower and upper operational limits on voltage magnitude $\lvert V_n\rvert$.
$\overline{I}_{mn}$	Operational limit on current magnitude $\lvert I_{mn}\rvert$.
$\tan\phi_d$	Reactive to active power ratio of device d (assumed constant for all devices).
T_d	Duration of a modulation signal sent to a flexible load.

ΔP_d Vector of length T_d representing the modulation signal sent to a flexible load.

N_{loads} Length of the history of load consumption tracked in the state.

N_{ir} Length of the history of solar irradiance tracked in the state.

N_v Length of the history of wind speed tracked in the state.

q_t Index of a quarter of an hour.

Variables: Note that some variables may have an additional subscript t. Also some variables are control variables, some represent the state of the system, and the remaining variables are exogenous stochastic processes.

$\boldsymbol{V}$ Vector of size $|\mathcal{N}|$, node voltages.

V_n Complex voltage at node n, i.e. n^{th} component of $\boldsymbol{V}$.

$\boldsymbol{I}$ Vector of size $|\mathcal{N}|$, current injected in the nodes.

I_i If $i = l$, it is the complex current in link l, if $i = n$, it is the complex current injected in bus n, i.e. n^{th} component of $\boldsymbol{I}$.

S_i Apparent power injected in bus. If $i = d$, it is the power injected by device d. If $i = n$, it is the total power injected by all devices connected at node n.

P_i Active power injected in bus. If $i = d$, it is the power injected by device d. If $i = n$, it is the total power injected by all devices connected at node n.

Q_i Reactive power injected in bus. If $i = d$, it is the power injected by one device. If $i = n$, it is the total power injected by all devices connected at node n.

S_{mn} Apparent power entering branch $l = (m, n)$ from the m side.

P_{mn} Active power entering branch $l = (m, n)$ from the m side.

Q_{mn} Reactive power entering branch $l = (m, n)$ from the m side.

ir_t Solar irradiance level at time t.

v_t Wind speed at time t.

$\boldsymbol{s}_t^{(1)}$ Vector representing the state of the devices at time t.

$\boldsymbol{s}_t^{(2)}$ Vector representing the state of the modulation instructions sent to controllable devices, at time t.

$\boldsymbol{flex}_t$ Vector representing the state of the flexible loads at time t, it is a part of $\boldsymbol{s}_t^{(2)}$.

$\boldsymbol{s}_t^{(3)}$ Part of the state of the system that, at time t, keeps track of past realizations of the uncertain phenomena.

$\boldsymbol{s}_t$ Global state of the system at time t.

$\boldsymbol{a}_t$ Vector of control actions taken at time t.

$\overline{\boldsymbol{p}}_t$ Maximum level of active power injection for period $t + 1$ and for each of the generators $g \in \mathcal{G}$, part of $\boldsymbol{a}_t$.

$\boldsymbol{act}_t$ Activation indicators of the flexibility services of the loads $d \in \mathcal{F}$, part of $\boldsymbol{a}_t$.

$act_{d,t}$	Component of $\boldsymbol{act}_t$ for flexible load $d \in \mathcal{F}$.
$\boldsymbol{w}_t$	Information on exogenous phenomena available at time t.

Operators and functions:

$\lvert\cdot\rvert$	Magnitude of a complex number or size of a set.
$\cdot^*$	Complex conjugate.
$f : \mathcal{S} \times \mathcal{A}_{\boldsymbol{s}} \times \mathcal{W} \to \mathcal{S}$	Transition function of the system.
$r : \mathcal{S} \times \mathcal{A}_{\boldsymbol{s}} \times \mathcal{S} \to \mathbb{R}$	Reward function.
$\pi : \mathcal{S} \to \mathcal{A}_{\boldsymbol{s}}$	Policy that returns an action for every feasible state.
$\mathcal{G}(n)$	Set of generators connected to node n.
$\mathcal{C}(n)$	Set of loads connected to node n.
$\mathcal{F}(n)$	Set of flexible loads connected to node n.

5.2 Introduction

Many authors have already attempted to provide solutions to the operational planning problem faced by a DSO wishing to implement ANM strategies. However, they mostly rely on different formulations and it can be difficult for one author to rebuild on top of another's work. These formulations can be considered as an extension of the *optimal power flow* (OPF) problem [61]. More specifically, they can be assimilated to sequential decision-making problems where, at each time step, constraints that are similar to those used for defining an OPF problem are met. Optimal power flow problems, although non-convex, have been solved for a long time using local nonlinear optimization methods. Interior-point methods are probably the most widespread class of methods dedicated to this problem [27]. If the solution they provide has no guarantee to be globally optimal, then they have been made popular by their convergence speed and their ability to solve problems of large dimensions fairly efficiently. Convexifications of the power flow equations have been successful, in particular in [62] where the author models power flows in a radial distribution system using second-order cone constraints. Recently, semidefinite programming (SDP) was applied as a convex relaxation to the OPF problem [22]. The authors report no duality gap on some standard meshed test systems and randomized versions of these test systems. The zero duality gap property was thus observed experimentally on standard test systems, and further research resulted in sufficient conditions. This is the case, for example, if the objective function is convex and monotonically increasing with the active power generation, and if the network has a radial topology [28, 29]. Another approach aiming at global optimality relies on Lagrangian relaxation (LR) [23]. The author also

describes a spatial branch and bound (B&B) algorithm to close the gap, should one exist. The ability of both SDP and LR to decrease the optimality gap within a B&B framework was evaluated in [30]. Although SDP appeared to be computationally more attractive, it showed that it could be very challenging to reach a significant gap reduction within reasonable time limits, even for small test systems. A different approach is considered in [63], where the authors present a linear approximation of the power flow equations with a focus on distribution networks. Multi-period applications related to energy storage are investigated in [31], where the SDP relaxation of [22] is successfully applied, as their particular application met the conditions of having no duality gap. The authors of [32] argue that extending [30] to a multi-period setting yields an SDP too large for current solvers to solve efficiently and suggest relaxing the time-coupling constraints using LR. However, it ended up being computationally too expensive to make the B&B approach worthwhile. Many papers consider the unit commitment problem over an AC network, which is an instance of a multi-period OPF with discrete variables. For instance in [33], a generalized Benders decomposition divides the problem into a linear master problem with discrete variables and nonlinear multi-period sub-problems. Benders cuts are generated from the sub-problems to tighten the MIP master problem. Finally, [64] focused on trying to solve a problem that is mathematically close to the one we consider and provides more information on related research.

A first objective of this work is to facilitate the comparison of solution techniques that have been developed in the research community. To that end, we first propose a generic formulation of ANM related decision-making problems. More specifically, we detail a procedure to state these problems as Markov Decision Processes (MDP), where the system dynamics describes the evolution of the electrical network and devices, while the action space encompasses the control actions that are available to the DSO. Afterwards, we instantiate this procedure on networks of 5, 33, and 77 buses, and use the elements of the resulting MDPs to build a simulator of these systems, which is available at `http://www.montefiore.ulg.ac.be/~anm/`. As a second contribution, we provide quantitative results for the resolution of the ANM problem cast as a stochastic mixed-integer nonlinear program (MINLP), as well as a mixed-integer second-order cone programming (MISOCP) relaxation and a mixed-integer linear programming (MILP) approximation, using state of the art open source and commercial solvers. We then perform a sensitivity analysis over the size of the distribution system, the amount of flexibility available in the system, and the number of scenarios considered in the deterministic equivalent of the stochastic program. Finally, a last contribution lies in the features modeled in this work. Compared to the work of [9] and [10], we explicitly account for uncertainty, and for discrete variables stemming from the activation of flexibility services. Compared to our work, [9] relies only on a continuous

nonlinear programming formulation, and thus does not analyze linear or second order cone programming formulations, but models a storage system, and [10] also models discrete decisions variables, but they are related to capacitor banks switching and storage system operation modes. The latter reference also uses MISOCP and MILP formulations.

The rest of this chapter is structured as follows. The ANM problem of a DN is described in Section 5.3, where the electrical model and the network operation details are explained, and the operational planning problem is formulated as a Markov decision process. This formulation is then cast as a stochastic mixed-integer nonlinear program in Section 5.4, where a second order cone relaxation and a linear approximation are also detailed. The test beds built around the different distribution systems are described in Section 5.5, and test results are presented in Section 5.6. Section 5.7 concludes and presents possible extensions of this work.

5.3 Problem Description

5.3.1 Model of the electrical distribution system

In this chapter, we are always considering that the network and all its devices are operating in alternating current mode. We also make the choice to represent complex numbers in rectangular coordinates.

The electrical distribution system can be mathematically represented by a graph, that is a set of nodes, and a set of links connecting nodes. A node is an electrical bus characterized by a voltage $V_n \in \mathbb{C}$. In addition to links connecting a bus to its neighbors, several devices may be connected to a bus. Devices are either injecting or withdrawing power. Every link $(m, n) \in \mathcal{L} \subset \mathcal{N}^2$ connects a pair of nodes $m, n \in \mathcal{N}$ and represents an overhead line, an underground cable, or a transformer. A link is represented by its π-model, composed of five complex parameters: two ratios t_{mn} and t_{nm}, a branch admittance $Y_{mn}^{(br)}$, and two shunt admittances $Y_{mn}^{(sh)}$ and $Y_{nm}^{(sh)}$ (see Fig. 5.1), that are considered fixed in this work, although opportunities to change them dynamically can exist in practice. More details on the π-model of specific links can be found in [65].

To ensure the proper operation of the devices connected to a bus, the voltage magnitude $|V_n|$ at note n should not deviate too much from its nominal voltage

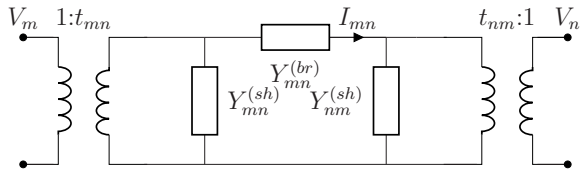

Figure 5.1: π-model of a link.

level:

$$\forall n \in \mathcal{N} : \underline{V}_n \leq |V_n| \leq \overline{V}_n \,. \tag{5.1}$$

If $I_{mn} \in \mathbb{C}$ is the branch current through link (m, n), its magnitude $|I_{mn}|$ should be kept below a pre-specified limit to prevent excessive heating of conductors and insulating materials:

$$\forall (m, n) \in \mathcal{L} : |I_{mn}| \leq \overline{I}_{mn}. \tag{5.2}$$

In reality, there are several limits depending on the magnitude and duration of the over-current. In this work we consider only the most conservative limit, since we want to keep a sufficient margin as we are taking decisions ahead of time with a relatively high uncertainty. The magnitude of the current I_l in link l connecting nodes m and n can be deduced from the voltage at these nodes by

$$|I_{mn}| = \left| \left(|t_{mn}|^2 V_m - (t_{mn}^{(l)})^* t_{nm}^{(l)} V_n \right) Y_{mn}^{(br)} \right| , \tag{5.3}$$

where $\cdot^*$ denotes the complex conjugate operator.

Before defining the power injections as a function of voltages, it is convenient to relate the current injected at nodes to the voltage by writing:

$$\boldsymbol{I} = \boldsymbol{Y}\boldsymbol{V} \,, \tag{5.4}$$

where $\boldsymbol{I} = (I_1, \ldots, I_{|\mathcal{N}|})$ is the vector of the current injection at nodes, $\boldsymbol{V} = (V_1, \ldots, V_{|\mathcal{N}|})$ is the vector of the voltage at nodes, and $\boldsymbol{Y}$ is the $|\mathcal{N}| \times |\mathcal{N}|$ nodal admittance matrix, which has its elements defined by

$$Y_{mn} = \begin{cases} -(t_{mn}^{(l)})^* t_{nm}^{(l)} Y_{mn}^{(br)} & \text{if } m \neq n \text{ and } \exists (m, n) \in \mathcal{L} \,, \\ \sum_{(m,k)\in\mathcal{L}} |t_{mk}|^2 (Y_{mn}^{(sh)} + Y_{mn}^{(br)}) & \text{if } m = n \,, \\ 0 & \text{otherwise} \,. \end{cases} \tag{5.5}$$

Regarding the active power P_n and reactive power Q_n injected at every node n,

they are related to the node voltages through the power flow equations [66]:

$$\forall n \in \mathcal{N} : S_n = P_n + jQ_n = V_n I_n^* = V_n \boldsymbol{Y}_{n\cdot}^* \boldsymbol{V}^*, \tag{5.6}$$

where S_n is the apparent power injection at bus n and $\boldsymbol{Y}_{n\cdot}$ denotes the n^{th} row of the nodal admittance matrix. By convention a power injection is positive if it supplies the network and negative if it takes energy from the network.

In summary, there are four quantities attached to each node $n \in \mathcal{N}$ that determine the electrical state of the system: P_n, Q_n, and real and imaginary parts of V_n. The power flow equations (5.6) provide $2|\mathcal{N}|$ relations. $2|\mathcal{N}|$ variables should thus be fixed to obtain a solution to this system of equations. In general, V_n is fixed on one side of the transformer between the MV network and the transmission system, to provide a reference voltage. At other nodes, the active power injection P_n is known, as well as either the reactive power Q_n or the voltage magnitude $|V_n|$, depending on the type of device connected at the node. In this work we consider that we have some control over the power flows in the system, hence we consider that less than $2|\mathcal{N}|$ variables are fixed and that we can act on P_n and Q_n at some nodes. The system is actually controlled by acting on the electrical devices attached to these nodes.

Electrical devices can be classified into two distinct subsets, the set $\mathcal{C} \subset \mathcal{D}$ of loads that withdraw power from the network, and the set $\mathcal{G} \subset \mathcal{D}$ of generators that inject power into the network. Within each subset, we also distinguish two types of device models. The first ones represent individual injection and withdrawal points. They can model certain types of DGs or consumers that are directly connected to the MV grid (e.g., wind farms, some companies and factories, etc.). The others model an aggregate set of devices that are assimilated to a single connection point at the MV grid (e.g., residential consumers and solar panels). Correspondences between some physical elements and their device model are illustrated in Fig. 5.2. At node 3, a set of residential loads and a set of distributed solar units have been aggregated into a single load model and a single generator model.

An active power injection value P_d and a reactive power injection value Q_d are associated with every device $d \in \mathcal{D}$, and, denoting the set of devices connected at node n by $\mathcal{D}(n) \subset \mathcal{D}$:

$$\forall n \in \mathcal{N} : S_n = P_n + jQ_n = \sum_{d \in \mathcal{D}(n)} (P_d + jQ_d). \tag{5.7}$$

Every device d has a restricted set $\mathcal{O}_d \subset \mathbb{R}^2$ of valid (P_d,Q_d) injection points. We assume that the loads are operating at a constant power factor, i.e. the ratio

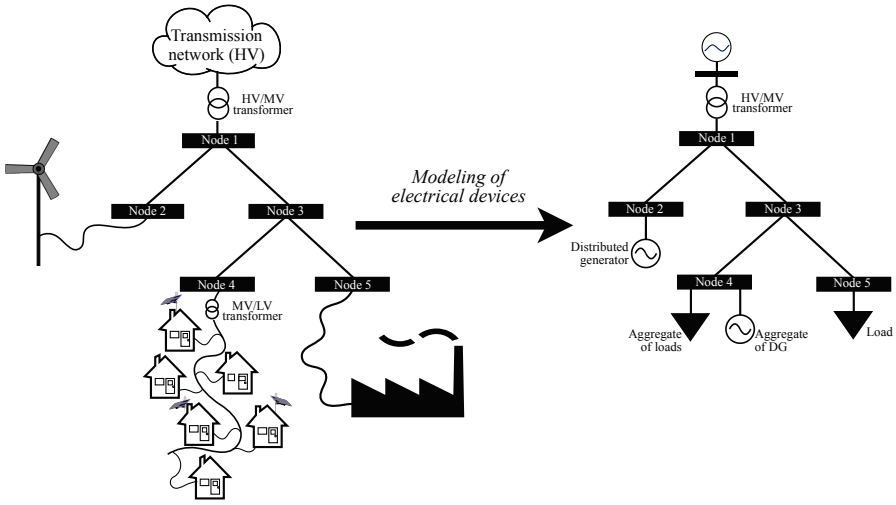

Figure 5.2: System model

between reactive and active powers - denoted as $\tan\phi_d$ - remains unchanged:

$$\forall d \in \mathcal{C} : \mathcal{O}_d = \{(P_d, Q_d) \in \mathbb{R}^2 \mid \frac{Q_d}{P_d} = \tan\phi_d\}\,. \tag{5.8}$$

For distributed generators, the injections points have to stay within a polyhedron, as illustrated in Fig. 5.3. This set is defined by lower and upper bounds on both P_d and Q_d, as well as by two linear constraints that prevent a full flexibility on Q_g when P_g is close to its maximum. These constraints model the limitations of the power converter and/or of the electric generator [67]. We have:

$$\begin{aligned}\forall g \in \mathcal{G} : \mathcal{O}_g = \{(P_d, Q_d) \in \mathbb{R}^2 \mid\ & P_{min,g} \leq P_g \leq P_{max,g}\,,\\ & Q_{min,g} \leq Q_g \leq Q_{max,g}\,,\\ & Q_g \leq \alpha_g^+ P_g + \beta_g^+\,,\\ & Q_g \leq \alpha_g^- P_g + \beta_g^-\}\,.\end{aligned} \tag{5.9}$$

5.3.2 Operational planning problem statement

Considering the model of the electrical distribution network presented in Section 5.3.1, operational planning is a recurring task performed by the DSO

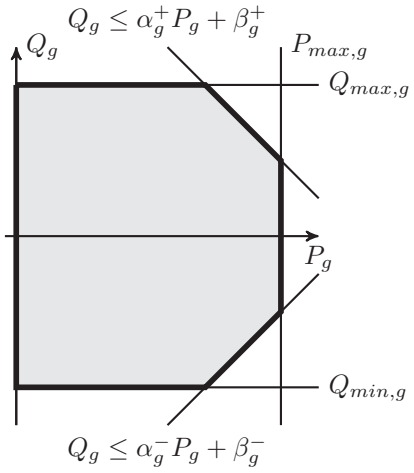

Figure 5.3: Illustration of a polyhedral set $\mathcal{O}_d$ defining the P-Q capability area of a distributed generator $g \in \mathcal{G}$.

to anticipate the evolution of the system, that is the impact of the evolution of the injection and the consumption patterns on the operational limits of the system, and take preventive decisions to stay within these limits. Among the available decisions in the considered timing of operations, we consider that acting on the power injected or consumed by a predefined set of devices is the only type of control the DSO has, as detailed in Section 5.3.1. We describe the evolution of the system by a discrete-time process having a time horizon $\mathcal{T}$, the number of periods used for the operational planning phase. The period duration is 15 minutes, by analogy with the typical duration of a market period. The power injection and withdrawal levels are constant within a single period, and we neglect the fast dynamics of the system, which may be handled by real time controllers [68]. The control actions in this section are aimed to directly impact these power levels and can introduce time-coupling effects, depending on the type of device. We now describe two control means of the system, the modulation of the generation and the modulation of the demand, as well as one of the possible interaction schemes between the actors of this system.

For each device belonging to the set $\mathcal{G} \subset \mathcal{D}$ of DGs, the DSO can impose a curtailment instruction, i.e. an upper limit on the generation level of the DG (cf. Fig. 5.4). This request can be performed until the time period immediately preceding the one concerned by the curtailment and it is acquired in exchange for a fee. This fee is used to compensate the producer for financial loss related to the energy that could not be produced during modulation periods. We assume that this fee is defined as a per unit compensation for the energy not produced, with respect to the actual potential that is known after the market

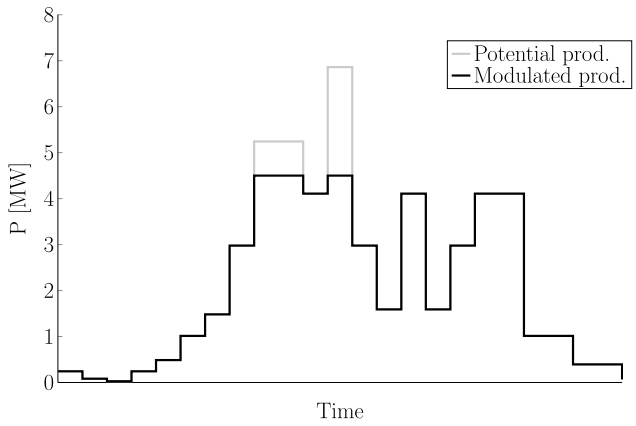

Figure 5.4: Curtailment of a distributed generator.

period.

We also consider that the DSO can modify the consumption of some flexible loads, a subset $\mathcal{F}$ of full set of the loads $\mathcal{C} \subset \mathcal{D}$ of the network. An activation fee is associated with this control mean and flexible loads can be notified of activation until the time immediately preceding the start of the service. Once the activation is performed at time t_0, the consumption of the flexible load d is modified by a certain value during T_d periods. For each of these modulation periods $t \in \{t_0 + 1, ..., t_0 + T_d\}$, this value is defined by the modulation function $\Delta P_d(t - t_0)$. An example of modulation function and its influence over the consumption curve are presented in Fig. 5.5. Loads cannot be modulated in an arbitrary way. There are constraints to be imposed on the modulation signal, which are inherited from the flexibility sources of the loads, such as an inner storage capacity (e.g. electric heater, refrigerator, water pump) or a process that can be scheduled with some flexibility (e.g., industrial production line, dishwasher, washing machine). In any case, we will always consider that the modulation signal ΔP_d has to satisfy the following conditions:

- A downward modulation is followed by an increase of the consumption, and conversely.
- The integral of the modulation signal is null in order to ensure that the consumption is only shifted, not modified.

Other approaches that we do not consider in this work exist to control the system, such as modulating the tariff signal(s), acting on the topology of the network, or using distributed storage sources. We do not model either the automatic regulation devices that often exist in distribution systems, such as On Load Tap Changers of transformers which automatically adapt to control the voltage level. This should be the case, obviously, in a real life application.

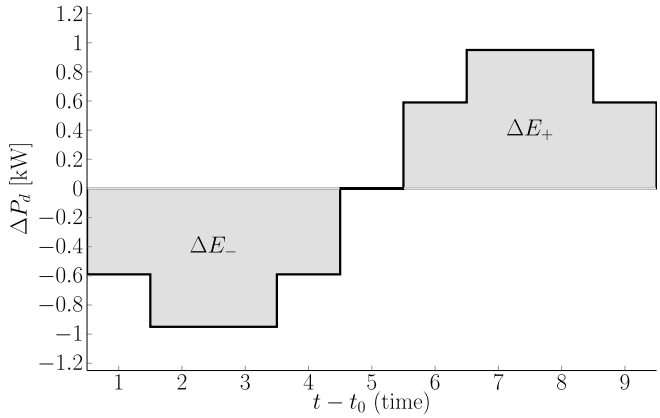

(a) Modulation signal of the consumption ($T_d = 9$).

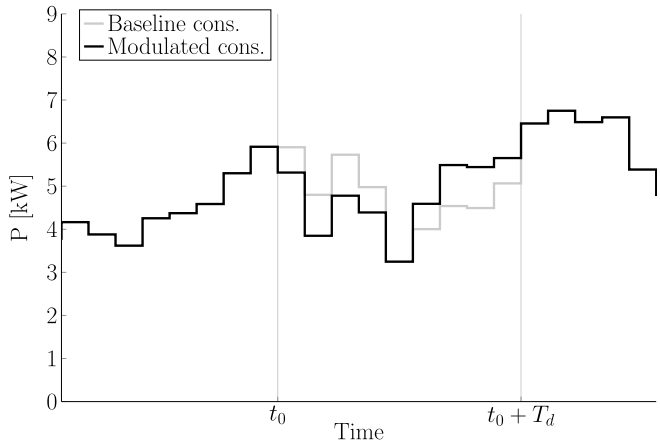

(b) Impact of the modulation signal over the consumption.

Figure 5.5: Illustration of flexibility services.

We will discuss in the conclusion what are the implications of these non-modeled control possibilities.

5.3.3 Optimal sequential decision-making formulation

We now formulate operational planning as an optimal sequential decision-making problem, that is, we explain how the time, the decision process, and uncertainty are included to extend the mathematical model described in Section 5.3.1. The sequential aspect is induced by the modulation service that

is provided by flexible loads. Indeed, if such a service is activated at time t_0 for a flexible load d, the action will influence the system for the set of periods $\{t_0+1, ..., t_0+T_d\}$. In addition to being a sequential problem, it is also stochastic, because the evolution of the system and the outcome of control actions are affected by several uncertain factors. These factors include, but are not limited to, the wind speed, the level of solar irradiance, and the consumption level of the loads. In this section, we model this problem as a Markov decision process with mixed-integer sets of states and actions. We thus consider that the transition probabilities of the state of the system from a period t to a period $t+1$ only depend on the state at time t. However, this state can encompass several past values of wind speed, solar irradiance, consumption levels, and any auxiliary modeling variables, in order to obtain a relevant model. An automatic procedure that determines an adequate number of past values to track in the state is presented in Section 5.5. Note that modeling the actual system as a Markovian system is not restrictive as all properly modeled systems are Markovian if the state variables capture all the information to model the system from time t and onwards [69]. Finally, the notion of optimality is defined using a reward function that associates an immediate reward (or score) to every transition of the system. The better the cumulated reward over a system trajectory, the better the sequence of control actions for this trajectory.

5.3.3.1 System state

The global state space $\mathcal{S}$ of the system is decomposed in three subsets:

$$\mathcal{S} = \mathcal{S}^{(1)} \times \mathcal{S}^{(2)} \times \mathcal{S}^{(3)}.$$

The power injections of the devices are sufficient to obtain the value of the electrical quantities through equations (5.6) and (5.7). These injections are determined from the realization of the exogenous consumption and generation processes at a given time period, and from the modulation instructions for that period. If the consumption processes require the representation of the individual consumption of every load, it is possible to obtain the production of DGs given the power level of their energy source (i.e. the wind speed or the level of solar irradiance). We thus define a first state set $\mathcal{S}^{(1)}$ such that the vectors $\boldsymbol{s}_t^{(1)} \in \mathcal{S}^{(1)}$ are defined by

$$\boldsymbol{s}_t^{(1)} = \left(P_{1,t}, \ldots, P_{|\mathcal{C}|,t}, ir_t, v_t\right),$$

where, at time $t \in \mathcal{T}$, the ir_t and v_t components represent the level of solar irradiance and the wind speed, respectively. If, for the sake of simplicity, we

consider only solar and wind generation, other types of generators could easily be integrated by increasing the dimension of $\mathcal{S}^{(1)}$. Note that the reactive power withdrawals of loads are known from $\boldsymbol{s}_t^{(1)}$ through equation (5.8).

The vector $\boldsymbol{s}_t^{(2)} \in \mathcal{S}^{(2)}$, defined as

$$\boldsymbol{s}_t^{(2)} = (\overline{P}_{1,t}, \hat{Q}_{1,t}, \ldots, \overline{P}_{|\mathcal{G}|,t}, \hat{Q}_{|\mathcal{G}|,t}, flex_{1,t}, \ldots, flex_{|\mathcal{F}|,t}),$$

contains the upper limits $\overline{P}_{g,t}$ on the active power injection and the reactive set-points $\hat{Q}_{g,t}$ of the DGs $g \in \mathcal{G}$, as authorized by the DSO, and the indicators $flex_{d,t}$ of the flexibility service state of the loads $d \in \mathcal{F}$:

$$flex_{d,t} = \begin{cases} \text{number of active periods left} & \text{if service is active} \\ 0 & \text{if service is inactive}\,. \end{cases}$$

We denote by $\boldsymbol{s}_t^{(3)} \in \mathcal{S}^{(3)}$ the part of the system's state that, at time $t \in \mathcal{T}$, keeps track of past realizations of the uncertain phenomena (i.e. wind speed, solar irradiance, and consumption levels) and contains the optional auxiliary modeling variables. Its purpose is to improve the accuracy of the stochastic modeling and to allow the representation of processes that are required for some reward functions (see Section 5.3.3.4). The number of past values can be different for each phenomenon and, we have

$$\begin{aligned} \boldsymbol{s}_t^{(3)} = (&P_{1,t-1}, \ldots, P_{1,t-N_{loads}+1}, \ldots, P_{|\mathcal{C}|,t-1}, \ldots, P_{|\mathcal{C}|,t-N_{loads}+1}, \\ &ir_{t-1}, \ldots, ir_{t-N_{ir}+1}, v_{t-1}, \ldots, v_{t-N_v+1}, \\ &s_{1,t}^{(\text{aux})}, \ldots, s_{N_{aux},t}^{(\text{aux})}) \end{aligned}$$

where N_{loads}, N_{ir}, $N_v \in \mathbb{Z}_0^+$, and $N_{aux} \in \mathbb{Z}^+$. The value of these parameters has to be determined when instantiating the presented abstract decision model (see Section 5.5). A value of 1 for the three former parameters means that the history of the corresponding phenomenon consists of $\boldsymbol{s}^{(1)}$ only, while a value of 0 for the latter parameter means that there is no auxiliary variable. We denote thereafter the vector of the N_{aux} auxiliary modeling variables by $\boldsymbol{s}_t^{(\text{aux})}$.

5.3.3.2 Control actions

The control means that are available to the DSO to control the system are modeled by the set $\mathcal{A}_{\boldsymbol{s}}$ of control actions. This set depends on the state $\boldsymbol{s}_t$ of the system because it is not possible to activate the flexibility service of a load

if it is already active. The components of vectors $\boldsymbol{a}_t \in \mathcal{A}_{\boldsymbol{s}}$ are defined by

$$\boldsymbol{a}_t = (\overline{\boldsymbol{p}}_t, \hat{\boldsymbol{q}}_t, \boldsymbol{act}_t)\,,$$

with $\overline{\boldsymbol{p}}_t, \hat{\boldsymbol{q}}_t \in \mathbb{R}^{|\mathcal{G}|}$ such that, for period $t+1$ and for each of the generators $g \in \mathcal{G}$, $\overline{p}_{g,t}$ and $\hat{q}_{g,t}$ indicate the maximum level of active power injection and the desired reactive set-point, respectively. On the other hand, the vector $\boldsymbol{act}_t$ represents the activation indicators of the flexibility services of the loads $d \in \mathcal{F}$, where each component $act_{d,t}$ belongs to $\mathcal{A}_{d,\boldsymbol{s}}$, which is defined as

$$\mathcal{A}_{d,\boldsymbol{s}} = \begin{cases} \{0,1\} & \text{if } flex_{d,t} = 0 \\ \{0\} & \text{if } flex_{d,t} > 0\,, \end{cases} \tag{5.10}$$

to ensure that a load which is already active is not activated.

By using this representation of the control actions, we consider that a curtailment or flexibility activation action targeting a period t must always be performed at the period $t-1$, as described in Section 5.3. We do not consider the possibility to notify control actions several periods ahead, because it would induce even larger time-coupling effects, while not improving the extent of control of the DSO since in the interaction model considered in this chapter the cost associated with an action is independent of the notification delay.

5.3.3.3 Transition function

The system evolution from a state $\boldsymbol{s}_t$ to a state $\boldsymbol{s}_{t+1}$ is described by the transition function f. The new state $\boldsymbol{s}_{t+1}$ depends, in addition to the preceding state, on the control actions $\boldsymbol{a}_t$ and on the realization of the stochastic processes:

$$f : \mathcal{S} \times \mathcal{A}_{\boldsymbol{s}} \times \mathcal{W} \to \mathcal{S}\,,$$

where $\mathcal{W}$ is the set of possible realizations of a random process. The general evolution of the system is thus governed by relation

$$\boldsymbol{s}_{t+1} = f(\boldsymbol{s}_t, \boldsymbol{a}_t, \boldsymbol{w}_t)\,, \tag{5.11}$$

where $\boldsymbol{w}_t \in \mathcal{W}$ represents the exogenous information and follows a probability law $p_{\mathcal{W}}(\,\cdot\,)$. We could write equivalently that $\boldsymbol{s}_{t+1} \sim p_{\mathcal{S}}(\,\cdot\,|\boldsymbol{s}_t, \boldsymbol{a}_t)$, which clearly highlights that the next state of the system follows a probability distribution that is conditional on the current state and on the action taken at the corresponding time step. However, we favor notation of equation (5.11) as it enables

an easier formulation of concepts that are introduced latter in this chapter. We now describe the various elements that constitute the transition function.

Load consumption The uncertainty about the behavior of consumers inevitably leads to uncertainty about the power level they draw from the network. However, over a one-day horizon, some trends can be observed. For example, consumption peaks arise in the early morning and in the evening for residential consumers, but at levels that fluctuate from one day to another and among consumers. We model the evolution of the consumption of each load $d \in \mathcal{C}$ by

$$P_{d,t+1} = f_d(P_{d,t}, P_{d,t-1}, \ldots, P_{d,t-N_{loads}+1}, \boldsymbol{s}_t^{(aux)}, \boldsymbol{w}_{d,t}) \,, \tag{5.12}$$

where $\boldsymbol{w}_{d,t} \sim p_{\mathcal{W}_d}(\,\cdot\,)$ denotes some components of $\boldsymbol{w}_t \sim p_{\mathcal{W}}(\,\cdot\,)$. Given the hypothesis of a constant power factor for the loads, the reactive power consumption can directly be deduced from $P_{d,t+1}$:

$$Q_{q,t+1} = \tan\phi_d \cdot P_{d,t+1} \,. \tag{5.13}$$

Speed and power level of wind generators The uncertainty about the production level of wind turbines is inherited from the uncertainty about the wind speed. The stochastic process that we consider governs the wind speed, which is assumed to be uniform across the network. The production level of the wind generators is then obtained by using a deterministic function that depends on the wind speed realization, this function is the power curve of the considered generator. We can formulate this phenomenon as:

$$v_{t+1} = f_v(v_t, \ldots, v_{t-N_v+1}, \boldsymbol{s}_t^{(aux)}, \boldsymbol{w}_t^{(v)}) \,, \tag{5.14}$$

$$P_{g,t+1} = \eta_g(v_{t+1}), \forall g \in \text{wind generators} \subset \mathcal{G} \,, \tag{5.15}$$

such that $\boldsymbol{w}_t^{(v)} \sim p_{\mathcal{W}^{(v)}}(\,\cdot\,)$ denotes some components of $\boldsymbol{w}_t \sim p_{\mathcal{W}}(\,\cdot\,)$ and where η_g is the power curve of generator g. A typical example of power curve $\eta_g(v)$ is illustrated in Fig. 5.6.

Irradiance and photovoltaic production Like wind generators, the photovoltaic generators inherit their uncertainty in production level from the uncertainty associated with their energy source. This source is represented by the level of solar irradiance, which is the power level of the incident solar energy per square meter. The irradiance level is the stochastic process that we model, while the production level is obtained by a deterministic function of the

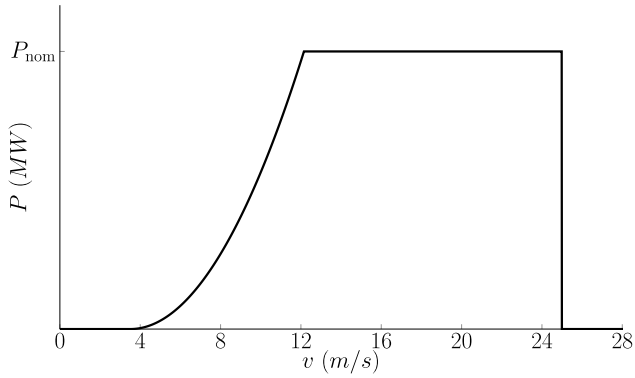

Figure 5.6: Power curve of a wind generator.

irradiance and of the surface of photovoltaic panels. This function is simpler than the power curve of wind generators and is defined as

$$P_{g,t} = \eta_g \cdot \text{surf}_g \cdot ir_t \,,$$

where η_g is the efficiency factor of the panels, assumed constant and with a typical value around 15%, while surf_g is the surface of the panels in m^2 and is specific to each photovoltaic generator. The irradiance level is denoted by ir_t and the whole phenomenon is modeled by the following process:

$$ir_{t+1} = f_{ir}(ir_t, \ldots, ir_{t-N_{ir}+1}, \boldsymbol{s}_t^{(aux)}, \boldsymbol{w}_t^{(ir)}) \,, \tag{5.16}$$

$$P_{g,t+1} = \eta_g \cdot \text{surf}_g \cdot ir_{t+1}, \forall g \in \text{solar generators} \subset \mathcal{G} \,, \tag{5.17}$$

such that $\boldsymbol{w}_t^{(ir)} \sim p_{\mathcal{W}^{(ir)}}(\,\cdot\,)$ denotes some components of $\boldsymbol{w}_t \sim p_{\mathcal{W}}(\,\cdot\,)$.

Auxiliary modeling variables The evolution of auxiliary modeling variables depends on their meaning and must be determined when instantiating the presented abstract decision model. The evolution of each component of $\boldsymbol{s}_t^{(\text{aux})}$ can be either stochastic or deterministic and, without loss of generality, we can write:

$$\boldsymbol{s}_{t+1}^{(\text{aux})} = f_{aux}(\boldsymbol{s}_t, \boldsymbol{w}_t^{(\text{aux})}) \,, \tag{5.18}$$

such that $\boldsymbol{w}_t^{(\text{aux})} \sim p_{\mathcal{W}^{(\text{aux})}}(\,\cdot\,)$ denotes some components of $\boldsymbol{w}_t \sim p_{\mathcal{W}}(\,\cdot\,)$.

Impact of control actions The stochastic processes that we described govern the evolution of the state $\boldsymbol{s}_t^{(1)} \in \mathcal{S}^{(1)}$ of the consumption of loads (flexibility services excluded) and of the power level of energy sources of DGs. We now

define the evolution of the components of $\boldsymbol{s}_t^{(2)} \in \mathcal{S}^{(2)}$ by integrating the control actions of the DSO. Concerning the modulation instructions of the generators, we have:

$$\forall g \in \mathcal{G}: \qquad \overline{P}_{g,t+1} = \begin{cases} \overline{p}_{g,t} & \text{if } (\overline{p}_{g,t}, \hat{q}_{g,t}) \in \mathcal{O}_g\,, \\ \max_{(p,\hat{q}_{g,t})\in\mathcal{O}_g} p & \text{otherwise}\,, \end{cases} \tag{5.19}$$

$$\forall g \in \mathcal{G}: \qquad \hat{Q}_{g,t+1} = \hat{q}_{g,t}\,, \tag{5.20}$$

where $\max_{(p,\hat{q}_{g,t})\in\mathcal{O}_g} p$ denotes the maximal active production level that generator g can sustain with a reactive set-point of $\hat{q}_{g,t}$. It is used if needed to ensure that the instructed $(\overline{P}_{g,t+1}, \hat{Q}_{g,t+1})$ point is a valid operating point, such a defined by equation (5.9). As for the components dedicated to the flexible loads, their evolution is governed by:

$$\forall d \in \mathcal{F}: \quad flex_{d,t+1} = \max(flex_{d,t} - 1\ ;\ 0) + act_{d,t} T_d\,, \tag{5.21}$$

$$\forall d \in \mathcal{F}: \qquad \Delta P_{d,t+1} = \begin{cases} \Delta P_d (T_d - flex_{d,t+1} + 1) & \text{if } flex_{d,t+1} > 0 \\ 0 & \text{if } flex_{d,t+1} = 0\,. \end{cases} \tag{5.22}$$

From vectors $\boldsymbol{s}_t^{(1)}$ and $\boldsymbol{s}_t^{(2)}$, we can determine the active and reactive power injections at nodes and thus obtain the value of the electrical quantities at nodes $n \in \mathcal{N}$ and links $(m,n) \in \mathcal{L}$ of the network:

$$P_{n,t} = \sum_{g\in\mathcal{G}(n)} \min(\overline{P}_{g,t}; P_{g,t}) + \sum_{d\in\mathcal{C}(n)} P_{d,t} + \sum_{d\in\mathcal{F}(n)} \Delta P_{d,t}\,, \tag{5.23}$$

$$Q_{n,t} = \sum_{g\in\mathcal{G}(n)} \hat{Q}_{g,t} + \sum_{d\in\mathcal{C}(n)} Q_{d,t} + \sum_{d\in\mathcal{F}(n)} \tan\phi_d \Delta P_{d,t}\,, \tag{5.24}$$

$$P_{n,t} - jQ_{n,t} = V_{n,t}^* \boldsymbol{Y}_n \cdot V_{n,t}\,, \tag{5.25}$$

$$|I_{mn,t}| = \left| \left(|t_{mn}|^2 V_{m,t} - (t_{mn}^{(l)})^* t_{nm}^{(l)} V_{n,t} \right) Y_{mn}^{(br)} \right|\,. \tag{5.26}$$

5.3.3.4 Reward function and goal

In order to evaluate the performance of a policy, we first specify the reward function $r : \mathcal{S} \times \mathcal{A}_{\boldsymbol{s}} \times \mathcal{S} \to \mathbb{R}$, which associates an instantaneous reward for

each transition of the system from a period t to a period $t+1$:

$$r(\boldsymbol{s}_t, \boldsymbol{a}_t, \boldsymbol{s}_{t+1}) = \underbrace{-\sum_{g\in\mathcal{G}} \max\{0, \frac{P_{g,t+1} - \overline{P}_{g,t+1}}{4}\} C_g^{curt}(\boldsymbol{s}_{t+1}^{(\text{aux})})}_{\text{curtailment cost of DGs}} \underbrace{- \sum_{d\in\mathcal{F}} act_{d,t} C_d^{flex}}_{\substack{\text{activation cost} \\ \text{of flexible loads}}} - \underbrace{\Phi(\boldsymbol{s}_{t+1})}_{\text{penalty function}}, \tag{5.27}$$

where $C_g^{curt}(\cdot)$ is a per-generator function that defines the curtailment price, while $C_d^{flex}(\cdot)$ defines the activation cost for each flexible load. In this generic definition of the reward, we allow both functions to depend on the auxiliary state variables so that it can model arbitrary processes. The function Φ aims at penalizing a policy that leads the system into an undesirable state (e.g. that violates the operational limits or induces many losses) and, together with C_g^{curt} and C_d^{flex}, it must be defined when instantiating the decision model. Note that equation (5.27) is such that the higher the operational costs and the larger the violations of operational limits, the more negative the reward function.

We can now define the *return over T periods*, denoted R_T, as the weighted sum of the rewards that are observed over a system trajectory of T periods

$$R_T = \sum_{t=0}^{T-1} \gamma^t r(\boldsymbol{s}_t, \boldsymbol{a}_t, \boldsymbol{s}_{t+1}), \tag{5.28}$$

where $\gamma \in]0;1[$ is the discount factor. Given that $\gamma^t < 1$ for $t > 0$, the further in time the transition from period $t = 0$, the less importance is given to the associated reward. Because the operation of a DN must always be ensured, it does not seem relevant to consider returns over a finite number of periods and we introduce the *return* R as

$$R = R_\infty = \lim_{T\to\infty} \sum_{t=0}^{T-1} \gamma^t r(\boldsymbol{s}_t, \boldsymbol{a}_t, \boldsymbol{s}_{t+1}), \tag{5.29}$$

that corresponds to the weighted sum of the rewards observed over an infinite trajectory of the system. Given that the costs have finite values, assuming the same for penalties, and observing that the reward function r is the sum of an infinite number of these costs and penalties, a constant C exists such that, $\forall(\boldsymbol{s}_t, \boldsymbol{a}_t, \boldsymbol{s}_{t+1}) \in \mathcal{S} \times \mathcal{A}_{\boldsymbol{s}} \times \mathcal{S}$, we have $|r(\boldsymbol{s}_t, \boldsymbol{a}_t, \boldsymbol{s}_{t+1})| < C$ and thus

$$|R| < \lim_{T\to\infty} C \sum_{t=0}^{T-1} \gamma^t = \frac{C}{1-\gamma}. \tag{5.30}$$

It means that even if the return R is defined as an infinite sum, it converges to a finite value. One can also observe that, because $\boldsymbol{s}_{t+1} = f(\boldsymbol{s}_t, \boldsymbol{a}_t, \boldsymbol{w}_t)$, a function $\rho : \mathcal{S} \times \mathcal{A} \times \mathcal{W} \to \mathbb{R}$ exists that aggregates functions f and r such that

$$\rho(\boldsymbol{s}_t, \boldsymbol{a}_t, \boldsymbol{w}_t) = r(\boldsymbol{s}_t, \boldsymbol{a}_t, f(\boldsymbol{s}_t, \boldsymbol{a}_t, \boldsymbol{w}_t)) = r(\boldsymbol{s}_t, \boldsymbol{a}_t, \boldsymbol{s}_{t+1})\,, \tag{5.31}$$

with $\boldsymbol{w}_t \sim p_{\mathcal{W}}(\cdot)$. Let $\pi : \mathcal{S} \to \mathcal{A}_{\boldsymbol{s}}$ be a policy that associates a control action to each state of the system. We can define, starting from an initial state $\boldsymbol{s}_0 = \boldsymbol{s}$, the expected return R of the policy π by

$$J^{\pi}(\boldsymbol{s}) = \lim_{T \to \infty} \mathop{\mathbb{E}}_{\substack{\boldsymbol{w}_t \sim p_{\mathcal{W}}(\cdot) \\ t=0,1,\ldots}} \{ \sum_{t=0}^{T-1} \gamma^t \rho(\boldsymbol{s}_t, \pi(\boldsymbol{s}_t), \boldsymbol{w}_t) | \boldsymbol{s}_0 = \boldsymbol{s} \}\,. \tag{5.32}$$

We denote by Π the space of all the policies π. For a DSO, addressing the operational planning problem described in Section 5.3 is equivalent to determine an optimal policy π^* among all the elements of Π, i.e. a policy that satisfies the following condition

$$J^{\pi^*}(\boldsymbol{s}) \geq J^{\pi}(\boldsymbol{s}), \forall \boldsymbol{s} \in \mathcal{S}, \forall \pi \in \Pi\,. \tag{5.33}$$

It is well known that such a policy satisfies the Bellman equation [70], which can be written

$$J^{\pi^*}(\boldsymbol{s}) = \max_{\boldsymbol{a} \in \mathcal{A}_{\boldsymbol{s}}} \mathop{\mathbb{E}}_{\boldsymbol{w} \sim p_{\mathcal{W}}(\cdot)} \left\{ \rho(\boldsymbol{s}, \boldsymbol{a}, \boldsymbol{w}) + \gamma J^{\pi^*}(f(\boldsymbol{s}, \boldsymbol{a}, \boldsymbol{w})) \right\}, \forall \boldsymbol{s} \in \mathcal{S}\,. \tag{5.34}$$

If we only take into account the space of stationary policies (i.e. that selects an action independently of time t), it is without loss of generality comparing to the space of policies $\Pi' : \mathcal{S} \times \mathcal{T} \to \mathcal{A}$ because the return to be maximized corresponds to an infinite trajectory of the system [71].

5.4 Lookahead optimization model

We now describe a look-ahead algorithm to build a policy based on stochastic programming. The principle is, at each time step $t \in \mathcal{T}$, to optimize a model $\mathcal{M}_t$ of the system over a finite time horizon $\mathcal{T}_t = \{t, ..., t + T - 1\}$ and to apply the control action $\hat{\boldsymbol{a}}_t^* = \hat{\pi}^*_{\mathcal{M}_t}(\boldsymbol{s}_t)$ that corresponds to the first stage of the

model. This approximate optimal policy $\hat{\pi}^*_{\mathcal{M}_t}$ can be formulated as

$$\hat{\pi}^*_{\mathcal{M}_t}(\boldsymbol{s}_t) = \arg\max_{\boldsymbol{a}_t} \max_{\substack{\boldsymbol{s}_{t'},\boldsymbol{a}_{t'} \\ \forall t' \in \mathcal{T}_t}} \mathbb{E}_{\boldsymbol{w}_{t'} \sim p_{\mathcal{W}}(\cdot)} \Big[\sum_{t'=t}^{t+T-1} \gamma^{t'-t} r(\boldsymbol{s}_{t'}, \boldsymbol{a}_{t'}, f(\boldsymbol{s}_{t'}, \boldsymbol{a}_{t'}, \boldsymbol{w}_{t'})) \Big] \quad (5.35)$$

$$\text{s.t.} \quad \boldsymbol{s}_{t'} = f(\boldsymbol{s}_{t'-1}, \boldsymbol{a}_{t'-1}, \boldsymbol{w}_{t'-1}) \,, \quad \forall t' \in \mathcal{T}_t \backslash \{t\} \quad (5.36)$$

$$\boldsymbol{a}_{t'} \in \mathcal{A}_{\boldsymbol{s}_{t'}} \,, \quad \forall t' \in \mathcal{T}_t \,, \quad (5.37)$$

where the shorter the horizon T, the higher the approximation error.

The finite lookahead time horizon is not the only source of approximation. First, there is no exact numerical method to solve (5.35)-(5.37) without requiring a discrete approximation of the continuous stochastic processes [17]. We detail in Section 5.4.2 how to build such a discrete approximation. Then, because of the nonlinearity of power-flow equations on the one hand, and the integer variables that model the activation of flexibility services on the other hand, the resulting mathematical problem is very complex to solve. For this reason, it is often required either to resort to local optimization techniques and heuristics, or to use relaxations and approximations of the power-flow equations. In particular, we describe in Section 5.4.5 several models of the electrical network of different complexity and accuracy.

5.4.1 Model instantiation

The decision model presented in Section 5.3.3 is generic on some of its elements. We now instantiate these elements to obtain a practical model that can be implemented to perform numerical simulations.

Auxiliary state variable We limit the vector $\boldsymbol{s}_t^{(\text{aux})}$ to a single auxiliary variable that indicates the time of the day:

$$\boldsymbol{s}_t^{(\text{aux})} = q_t \,, \quad (5.38)$$

which takes values in $\{0, \dots, 95\}$ to identify the quarter of an hour in the day. This information will be used as an input of the modulation price functions and of the transition function of both production and consumption processes. The relation that governs the evolution of q_t can be stated as a function $f_{aux} : \{0, \dots, 95\} \mapsto \{0, \dots, 95\}$, which is defined as:

$$q_{t+1} = f_{aux}(q_t) = (q_t + 1) \bmod 96 \quad . \quad (5.39)$$

Modulation prices For the sake of simplicity, we consider that the curtailment price functions C_g^{curt} depend exclusively on q_t. The time of the day being deterministic, these functions are deterministic too and correspond to arrays of 96 price values, which span a whole day. Concerning the activation costs C_d^{flex}, they are assumed to be constant on a per-load basis. The values of both the arrays and constants are specified in Section 5.5 when presenting the test instances.

Penalty function We choose to penalize a policy for violating operational limits and for the active losses in the network. This is implemented using the following function:

$$\begin{aligned}\Phi(\boldsymbol{s}_{t+1}) = k.\Big(&\sum_{n\in\mathcal{N}} [\max(0, |V_{n,t+1}| - \overline{V}_n) + \max(0, \underline{V}_n - |V_{n,t+1}|)] \\ &+ \sum_{(m,n)\in\mathcal{L}} \max(0, |I_{mn,t+1}| - \overline{I}_{mn}) \Big) \\ &+ C_{loss}(q_{t+1}) \sum_{n\in\mathcal{N}} \frac{P_{n,t+1}}{4}\,, \end{aligned} \tag{5.40}$$

where $|V_{n,t+1}|$ ($n \in \mathcal{N}$) and $I_{mn,t+1}$ ($(m,n) \in \mathcal{L}$) are determined from $\boldsymbol{s}_{t+1}$ using equations (5.23)-(5.26), and where $k \in \mathbb{R}_0^+$ is a typically large constant. The per-unit price $C_{loss}(q_{t+1})$ of losses is a deterministic function of the quarter of hour and corresponds to an array of 96 price values.

Production and consumption processes The instantiated versions of transition functions (5.12), (5.14), and (5.16), of the stochastic quantities (i.e. the consumption of the loads, the wind speed, and the level of solar irradiance) have the following structure:

$$x_{t+1} = f_x(x_t, \ldots, x_{t-N_x+1}, q_t, w_t^{(x)})\,, \tag{5.41}$$

$$= \mu_{x,t+1} + \sigma_{x,t+1} \cdot w_t^{(x)}\,, \tag{5.42}$$

$$\text{with } w_t^{(x)} \sim p_{\mathcal{W}^{(x)}}\left(\cdot \,|\, \frac{x_t - \mu_{x,t}}{\sigma_{x,t}}, \ldots, \frac{x_{t-N_x} - \mu_{x,t-N_x+1}}{\sigma_{x,t-N_x+1}} \right)\,, \tag{5.43}$$

where x denotes the considered process, and where $\mu_{x,t\pm\Delta t}$ and $\sigma_{x,t\pm\Delta t}$ are shortcuts for the following per-process functions:

$$\mu_{x,t\pm\Delta t} = \mu_x\Big((q_t \pm \Delta t) \bmod 96\Big)\,, \tag{5.44}$$

$$\sigma_{x,t\pm\Delta t} = \sigma_x\Big((q_t \pm \Delta t) \bmod 96\Big)\,. \tag{5.45}$$

These functions normalize the processes and remove their diurnal seasonality, and the conditional distribution of $w_t^{(x)}$ is then assumed to be stationary. The details of the conditional density functions are not required for the development of the lookahead optimization model, we specify in Section 5.5 a possible procedure to learn these functions from time series of measurements.

5.4.2 Discretization of the random process

The random process needs to be discretized over the look-ahead horizon to implement the policy with a computer program. A prevalent technique is to use a scenario tree [25] for this purpose. At each time step $t \in \mathcal{T}$, the evolution of the stochastic components is aggregated as a finite set $\tilde{\mathcal{W}}_t^T$ of outcome trajectories of the exogenous variables:

$$\tilde{\mathcal{W}}_t^T = \{(\boldsymbol{w}_t^{(k)}, \dots, \boldsymbol{w}_{t+T-1}^{(k)}) | k = 1, \dots, W\}, \tag{5.46}$$

and a probability $\mathbb{P}_k$ is associated to each trajectory $k \in \{1, \dots, W\}$. If two trajectories i and j share the same outcomes up to stage o, i.e. if $(\boldsymbol{w}_{t'}^{(i)}, \dots, \boldsymbol{w}_{t'+o}^{(i)}) = (\boldsymbol{w}_{t'}^{(j)}, \dots, \boldsymbol{w}_{t'+o}^{(j)})$, they can be interpreted as a single trajectory of probability $\mathbb{P}_i + \mathbb{P}_j$ up this stage. Fig. 5.7 provides an example of such a scenario tree, where the nodes represent the outcomes and the edges correspond to the transition probabilities.

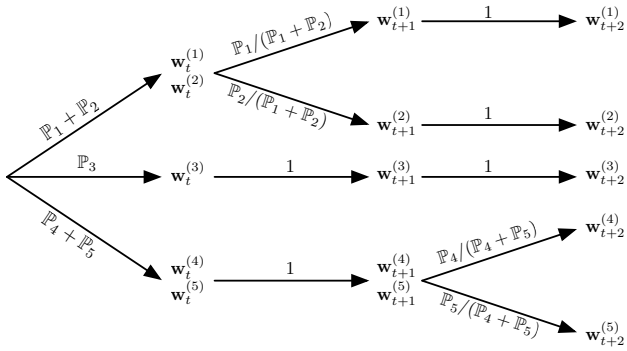

Figure 5.7: Example of scenario tree with $T = 3$ and $W = 5$.

5.4.3 Mathematical program

The purpose of the first term in the penalty function is to be an incentive to prevent the policy to bring the system in a state that violates operational limits. This definition allows to evaluate any kind of policy. In a mathematical programming setting, we remove this term from the objective function and add operational constraints defined in equations (5.1) and (5.2) to (5.35)-(5.37). The new objective function becomes:

$$\begin{aligned}\text{cost}(\boldsymbol{s}_t, \boldsymbol{a}_t, \boldsymbol{s}_{t+1}) = &\sum_{g\in\mathcal{G}} \max\{0, \frac{P_{g,t+1} - \overline{P}_{g,t+1}}{4}\} C_g^{curt}(q_{t+1}) + \sum_{d\in\mathcal{F}} act_{d,t} C_d^{flex} \\ &+ C_{loss}(q_{t+1}) \sum_{n\in\mathcal{N}} \frac{P_{n,t+1}}{4}\,. \end{aligned} \tag{5.47}$$

Taking into account the discretization of the stochastic processes, the objective function defined in equation (5.47), and the additional constraints, we can formulate a new approximate optimal policy $\hat{\pi}^*_{\hat{\mathcal{M}}_t}$ as

$$\hat{\pi}^*_{\hat{\mathcal{M}}_t}(\boldsymbol{s}_t) = \underset{\substack{\boldsymbol{a}_t \\ \boldsymbol{s}_t^{(k)},\ldots,\boldsymbol{s}_{t+T}^{(k)}, \\ \boldsymbol{a}_t^{(k)},\ldots,\boldsymbol{a}_{t+T-1}^{(k)}, \\ \forall k\in\{1,\ldots,\mathcal{W}\}}}{\arg\min} \sum_{k=1}^{W} \sum_{t'=t}^{t+T-1} \left[\mathbb{P}_k \gamma^{t'-t} \text{cost}(\boldsymbol{s}_{t'}^{(k)}, \boldsymbol{a}_{t'}^{(k)}, \boldsymbol{s}_{t'+1}^{(k)})\right] \tag{5.48}$$

$$\begin{aligned} \text{s.t.} \quad & \forall t' \in \mathcal{T}_t : \\ & \quad \forall i, j \text{ s.t. } (\boldsymbol{w}_t^{(i)},\ldots,\boldsymbol{w}_{t'}^{(i)}) = (\boldsymbol{w}_t^{(j)},\ldots,\boldsymbol{w}_{t'}^{(j)}) : \\ & \quad\quad \boldsymbol{a}_{t'}^{(i)} = \boldsymbol{a}_{t'}^{(j)}, && (5.49) \\ & \forall (k, t') \in \{1,\ldots,W\} \times \mathcal{T}_t : \\ & \quad \boldsymbol{s}_{t'+1}^{(k)} = f(\boldsymbol{s}_{t'}^{(k)}, \boldsymbol{a}_{t'}^{(k)}, \boldsymbol{w}_{t'}^{(k)})\,, && (5.50) \\ & \quad \boldsymbol{a}_{t'}^{(k)} \in \mathcal{A}_{\boldsymbol{s}_{t'}^{(k)}}\,, && (5.51) \\ & \forall (n, k, t') \in \mathcal{N} \times \{1,\ldots,W\} \times \mathcal{T}_t : \\ & \quad \underline{V}_{n,t'}^{(k)} \le |V_{n,t'}^{(k)}| \le \overline{V}_{n,t'}^{(k)}\,, && (5.52) \\ & \forall (m, n, k, t') \in \mathcal{L} \times \{1,\ldots,W\} \times \mathcal{T}_t : \\ & \quad |I_{mn,t}| \le \overline{I}_{mn}\,, && (5.53) \end{aligned}$$

where (5.50) stands for equations (5.12)-(5.26), and (5.51) for equation (5.10). The model takes into account that decisions at stage $t' \in \mathcal{T}_t$ only depend on exogenous information up to stage t', i.e. that future unknown data is not used, which is why we integrate the nonanticipativity constraints [17] to the

mathematical program using equation (5.49). Problem (5.48)-(5.53) is a mixed-integer program (MIP). For a given distribution system, its complexity depends mainly on the network model chosen to represent power-flow equations (cf. Section 5.4.5), and on the number of scenarios representing the uncertainty.

5.4.4 Detailed model of control actions

Implementing the model of control actions of Section 5.3.3.2 in a mathematical program is not straightforward. We now present how it can be implemented in problem (5.48)-(5.53).

5.4.4.1 Generation curtailment

This section focuses on the curtailment decision model. To ease the reading, we focus on one particular generator and thus omit subscript g. Note first that the active power injection term of equation (5.23) that follows a curtailment instruction $\overline{p}_t \geq 0$ from stage t, i.e. $\min(\overline{P}_{t+1}; P_{t+1})$, is translated in the mathematical program by

$$\min(\overline{P}_{t+1}; P_{t+1}) = P_{t+1} - p_{curt,t+1}\,, \tag{5.54}$$

where $p_{curt,t+1} \geq 0$ is the amount of active power curtailment induced by the power limit instruction. This quantity is easy to determine in a deterministic setting:

$$\overline{P}_{t+1} = \overline{p}_t\,, \tag{5.55}$$

$$p_{curt,t+1} = P_{t+1} - \overline{P}_{t+1}\,, \tag{5.56}$$

where P_{t+1} is the potential active production level at time step $t+1$.

Considering several scenarios leads to a less obvious definition of the amount of curtailment. Let $\overline{p}_t$ denote the curtailment instruction that, at time t, is shared by all scenarios $j \in \{1, \ldots, W\}$ such that $(\ldots, \boldsymbol{w}_{t-1}^{(k)}, \boldsymbol{w}_t^{(k)}) = (\ldots, \boldsymbol{w}_{t-1}^{(j)}, \boldsymbol{w}_t^{(j)})$. For one generator, the maximum power allowed and the curtailed power are

defined by the following set of constraints for each scenario k:

$$\overline{P}_{t+1}^{(k)} = \overline{p}_t \,, \tag{5.57}$$

$$\Delta p_{t+1}^{(k)} = P_{t+1}^{(k)} - \overline{P}_{t+1}^{(k)} \,, \tag{5.58}$$

$$p_{curt,t+1}^{(k)} = \max(0, \Delta p_{t+1}^{(k)}) \,, \tag{5.59}$$

where $P_{t+1}^{(k)}$ is the potential active production level in scenario k, and $\Delta p_{t+1}^{(k)}$ is an auxiliary variable that has no physical meaning, since it can be negative when $\overline{p}_t$ is not restrictive for scenario k (i.e. when $\overline{p}_t \geq P_{t+1}^{(k)}$). The variable $p_{curt,t+1}^{(k)}$ would be the power curtailed if scenario k realizes. It contributes linearly to the value of the objective function, proportional to the curtailment cost and weighted by the probability of scenario k. A common relaxation of the max operator of constraint (5.59) for a variable that tends to be minimized is

$$p_{curt,t+1}^{(k)} \geq \Delta p_{t+1}^{(k)} \,. \tag{5.60}$$

However, this holds only if constraint (5.60) is always tight, which is not always true in problem (5.48)-(5.53). Without preventing $p_{curt,t+1}^{(k)}$ to be greater than $\Delta p_{t+1}^{(k)}$, it would allow to discriminate the curtailment decisions between different scenarios even though the nonanticipativity constraint (5.49) is respected. Indeed, the amount of power curtailed could be increased beyond $P_{t+1}^{(k)} - \overline{P}_{t+1}^{(k)}$ and it would differ from the set point $\overline{p}_t$, which is guaranteeing nonanticipativity by being common for all subsequent scenarios.

From this analysis, we conclude that a continuous implementation of equation (5.59) is not possible and we model it using equation (5.60) and the following additional constraints:

$$p_{curt,t+1}^{(k)} \leq \Delta p_{t+1}^{(k)} - y^{(k)} \underline{\Delta P}_{t+1}^{(k)} \,, \tag{5.61}$$

$$p_{curt,t+1}^{(k)} \leq (1 - y_{t+1}^{(k)}) \, \overline{\Delta P}_{t+1}^{(k)} \,, \tag{5.62}$$

$$y_{t+1}^{(k)} \in \{0, 1\} \,, \tag{5.63}$$

where $\overline{\Delta P}_{t+1}^{(k)}$ and $\underline{\Delta P}_{t+1}^{(k)}$ are parameters that indicate the maximal and minimal values that $\Delta p_{t+1}^{(k)}$ can take, respectively. It corresponds to a *big M* formulation [72] and can be interpreted as follow:

- if $\Delta p_{t+1}^{(k)} < 0$, constraint (5.61) is satisfied only if $y_{t+1}^{(k)} = 1$, and constraint (5.62) then forces $p_{curt,t+1}^{(k)} = 0$;
- if $\Delta p_{t+1}^{(k)} \geq 0$, constraints (5.60) and (5.61) can be satisfied simultaneously only if $y_{t+1}^{(k)} = 0$.

Parameters $\underline{\Delta P}_{t+1}^{(k)}$ and $\overline{\Delta P}_{t+1}^{(k)}$ should be chosen such that the continuous relaxation is as tight as possible. For instance for a wind turbine $\overline{\Delta P}_{t+1}^{(k)} = P_{t+1}^{(k)}$ and $\underline{\Delta P}_{t+1}^{(k)} = P_{t+1}^{(k)} - \max_j P_{t+1}^{(j)}$.

Finally, the curtailment instruction $\overline{p}_{g,t}$ are recovered from the solution of $\hat{\mathcal{M}}_t$ upon the following processing of the solution:

$$\forall g \in \mathcal{G} : \overline{p}_{g,t} \leftarrow \begin{cases} \overline{p}_{g,t} & \text{if } \exists k \in \{1, ..., W\} \text{ s.t. } \overline{p}_{g,t} < P_{g,t+1}^{(k)}\,, \\ +\infty & \text{otherwise}\,, \end{cases} \tag{5.64}$$

This processing is introduced because, in $\hat{\mathcal{M}}_t$, the value of $\overline{p}_{g,t}$ has no meaning when it does not induce an actual curtailment for at least one scenario. Therefore, it makes no sense to interpret these variables as curtailment instructions and equation (5.64) makes sure that curtailment actions sent to the system actually corresponds to curtailment decisions in the optimization model.

5.4.4.2 Activation of flexibility services

This section details how the control actions $act_{d,t}$ defined in Section 5.3.3.2 are computed. To ease the reading, we focus on one particular device and thus omit subscript d in this section. The superscript (k) is also dropped and the following equations simply needs to be repeated for each scenario of the lookahead model, with equation (5.49) guaranteeing the nonanticipativity of the model. We first define several auxiliary variables:

- $z_t \in \{0, 1\}$ is a binary variable used to model the max operator for state transitions;
- $m_t \in \mathbb{Z}_+$ is a integer variable used for state transitions.

Ignoring the activation signal, the transition rule of the flexible state, i.e.

$$m_{t+1} = \max(0, flex_t - 1)\,,$$

is implemented through the following *big M* formulation:

$$m_{t+1} \leq flex_t - 1 + z_t \tag{5.65}$$
$$m_{t+1} \leq T\,(1 - z_t) \tag{5.66}$$
$$m_{t+1} \geq flex_t - 1\,. \tag{5.67}$$

The influence of the activation signal is then incorporated to the flexible state:

$$flex_{t+1} = m_{t+1} + act_t T\,, \tag{5.68}$$

while the following constraint prevents a double activation of a flexibility service:

$$a_t + \frac{flex_t}{T} \leq 1\,. \tag{5.69}$$

Finally, the value of the effective modulation signal, defined in equation (5.22), is implemented as:

$$\Delta P_t = \sum_{t':t-t'\leq T} a_{t-t'} \Delta P(t-t')\,, \tag{5.70}$$

where $\Delta P(\,\cdot\,)$ is the modulation curve of the load, which produces parameters for the mathematical program.

5.4.5 Detailed network models

We detail how the network model described in Section 5.3.1 is precisely instantiated in the AC non-convex case, then we describe a linearization approach and finally a second order cone program (SOCP) model. To ease reading we consider only one time step and omit the subscripts t and the scenario notation, but in reality these equations are replicated for each time step or node of the scenario tree. In this section, we define

$$g_{mn} + jb_{mn} = Y_{mn}^{(br)}$$

and

$$g_m^{(sh)} + jb_m^{(sh)} = \sum_{n:(m,n)\in\mathcal{L}} Y_{mn}^{(sh)}.$$

We also consider arbitrarily that node 1 is a slack bus which sets a reference phase angle of 0 and a fixed voltage magnitude.

5.4.5.1 Non-convex AC model

We chose to express relations (5.6) in rectangular coordinates. Hence we define variables

- e_n as the real part of V_n
- f_n as the imaginary part of V_n
- P_{mn} as the active power leaving bus m and flowing in link (m,n)
- Q_{mn} as the reactive power leaving bus m and flowing in link (m,n)
- P_n^{shunt} as the active power shunted at bus n
- Q_n^{shunt} as the reactive power shunted at bus n.

The above powers are defined as

$$\begin{aligned}
&\forall (m,n) \in \mathcal{L}: \\
&\quad P_{mn} = e_m \left(g_{mn}(e_m - e_n) - b_{mn}(f_m - f_n)\right) \\
&\qquad\quad + f_m \left(b_{mn}(e_m - e_n) + g_{mn}(f_m - f_n)\right), \qquad (5.71)\\
&\quad Q_{mn} = f_m \left(g_{mn}(e_m - e_n) - b_{mn}(f_m - f_n)\right) \\
&\qquad\quad - e_m \left(b_{mn}(e_m - e_n) + g_{mn}(f_m - f_n)\right), \qquad (5.72)\\
&\quad \forall n \in \mathcal{N}: \\
&P_n^{shunt} = g_n^{(sh)}(e_n^2 + f_n^2), \qquad (5.73)\\
&Q_n^{shunt} = b_n^{(sh)}(e_n^2 + f_n^2). \qquad (5.74)
\end{aligned}$$

Then the voltage operational limits are defined for every node n as

$$\underline{V_n}^2 \leq e_n^2 + f_n^2 \leq \overline{V_n}^2, \quad \forall n \in \mathcal{N}, \qquad (5.75)$$

and the thermal limits by

$$I_{mn}^2 \leq \overline{I}_{mn}^2, \quad \forall (m,n) \in \mathcal{L}, \qquad (5.76)$$

with

$$\begin{aligned}
I_{mn}^2 &= I_{real}^2 + I_{imag}^2, \qquad (5.77)\\
I_{real} &= g_{mn}(e_m - e_n) - b_{mn}(f_m - f_n), \qquad (5.78)\\
I_{imag} &= b_{mn}(e_m - e_n) + g_{mn}(f_m - f_n). \qquad (5.79)
\end{aligned}$$

5.4.5.2 Linearized model

This model proposed in [63] approximates linearly (5.71) and (5.72). Note that this approximation does not include the shunt powers, i.e. $P_n^{shunt} = Q_n^{shunt} = 0$,

$\forall n \in \mathcal{N}$. This yields

$$P_{mn} = g_{mn}(e_m - e_n) - b_{mn}(f_m - f_n), \quad \forall (m,n) \in \mathcal{L} \tag{5.80}$$
$$Q_{mn} = -b_{mn}(e_m - e_n) - g_{mn}(f_m - f_n), \quad \forall (m,n) \in \mathcal{L}. \tag{5.81}$$

The upper voltage limits and the thermal limits are approximated by a regular polyhedron inscribed in the respective circles of the original limits. The lower voltage operational limit is simply modeled as a lower bound on e_n, which means that we make the hypothesis that the angles are small. An iterative method could be set up if the approximated solutions are far from feasible solutions of the AC model. However, this turned out to be unnecessary as the decisions taken are most of the time very coherent with those obtained with other models, as illustrated in Section 5.5. This formulation does not account for losses.

5.4.5.3 Convex SOCP model

By introducing variables $u_n \geq 0$, $R_{mn} \geq 0$ and $T_{mn} \in \mathbb{R}$ that substitute the expressions

$$\frac{e_n^2 + f_n^2}{\sqrt{2}}, \quad e_m e_n + f_m f_n, \quad f_m e_n - e_m f_n,$$

respectively, constraints (5.71)-(5.74) can be rewritten without e and f as

$$P_{mn} = g_{mn}\sqrt{2}u_m - g_{mn}R_{mn} - b_{mn}T_{mn}, \quad \forall (m,n) \in \mathcal{L} \tag{5.82}$$
$$Q_{mn} = -b_{mn}\sqrt{2}u_m + b_{mn}R_{mn} - g_{mn}T_{mn}, \quad \forall (m,n) \in \mathcal{L} \tag{5.83}$$
$$P_n^{shunt} = g_n^{(sh)}\sqrt{2}u_n, \quad \forall n \in \mathcal{N} \tag{5.84}$$
$$Q_n^{shunt} = b_n^{(sh)}\sqrt{2}u_n, \quad \forall n \in \mathcal{N}. \tag{5.85}$$

The additional set of constraints

$$2u_m u_n = R_{mn}^2 + T_{mn}^2, \quad \forall (m,n) \in \mathcal{L} \tag{5.86}$$

are imposed to maintain a relationship between the newly introduced variables. They are then relaxed to obtain a convex second order cone program:

$$2u_m u_n \geq R_{mn}^2 + T_{mn}^2, \quad \forall (m,n) \in \mathcal{L}. \tag{5.87}$$

Voltage limits can be easily rewritten as a function of u_n as

$$\underline{V_n}^2 \leq \sqrt{2}u_n \leq \overline{V_n}^2, \quad \forall n \in \mathcal{N}. \tag{5.88}$$

Thermal limits are approximated in the same way as for the non-convex AC model. Note that as $R_{mn} = R_{nm}$ and $T_{mn} = -T_{nm}$, they are in practice replaced by a single variable per branch and constraints (5.82) and (5.83) are updated accordingly. It is shown in [62] that this relaxation is tight for radial networks under some conditions on the objective function. These conditions are not met in our formulation since minimizing curtailment is equivalent to maximizing the renewable generation. To mitigate this issue, the losses term in the objective function must be scaled with a coefficient sufficiently large so that (5.87) are tight, but not too large so that the original objective function is still guiding the solution. This tradeoff is further discussed in Section 5.5.

5.5 Test instances

We describe below the three test instances of the ANM problem that are used in the results section. The set of models and parameters that are specific to these instances, as well as documentation for their usage, are accessible at `http://www.montefiore.ulg.ac.be/~anm/` as Python code. It has been developed to provide a black-box-type simulator that is quick to set up. The DNs on which these instances are based are a toy 5-bus radial test system, a 33-bus non-radial test system [73], and a 77-bus radial test system [74]. Table 5.1 summarizes some relevant data about these instances. The test systems are also illustrated in Figures 5.8, 5.9, and 5.10. The location of the wind generators, which we assume to be curtailable, is indicated by a circled W. The 77-bus instance also includes non-curtailable generators that model residential photovoltaic panels.

case	**case5**			**case33**			**case77**		
flex level	low	medium	high	low	medium	high	low	medium	high
$\lvert\mathcal{N}\rvert$			5			33			77
$\lvert\mathcal{L}\rvert$			4			37			76
$\lvert\mathcal{G}\rvert$			1			4	6 curtailable (out of 59)		
$\lvert\mathcal{C}\rvert$			3			32			53
$\lvert\mathcal{F}\rvert$	1	2	3	11	22	32	11	22	33
max flex (MW)	0.3	0.6	0.9	0.62	1.3	2	1.71	3.41	5.01
∼peak load (MW)			11			9			18
$\mathcal{O}_g$, $\forall g \in$ *wind turbines*	$0 \le P_g \le 20$ $-5 \le Q_g \le 5$ $Q_g \le -0.24P_g + 6.8$ $Q_g \le 0.24P_g - 6.8$			$0 \le P_g \le 4.5$ $-1 \le Q_g \le 1$ $Q_g \le -0.2P_g + 1.3$ $Q_g \le 0.2P_g - 1.3$			$0 \le P_g \le 4.5$ $-1 \le Q_g \le 1$ $Q_g \le -0.2P_g + 1.3$ $Q_g \le 0.2P_g - 1.3$		

Table 5.1: Summary of test instances.

We consider that the per-unit curtailment prices are the same for all the generators. As described in Section 5.4.1, this price varies through the day and

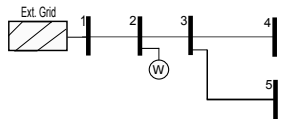

Figure 5.8: 5-bus test system.

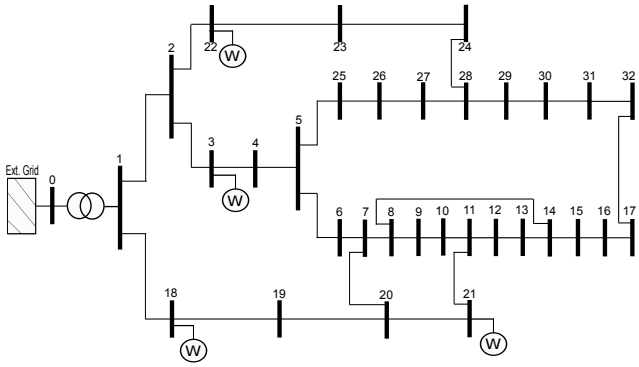

Figure 5.9: 33-bus test system.

Figure 5.11 specifies the values considered in the test instances. We also use these values for the per-unit cost of the losses, i.e. $C_{loss}(\cdot)$, while the constant k that appear in equation (5.40) is set to 10^4. Concerning flexible loads, three different penetration levels exist for each test case. For every configuration, about half of the flexible services offer a downward modulation, followed by an upward rebound effect, and inversely for the other half. The maximal and cumulated modulation magnitude is reported in Table 5.1 to illustrate the

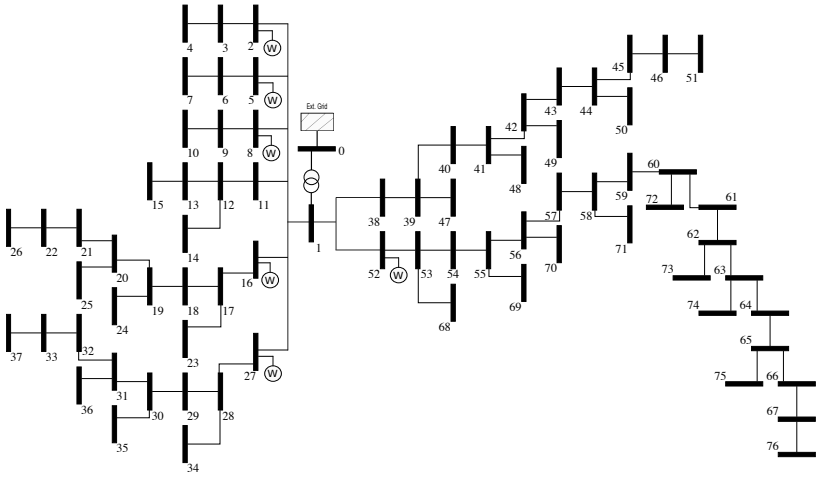

Figure 5.10: 77-bus test system.

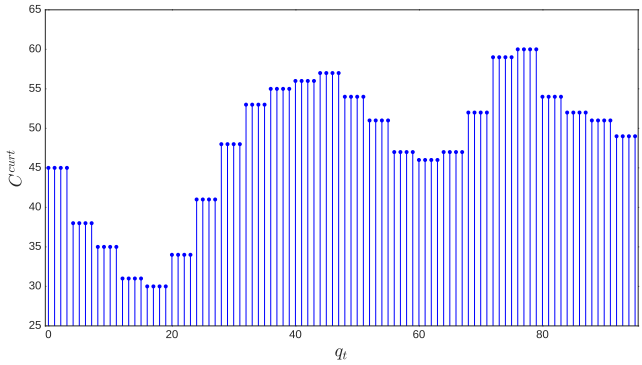

Figure 5.11: Curtailment prices used in the test instance.

potential offered by flexible loads in every configuration. Finally, the duration of the modulation signals is of 7 time periods for the 5-bus instances, and from 6 to 24 time periods for the 33 and 77-bus instances.

The conditional density functions defined in equation (5.43) are built using a parametric model $\mathcal{P}_{(N,n)}$ that relies on a mixture of n Gaussians to represent the probability distribution $p(w_{t+1}|w_t, \ldots, w_{t-N+1})$ of the next outcome of the process, conditionally to the last N observed outcomes. In particular, the following procedure allows to fit a model $\mathcal{P}_{(N,n)}$ to a set $\{(w_1^{(i)}, w_2^{(i)}, \ldots, w_L^{(i)}), i = 1, \ldots, I\}$ of time series of normalized realizations of the process of interest:

1. build a dataset of tuples $(w_{t-N+1}^{(i)}, \ldots, w_t^{(i)}, w_{t+1}^{(i)}), \forall (i,t) \in \{1, \ldots, I\} \times \{N, \ldots, L-1\}$;

2. model the joint distribution $p(w_{t-N+1}, \ldots, w_{t+1})$ of the dataset using a mixture of n Gaussians, by performing a maximum likelihood estimation [59] of the mixture's parameters (i.e. the weight η_i, mean $\boldsymbol{\mu}_i$, and covariance matrix $\boldsymbol{\Sigma}_i$ of every Gaussian $i \in \{1, \ldots, n\}$);

3. $\forall i \in \{1, \ldots, n\}$, deduce from $\boldsymbol{\mu}_i$ and $\boldsymbol{\Sigma}_i$ the functions $\mu_i^{\cdot|\cdot}(w_{t-N+1}, \ldots, w_t)$ and $\sigma_i^{\cdot|\cdot}(w_{t-N+1}, \ldots, w_t)$ that define the mean and standard deviation of w_{t+1}, according to the i$^{\text{th}}$ Gaussian in the mixture and conditional to $w_{t-N+1}, \ldots, w_t$ [58];

4. produce $p(\cdot|w_t, \ldots, w_{t-N+1})$ as the following mixture of conditional

Table 5.2: Parameters of the stochastic models used in the implementation of the benchmark.

	N	n
Wind speed (N_v)	1	1
Solar irradiance (N_{ir})	1	10
Load consumption (N_{loads})	2	10

Gaussian distributions:

$$p(\cdot\,|w_t,\ldots,w_{t-N+1}) = \sum_{i=1}^{n} \eta_i \mathcal{N}\Big(\mu_i^{\cdot\,|\,\cdot}(w_{t-N+1},\ldots,w_t), \sigma_i^{\cdot\,|\,\cdot}(w_{t-N+1},\ldots,w_t)\Big). \quad (5.89)$$

In order to determine an adequate value of the model's hyper-parameters n and N for each process, we relied on an Approximate Bayesian Computation (ABC) method [75]. Such an approach consists in sampling trajectories from each model and to compare them with the original data to estimate its posterior probability among the set Θ of candidate models [76]. Using $\Theta = \{\mathcal{P}_{(N,m)}|_{n\in\{1,\ldots,20\},N\in\{1,\ldots,3\}}\}$, the most likely parameters identified by this model choice technique are presented in Table 5.2. We refer the interested reader to [77] for more details on the modeling approach.

The datasets that we used are real measurements of the wind speed[i] and of the solar irradiance[ii]. For the residential consumption data, a single stochastic model has been learned from measurements of a Belgian distribution network and it is used for all the loads of the test instance. However, this model differs among the loads through the use of a scaling factor. The implementation of the statistical algorithms relies on both SciPy [78] and Scikit-learn [60], two Python libraries.

5.6 Numerical results

The goals of this section are to illustrate the operational planning problem and the test instances, as well as to provide some empirical evaluations of the proposed lookahead policy for the considered network models and for scenario trees of varying complexity. In particular, the policy $\hat{\pi}^*_{\hat{\mathcal{M}}_t}(\boldsymbol{s}_t)$ defined

[i] http://www.nrel.gov/electricity/transmission/eastern_wind_dataset.html
[ii] http://solargis.info/

by problem (5.48)-(5.53) was applied to every test instance and penetration level of the flexible loads. The empirical expected return of the policy, for a given test instance, level of flexibility, network model, and scenario tree complexity, is determined from 50 runs of 288 time steps (i.e. of 3 days), each run i corresponding to the following sequence:

1. Initialize the state vector $\boldsymbol{s}_0$ by setting all the flexible loads as inactive and by sampling stochastic components from the joint distributions learned when building the test instance.

2. Run a simulation of 288 time steps, where, at every time step, problem (5.48)-(5.53) is implemented as follow:

   a) sample 100 trajectories of the exogenous variables over a lookahead horizon of length $T = 10$, i.e. trajectories $(\boldsymbol{w}_t^{(j)}, \ldots, \boldsymbol{w}_{t+9}^{(j)})$, with $j = 1, \ldots, 100$;

   b) determine the corresponding trajectories of the potential (i.e. not accounting for modulation instructions) power injections of the devices, as they are fully determined by the current state $\boldsymbol{s}_t$ and by $(\boldsymbol{w}_t^{(j)}, \ldots, \boldsymbol{w}_{t+9}^{(j)})$;

   c) cluster the 100 trajectories of power injections into W scenarios, using a hierarchical clustering method and Ward's distance [79];

   d) build the corresponding clusters of outcome trajectories, i.e.

   $$\tilde{\mathcal{W}}_t^T = \{(\tilde{\boldsymbol{w}}_t^{(k)}, \ldots, \tilde{\boldsymbol{w}}_{t+9}^{(k)}) | k = 1, \ldots, W\},$$

   where $\tilde{\boldsymbol{w}}_{t'}^{(k)}$ denotes the centroid of cluster k at time $t' \in \{t, \ldots, t+9\}$, and compute the probabilities $\mathbb{P}_k$ of the resulting scenarios as

   $$\mathbb{P}_k = \frac{\text{number of trajectories in cluster } k}{100};$$

   e) solve problem $\hat{\mathcal{M}}_t$ with a discount factor $\gamma = 0.99$ and over the scenario tree defined by outcomes of $\tilde{\mathcal{W}}_t^T$ and probabilities $(\mathbb{P}_1, \ldots, \mathbb{P}_W)$;

   f) recover the action vector $\boldsymbol{a}_t$ to apply to the system.

The motivation behind the use of Ward's method to cluster trajectories is that it is a minimum variance method, which means that the trajectories of a cluster were selected because they are close to its centroid, in comparison to trajectories of other clusters. Consequently, the scenarios used in the optimization model, which are the centroids of the clusters, differ minimally from the trajectories it summarizes.

The implementation has been done using the Python code mentioned in Section 5.5 to simulate the system and Pyomo [80] to build the mathematical programs. These programs were solved by BONMIN [81] in the MINLP case, and by Gurobi in the MISOCP and MILP cases. At each time step, a budget of 10 minutes is allowed to solve the mathematical program. If the solver reaches the time limit, the current best solution is applied to the system if a feasible solution is available, or the whole simulation run fails if no solution was found. Both solvers stop before the time limit if they reach a relative optimality gap of 1%. Note that BONMIN performs local optimization and must be seen as an heuristic method to solve the non-convex MINLPs, as it comes with no optimality guarantees. In the MISOCP case, the scaling factor of the losses discussed in Section 5.4.5.3 was fixed empirically to 3. For every combination of test instance, level of flexibility, and network model, the same runs were performed with a scenario tree $\tilde{\mathcal{W}}_t^T$ of one scenario (i.e. the mean of the sampled trajectories) and of three scenarios. A version of the problem with perfect information, i.e. with a scenario tree consisting of the actual future trajectory of the exogenous information, was also simulated to obtain a reference value of performance. The overall simulation was carried on in a high-performance computing environment with 128 cores. Each run being limited to a single core, such an infrastructure enabled hundreds of simulations to run in parallel and thus to speed up computations by the same factor. Ignoring failed simulation runs, more than 1 million of mathematical programs were solved for a cumulated time budget of approximately 1122 days.

The empirical estimations of the expected return reported in the following results are computed as:

$$\mathop{\mathbb{E}}_{\boldsymbol{s}\sim p_0(\,\cdot\,)}\left\{J^{\hat{\pi}^*}(\boldsymbol{s})\right\} \approx \frac{1}{50}\sum_{i=1}^{50}\sum_{t=0}^{287} 0.99^t r_t^{(i)}\,, \tag{5.90}$$

where $r_t^{(i)}$ corresponds to the instantaneous reward observed during the n^{th} simulation run at time step t, and where $p_0(\,\cdot\,)$ denotes the probability distribution described at step (1). Tables 5.3, 5.4, and 5.5, summarize the results of the simulation runs for the 5-bus, 33-bus, and 77-bus test systems, respectively. The first columns identifies the test instance configuration and the two latter columns report the expected return and the distribution of solution time. The blue and red bars denote the contributions to the expected return of the expected costs (including losses) and of the penalties from constraint violations, respectively. The box plots' whiskers cover the whole range of the observed solution times and the red makers indicate the median time.

We can first observe from the simulation results of the 5-bus test system that having a perfect forecast of the evolution of the system yields significantly

better returns than when decisions are subject to uncertainty. It also shows that considering three possible future scenarios can significantly improve over an optimization performed on the average future scenario, to the expense of the solution time. Among the three network models, the SOCP relaxation is the one that induces the most penalties. These penalties also appear in the deterministic case, which implies that the relaxation is not always tight. We also observe that the policy slightly benefits from an increase of the flexibility level of loads in the deterministic setting but not in the presence of uncertainty. Given the small size of the 5-bus test system, the solution times are very good for every configuration with the exception of the MINLPs, for which worst-case solution time already reaches the time limit for all lookahead models.

The results for the 33-bus test system are quite similar, with the notable exception of the solution times. Both the SOCP and LP network models still produce mathematical programs that can be solved within a reasonable time budget. On the other hand, the time limit is very often reached when solving the MINLPs[iii]. The simulation runs even failed in the two most complex configurations as the solver could not find any feasible solution within the time limit. This observation can be extended to the simulation results of the 77-bus test system, with the difference that, in the 1-scenario configurations, the mean and median solution times are lower while the worst-case time is even larger. None of the 3-scenario runs succeeded for the NLP network model and even the SOCP model produces significantly increased solution times, with worst cases reaching the time limit.

Finally, a part of a 5-bus and low-flexibility simulation run is illustrated in Figures 5.12, 5.13, and 5.14, with a 3-scenarios lookahead model and a NLP, SOCP, and linear network model, respectively. The dashed lines in the upper-left subplots represent the estimated production in the 3 scenarios of the lookahead model at time step 101 (i.e. when computing decisions for time step 102 and onwards). The bottom-right subplots represent the generator's P-Q operating points for the whole simulation and the red point corresponds to time step 102. Notable differences can be observed among the network models. At time step 102, both the NLP and LP approaches show a violation of a thermal constraint because of an inadequate scenario tree, but the SOCP model is, on the contrary, quite conservative. This behavior is likely due to the scaling of the losses term in this latter model, as suggested by its chart of P-Q set-points. The policy did not explicitly computed a curtailment of active power but chose an aggressive Q set-point, which led to a power curtailment due to the P-Q capabilities of the generator. This phenomenon is observed several times in the reported simulation, in particular at and prior to time step 102. The NLP

[iii] Reported solution time can be larger than the time limit. It happens when the solver is executing a complex routine for some amount time before being able to check the limit.

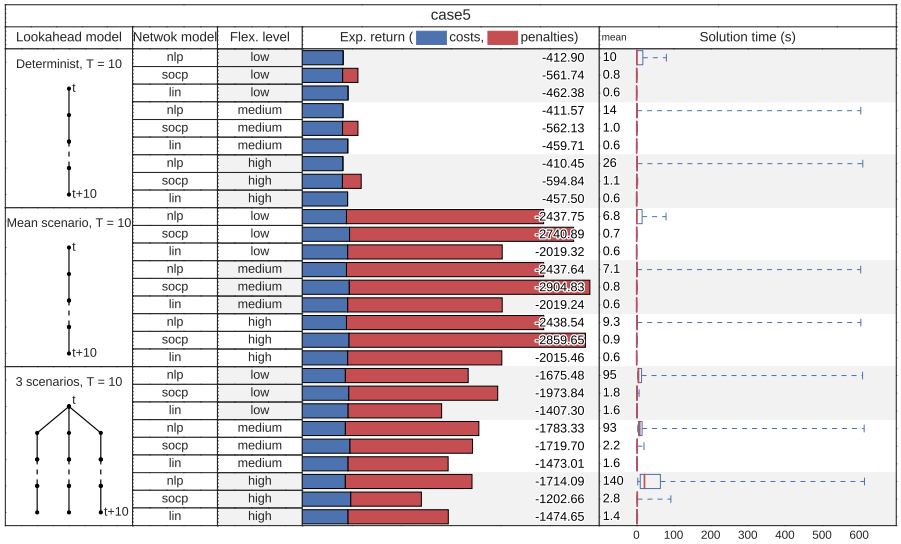

Table 5.3: Estimation of expected return and distribution of solver time for the 5-bus test system.

and LP models show a similar curtailment pattern, with the latter inducing more curtailment and an over-satisfaction of the thermal limit. We suspect the cause to be the non-inclusion of the losses in the LP model, which may also explain why this approach activates more flexible services than the two other approaches. Another consequence of not accounting for the losses is that the policy makes little use of the generator's reactive capabilities, as shown by the lower-right subplot of Figure 5.14. In accordance with results of Tables 5.3, 5.4, and 5.5, the SOCP network model is not always tight and, around time step 110, shows constraint violations in the lower-left subplot of Figure 5.13, while the two other network models keep the system within the operational limits.

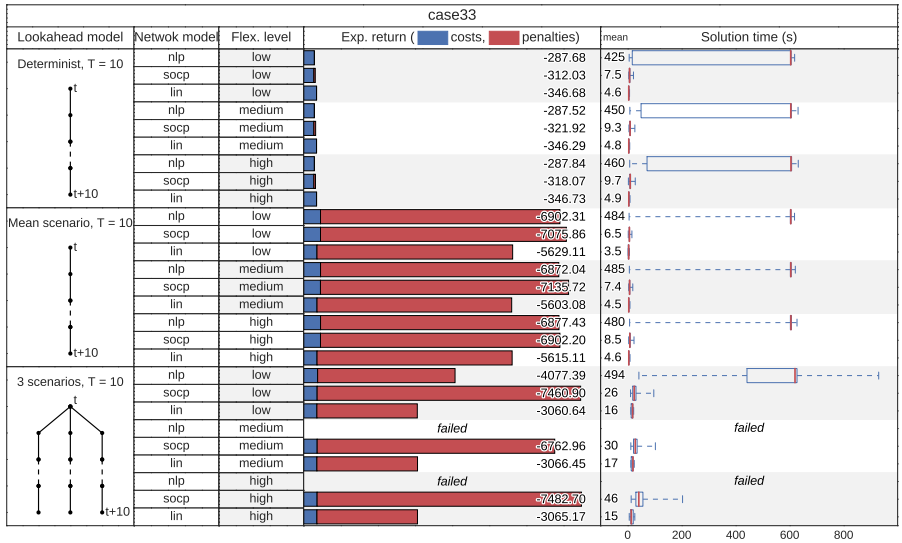

Table 5.4: Estimation of expected return and distribution of solver time for the 33-bus test system.

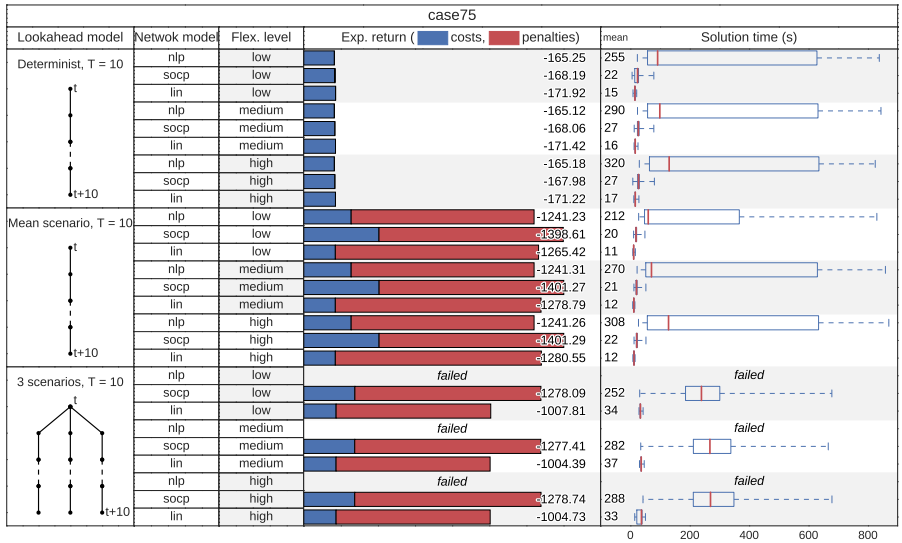

Table 5.5: Estimation of expected return and distribution of solver time for the 77-bus test system.

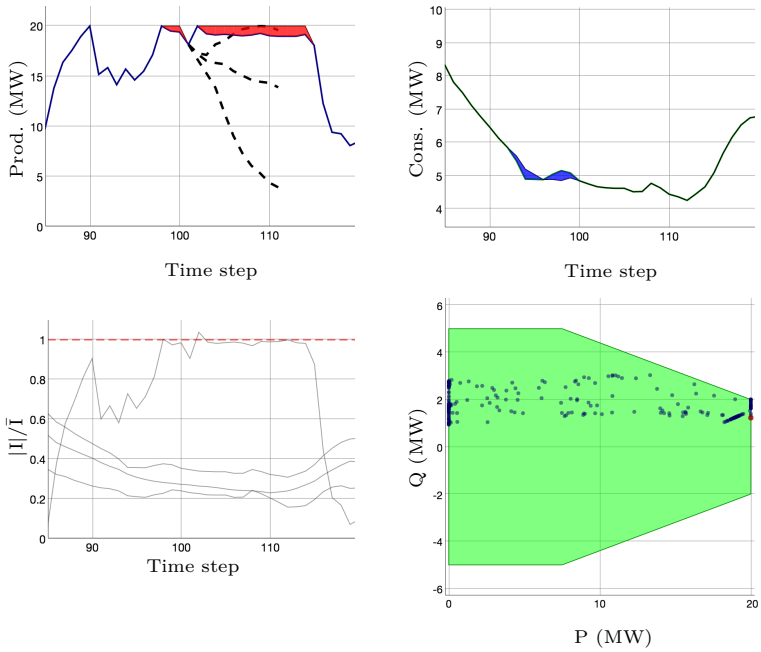

Figure 5.12: Illustrations of part of a 5-bus and low-flexibility simulation run, with a 3-scenarios lookahead model and a NLP network model.

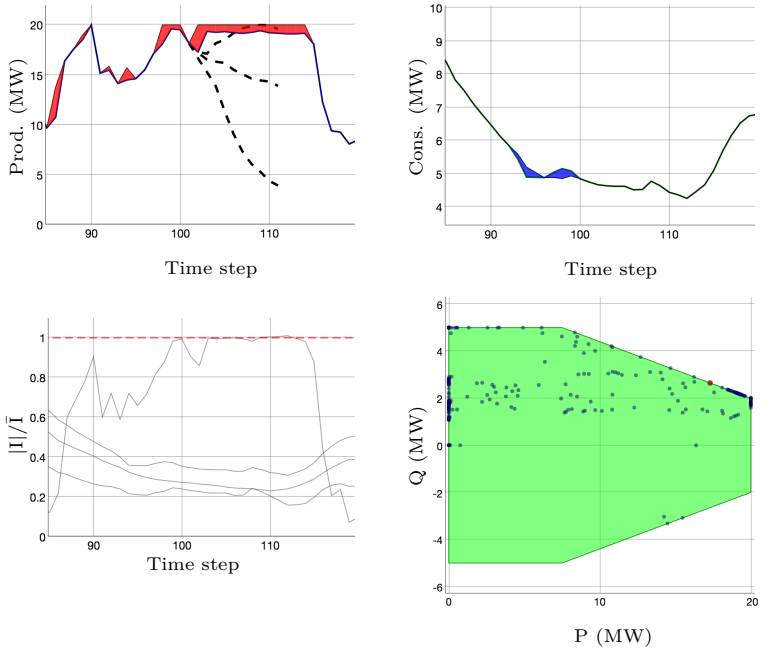

Figure 5.13: Illustrations of part of a 5-bus and low-flexibility simulation run, with a 3-scenarios lookahead model and a SOCP network model.

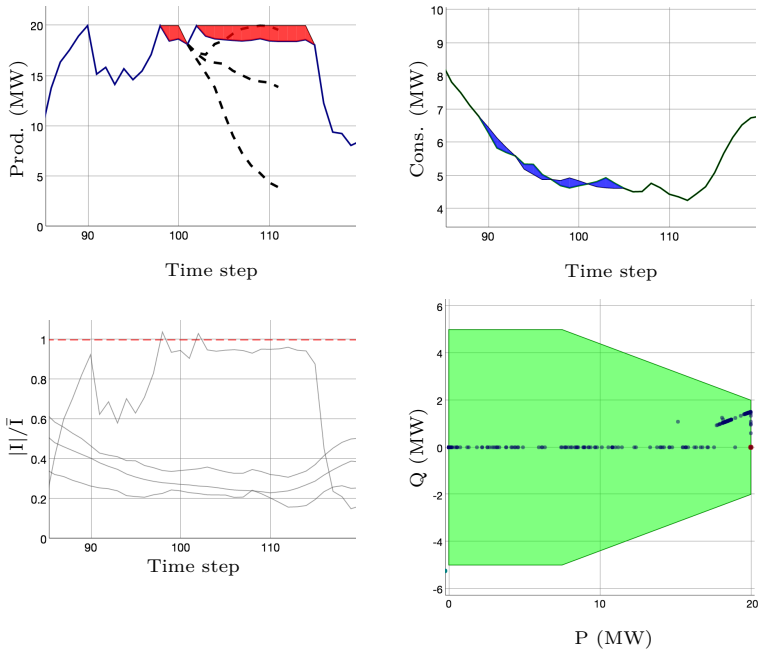

Figure 5.14: Illustrations of part of a 5-bus and low-flexibility simulation run, with a 3-scenarios lookahead model and a linear network model.

5.7 Conclusions

Active Network Management is an alternative or a complement to network reinforcement in case of massive integration of renewable energy in distribution systems in the future. Mathematically, operational planning, which is the preventive version of active network management we consider in this chapter, is an optimal sequential decision-making problem under uncertainty. The properties of the operational planning problem that we want to highlight are the need to optimize over a sufficiently long time horizon, to account for uncertainty of generation and consumption, and to model the discrete decisions related to the activation of flexibility services. In an attempt not to restrict ourselves to one solution method and one research community, we provide a formulation of this problem as a Markov Decision Process (MDP), which does not call for a particular solution method. We provide a simulator and several test beds at `http://www.montefiore.ulg.ac.be/~anm/` along with this formulation to foster research in this field, and ease future comparison of results. Although these benchmarks are not taken from real systems, their properties are coherent with what system operators could face in real life. We detail one possible solution method, which is a lookahead optimization model, then cast the MDP as a sequence of MINLPs, MISOCPs, or MILPs, and provide results on the benchmarks we created. Results show that state of the art open source local solvers for MINLP can show good performance on the test instances of limited size, at least when we approximate the stochastic program with few scenarios. Solving the MISOCPs and MILPs is however much more tractable, to the expense of the network model accuracy. In particular, the results of the MILP approximation suggest that it could scale to larger test systems and scenario trees. On the modeling side, we considered that all buses except the slack bus are P-Q buses, and that the power factors of the loads are constant while the generators are flexible as defined by their P-Q capabilities. Possible extensions of this work could be to consider the control of steerable synchronous generation, and of generators with time coupling constraints (e.g. combined heat and power generation). As mentioned in Section 5.3.2, other approaches exist to control the system, such as modulating the tariff signal(s), acting on the topology of the network, or using distributed storage sources. We did not model either the automatic regulation devices that often exist in distribution systems, such as On Load Tap Changers (OLTCs) of transformers that automatically adapt to control the voltage level. These automatic regulation devices have been recently addressed in [10]. We believe that all of these aspects should be considered in a real life solution. However, computational experiments show that we are at the limit of what can be

achieved with modern computers and standard mathematical programing tools. Furthermore, including a more detailed representation of the physical system makes the problem yet more discrete (OLTCs), and more uncertain (for instance, if flexibility services are not as well characterized as what we have assumed). Our experiments also show that increasing the number of scenarios, or stages of the stochastic program, would probably significantly improve the policies. All these observations suggest further research for tailored approximation or decomposition techniques, for instance techniques relying on the dynamic programming framework, in particular *approximate dynamic programming*, or simulation methods, such as *direct policy search* [82] or *Monte-Carlo tree search* [83, 84], or other approaches from the robust and stochastic programming community [85]. Actually the benchmarks that we proposed makes the comparison of new techniques possible.

6

Applications to a real distribution system

This chapter confronts the tools studied in this thesis with an actual distribution test system. The test system has been provided by a Belgian distribution system operator and has undergone some adjustments to picture its expected operating conditions in 2020. The production of wind and solar distributed generators is governed by generation data recorded in 2013 in the distribution system surroundings. A lookahead policy is evaluated over a batch of two-week-long simulations in a deterministic setting, as well as with 3-scenario and 5-scenario lookahead models. For each run, the stochastic models are learned from time series spanning the six weeks preceding the run.

Contents

6.1 The Ylpic test system

The Ylpic test system originates from a real distribution system that is operated by ORES, a Belgian DSO. The original grid was slightly modified for the following reasons:

- sensitive information were made anonymous;
- generation and consumption devices were updated to illustrate what the grid could face in 2020.

This latter update were performed by using the present data available to the DSO and a potential scenario of evolution of the Walloon electricity sector, such as defined within the GREDOR project [86].

The electrical grid of this test system has a radial configuration and is made of 328 MV buses. It is illustrated in Figure 6.1. The larger rectangle in this figure corresponds to the main substation, which is connected to the transmission network. The DSO does not own nor operate the HV/MV transformer but knows that the voltage magnitude at this substation is regulated. We consider this magnitude to be constant and set to 1.02 p.u. This value has been chosen to prevent the consumption processes (described in Section 6.2) to cause unrealistic undervoltage issues.

The considered operational constraints are:

- the voltage magnitude, which must stay within the $[0.95p.u., 1.05p.u.]$ interval for all the buses;
- the thermal limit of cables and lines, which is defined on a per-link basis.

As for the other chapters, we focus on the operational planning of the system. Fast dynamics is neglected and the physical quantities are assumed constant within a time period of a quarter of hour. The operation of the grid within such a time period falls within the scope of real-time controllers [68].

6.2 Generation and consumption processes

In addition to the grid, one-year-long time series describe the power production and consumption of all the devices of test instances. We first explain how these

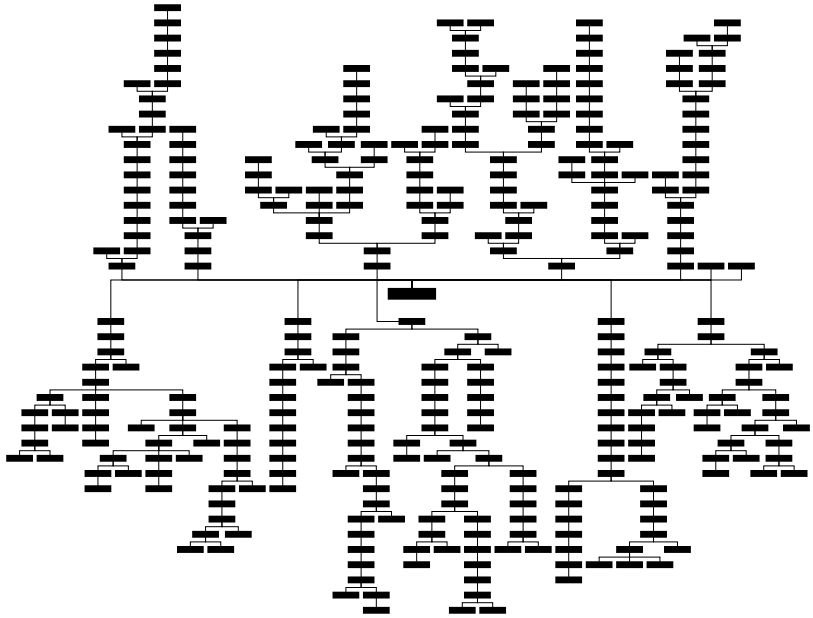

Figure 6.1: The Ylpic distribution test sytem.

time series govern the generation devices and then present the consumption case.

6.2.1 Generation

Data consisting of one year of power production acquired from a wind farm and a solar installation are used to set the injection of these two types of devices. These data take the form of time series of the production level of the generator, measured on a 15 minutes basis and covering the whole year 2013.

By contrast with the stochastic processes used in Chapter 5, i.e. the wind speed and the solar irradiance, the ones considered here are the normalized active production levels. A snapshot of these normalized production levels is plotted in Figure 6.2. The actual production level of a generator is then its generation capacity multiplied by the normalized production level. This

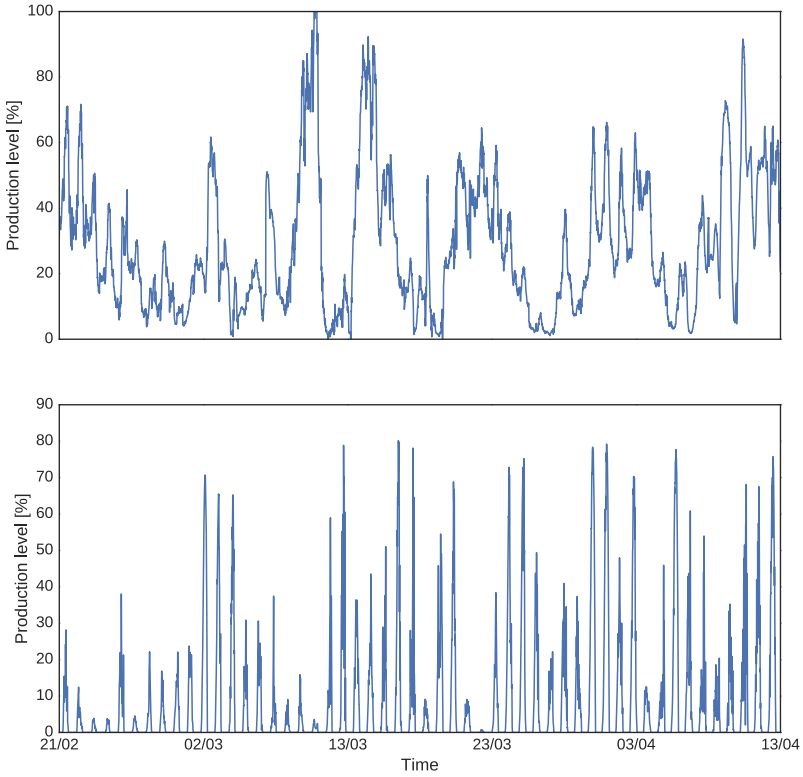

Figure 6.2: Snapshot of the wind and solar power levels.

implies some adjustments to equations (5.14)-(5.17), which become:

$$p_{t+1}^{(wind)} = f_{p^{(wind)}}(p_t^{(wind)}, \ldots, p_{t-N_v+1}^{(wind)}, \boldsymbol{s}_t^{(aux)}, \boldsymbol{w}_t^{(wind)}), \tag{6.1}$$

$$P_{g,t+1} = C_g p_{t+1}^{(wind)}, \forall g \in \text{wind generators} \subset \mathcal{G}, \tag{6.2}$$

$$p_{t+1}^{(sun)} = f_{p^{(sun)}}(p_t^{(sun)}, \ldots, p_{t-N_{ir}+1}^{(sun)}, \boldsymbol{s}_t^{(aux)}, \boldsymbol{w}_t^{(sun)}), \tag{6.3}$$

$$P_{g,t+1} = C_g p_{t+1}^{(sun)}, \forall g \in \text{solar generators} \subset \mathcal{G}, \tag{6.4}$$

where C_g [MW] denotes the generation capacity of generator g.

The time series of power levels cover a whole year and this will allow to evaluate the adequacy of the lookahead policy for quite different production patterns. Figures 6.3 and 6.4 illustrate the difference between July and December, for the solar and wind production, respectively. The cumulative density function (CDF) of the production levels shows, as expected, that the solar generation is much more important in July than in December, and inversely for the wind generation.

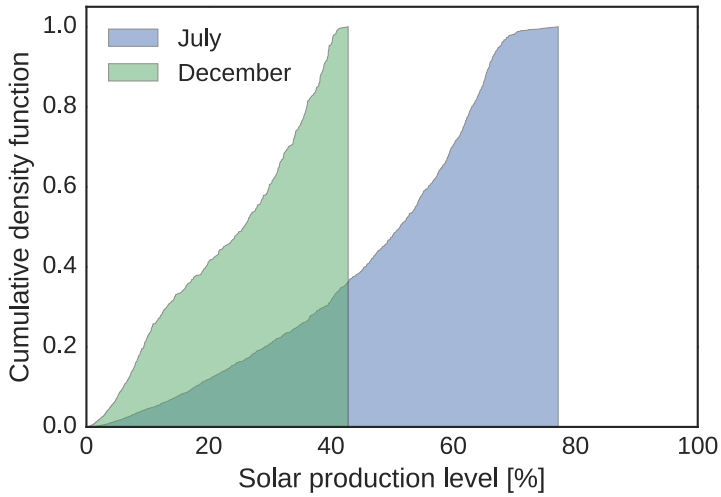

Figure 6.3: Comparison of the CDF of the solar production level in July and December.

The test system also includes combined heat and power (CHP) units. Their production dispatch is assumed to be known before the operational planning stage and they are then considered as deterministic exogenous variables.

The reactive power injection of all generators is assumed to be null unless otherwise instructed by the control actions of the DSO. The set of acceptable P-Q operating points is described in Section 6.3.

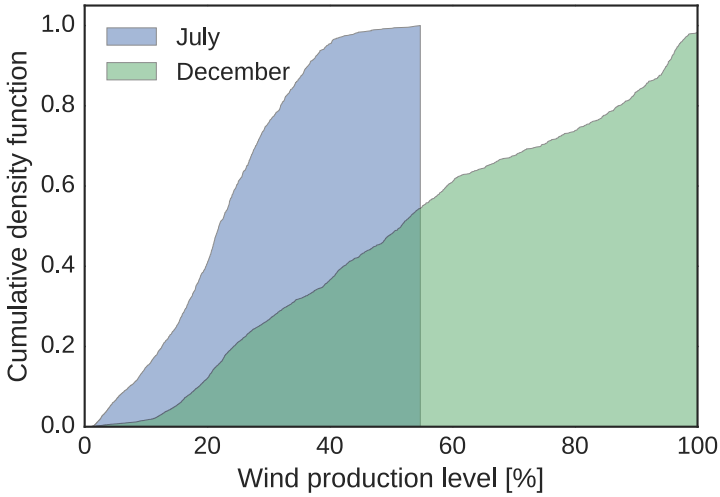

Figure 6.4: Comparison of the CDF of the wind production level in July and December.

6.2.2 Consumption

The consumption is defined on a per-load basis. A time series of the active and reactive consumption has been provided by the DSO for every load. A snapshot of the total active consumption within the system is presented in Figure 6.5.

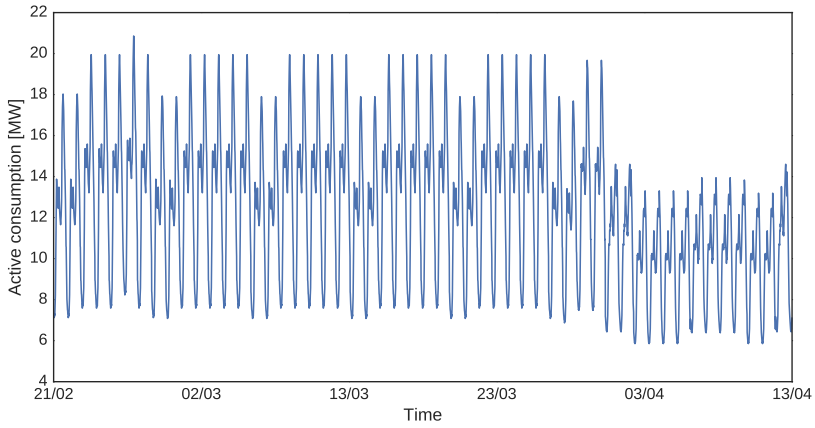

Figure 6.5: Snapshot of the total active consumption.

Similarly to the generation data, the consumption patterns vary within the year. This variability also occurs between weekdays and weekends. Figure 6.6 illustrates the difference between July and December, for the total active consumption within the system. A much higher power demand is observed in December than in July.

6.3 Flexibility

The considered control scheme is the one described in Section 5.3.3.2. The available control actions consist of active production limits, reactive injection set-points, and activation of load flexibility services.

The wind and CHP generators support both curtailment and reactive control. On the other hand, we assume that the solar generators, which mainly consist of residential units, can not be controlled in any way. The curtailment price is function of the time of the day and is illustrated in Figure 5.11 for CHP

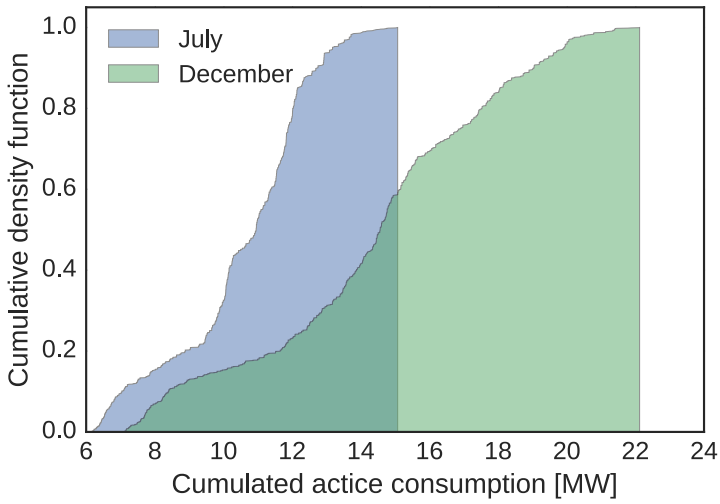

Figure 6.6: Comparison of the CDF of the total active consumption in July and December.

units. For wind generators, 60€ is added to this price to reflect the support mechanism that exists for renewables in Wallonia.

The extend of reactive support that a generator can provide is constrained by its set of acceptable injection points, which differs for wind and CHP generators. In both cases, the region of valid P-Q set-points is a polyhedron such as defined by equation (5.9). This region is symmetric with respect to the P-axis for wind generators, while it is not in the CHP case. These areas have been defined by the DSO within the GREDOR project. Figures 6.7a and 6.7b illustrate the P-Q area of a wind farm and CHP generator, respectively.

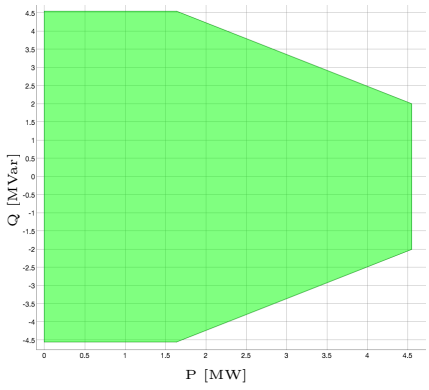

(a) Wind farm.

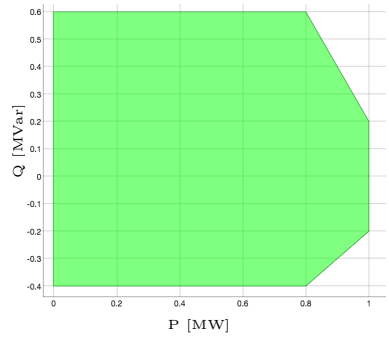

(b) CHP generator.

Figure 6.7: Examples of region of valid P-Q set-points.

Finally, the test system includes 100 flexible loads and each of them has its modulation signal and price. These signals are similar to the one illustrated in Figure 5.5a and differ in terms of length and magnitude. The distribution of these two parameters among the flexible loads is presented in Figure 6.8. Half of the signals starts with a downward modulation, and inversely for the other half. The activation cost of the services is defined as 5€/MWh of demand that is shifted by the modulation signal. This price is lesser that for curtailment and has been chosen in order to foster, when possible, the recourse to load flexibility.

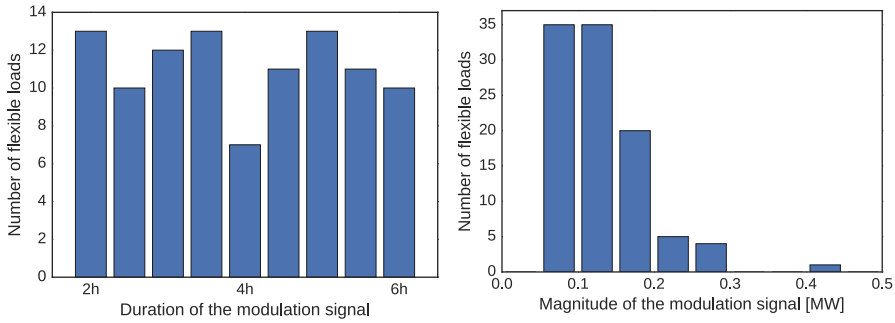

Figure 6.8: Description of the modulation signals.

6.4 Experimental setting

The design of the experimental setting has been driven by the aim of evaluating the performance of the lookahead policy described in Section 5.4 at operating the realistic Ylpic test system. In addition, the GMM approach presented in Chapter 4 is used to model the stochastic processes.

The one-year-long generation and consumption processes described in Section 6.2 are divided into overlapping time intervals of 8 consecutive weeks, an interval starting every 2 weeks of the year. Within each time interval, the first six weeks are used to learn the stochastic models and the last two weeks drive the simulation of the test system. This scheme is described in Figure 6.9.

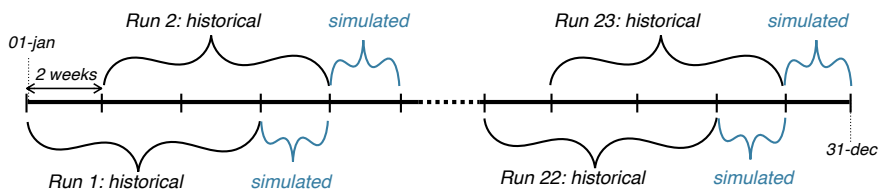

Figure 6.9: The experimental setting takes the form of a batch of 23 simulation runs.

6.4.1 Lookahead optimization model

The learned processes are the normalized production levels of wind and solar generators, i.e. equations (6.1) and (6.3), while the demand is considered to be deterministic. This assumption is motivated by the lack of real consumption data. The available time series of power demand are synthetic data, which do not exhibit the variability, temporal correlation, or spatial correlation that we could expect from actual measurements. Relying on arbitrary stochastic models could have biased the interpretation of the results.

The learning procedure for the Gaussian mixture parameters is described in Section 4.3, while the selection of the hyper parameters (i.e. the number of mixture components and the Markovian order) is performed using a grid search with cross validation. For every stochastic process and every hyper parameter value, a GMM is learned on the historical data but one week. The score of the GMM is defined as the log-likelihood of the left out data under the learned model [87]. The score of a hyper parameter value is then the average of the associated GMMs for every left out week. The considered set Ω of candidate hyper parameters $\omega = (L, N)$, where L is the Markovian order and N is the number of mixture components, is $\Omega = \{5\} \times \{1, 5, 10, 15, 20, 25, 30, 35, 40\}$. This set is restricted to a single Markovian order to limit the computational burden of the approach. We chose 5 as it consistently produced good models in the empirical analyses of Chapter 4.

6.4.2 Lookahead optimization model

The mathematical program that implements the lookahead policy is defined by equations (5.48)-(5.53), with the linearized network model of Section 5.4.5.2.

The two other network models were excluded as they do not exhibit the scalability requirements for such a large test system.

The policy is applied to the test system using the procedure (2a)-(2f) of Section 5.6, with 3 and 5 scenarios in the lookahead model.

6.4.3 Computational environment

Each batch of 23 simulations ran concurrently on a machine with 40 logical cores of 2.4Ghz and 64Go of RAM. Gurobi was used to solve MILPs, and we relied on Scikit-learn [60] to implement the learning of GMMs and the clustering of trajectories into scenarios.

6.5 Numerical results

The parameters and results of the simulation runs are summarized in Table 6.1. This table reports the empirical mean and standard deviation of both the expected return and solver time, for the three different lookahead models as well as when no policy is applied to the system. As expected, the deterministic case is the most favorable one and the worst performance is reached when there is no policy. The 5-scenario configuration produces a slightly better expected return than the 3-scenario one but at the cost of a substantial increase in solver time.

	Parameters		Expected return		Solver time	
	T	γ	Mean	Std. dev.	Mean	Std. dev.
Deterministic	10	0.999	−2357.9	904.4	53.4s	3.1s
5 scenarios			−2884.6	1858.3	269.1s	29.1s
3 scenarios			−2889.3	1859.4	145.9s	12.3s
No policy	N/A		−9853.0	13543.8	N/A	N/A

Table 6.1: Simulation results and parameters.

The cumulated operational costs and magnitude of constraint violations are plotted in Figure 6.10, for every policy. In order to improve the readability of these results, we only considered the five simulation runs that have the most operational issues (i.e. the largest magnitude of violations) without policy.

The deterministic case is naturally the one that leads to the least costs and violations. Among the two stochastic cases, the 5-scenario policy produces smaller violations but at a higher cost.

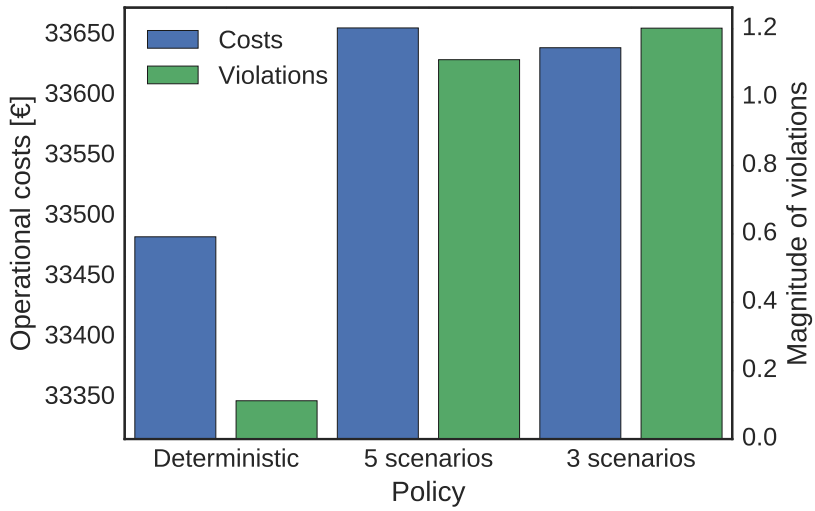

Figure 6.10: Operational costs and constraint violations for every policy.

When analyzing the results on a per-run basis, we observe that, in the stochastic setting, the policies perform poorly for two particular runs. This performance drop does not occur in the deterministic case. Figure 6.11 plots the cumulated active production in the distribution system, both in the deterministic setting and in the stochastic setting with the 3-scenario policy. At this time in the simulation, the policy must take adequate control actions to prevent over-voltages when the cumulated active production exceeds around 20 MW. In the deterministic case, the policy activates flexible loads and, as shown in red in the figure, performs generation curtailment. In the stochastic case however, the scenarios in the lookahead model, illustrated by dashed black lines in the figure, are very inaccurate and the policy can not anticipate the operational issues. A further analysis reveals that the inaccuracy comes from the stochastic model of the wind production levels. For the two defective runs, the 6-week-long historical data are not representative of the stochastic process for the next two weeks. The difference between the historical and simulated data is presented in Figure 6.12 for one of these runs. The cumulative density function (CDF) highlights that the production levels in the simulation reach much higher values than in the historical data, which led to learn an inadequate stochastic model. By contrast, Figure 6.13 shows a case where the CDFs match quite well. This corresponds to a run where the policies perform well in the stochastic setting.

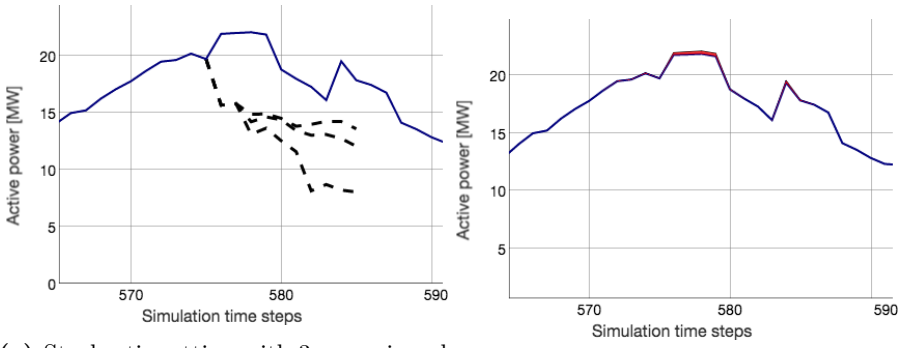

(a) Stochastic setting with 3-scenario policy.

(b) Deterministic setting.

Figure 6.11: Snapshot of a run where the stochastic policies perform poorly.

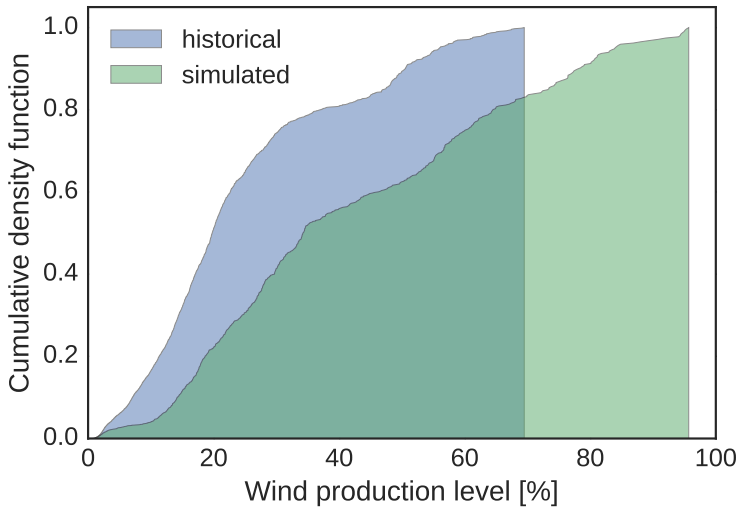

Figure 6.12: CDF of the wind production level for the historical and simulated data of a run in September.

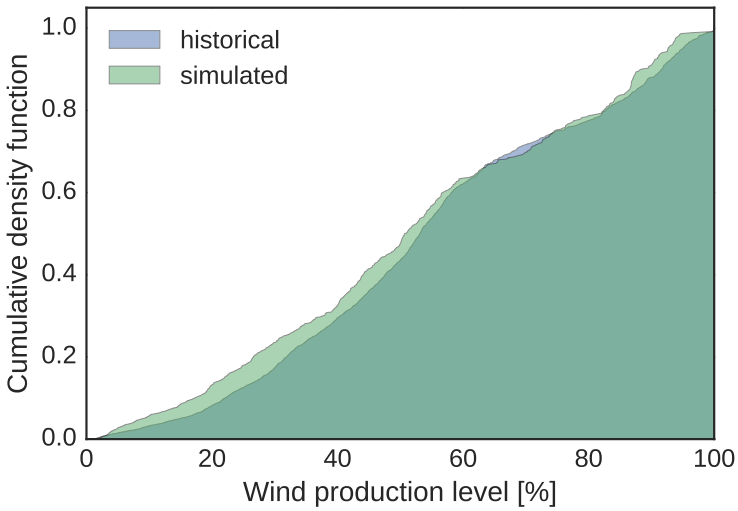

Figure 6.13: CDF of the wind production level for the historical and simulated data of a run in November.

6.6 Conclusion

In this chapter, we confronted the tools presented throughout this dissertation with a test system designed based on a real distribution system. The time series considered to simulate the operation of the grid and to learn the stochastic models are real datasets of measurements for the generation.

Two lookahead policies with 3 and 5 scenarios were compared to a deterministic configuration as well as when no policy is applied to the system. They exhibited much better performances than without policy in terms of expected return, but they can not reach the performance level of the (unrealistic) deterministic case. The policy with 5 scenarios has a slight lead over the 3-scenario version, but requires a significantly higher computational cost. It is likely that to obtain good performances within an acceptable time, the construction of scenarios should be revised to limit the number of scenarios needed to reach a given performance level.

The simulations have also highlighted how critical it is to have adequate learning data to produce the stochastic models. The available historical data were scarce and augmenting the historical data with measurements acquired at similar periods of the year but covering several years would likely improve the quality

of the stochastic models. Improving the generalization abilities of the models, e.g. by differentiating the time series, could also help to mitigate this issue.

7

Conclusion

Contents

This thesis focused on the operational planning problem of distribution systems, which is the preventive part of ANM. In this chapter, we first summarize the material of the dissertation and then highlight further research directions.

7.1 Summary

A formulation of the ANM problem that allows utilization of demand-side operational flexibility was presented in Chapter 2. This work highlighted both the sequential and the uncertain nature of the ANM problem and addressed it as an optimal sequential decision-making problem under uncertainty. A case study was designed to demonstrate that it is critical to explicitly take into account the uncertainty to efficiently operate demand-side flexibility.

In Chapter 3, we described a novel relaxation for multi-period OPF problems with discrete variables that is based on a network-flow reformulation. The relaxation produces lower bounds that are comparable with a Lagrangian relaxation, but reduces the level of infeasibility of the relaxed solutions.

We presented in Chapter 4 a novel approach that relies on Gaussian mixtures to model a stochastic process from a set of time series of observations. The hyper parameters of the model, i.e. the Markov order and the number of mixture components, are determined using a multi-armed bandit technique, while the mixture parameters are learned from the data using an EM algorithm. Empirical results showed that the proposed approach outperforms an ARMA approach for the considered application of lookahead security analysis, for datasets of residential power consumption and of wind speed.

In Chapter 5, the ANM problem was formulated as a Markov Decision Process (MDP), which does not call for a particular solution method. We provided a simulator and several test beds along with this formulation to foster research in this field, and ease future comparison of results. One possible solution method was detailed, which is a lookahead optimization model. The MDP was then cast as a sequence of MINLPs, MISOCPs, or MILPs, and we provided results on the benchmarks we created. The results showed that state-of-the-art open source local solvers for MINLP can show good performance on the test instances of limited size, at least when we approximate the stochastic program with few scenarios. Solving the MISOCPs and MILPs is, however, much more tractable, to the expense of the network model accuracy. In particular, the results of the MILP approximation suggest that it could scale to larger test systems and scenario trees.

Finally, the tools presented throughout this dissertation were evaluated on a test system designed based on a real distribution system in Chapter 6. The time series considered to simulate the operation of the grid and to learn the stochastic models were real datasets of measurements for the generation. Two lookahead policies with three and five scenarios were compared to a deterministic configuration as well as when no policy is applied to the system. They exhibited much better performances than without policy in terms of expected return, but they cannot reach the performance level of the (unrealistic) deterministic case. The policy with five scenarios has a slight lead over the three-scenario version, but requires a significantly higher computational cost.

7.2 Future Work

7.2.1 Approximation and decomposition techniques

The discretization of uncertainty into a set of scenarios could be refined to preserve the quality of the lookahead model as much as possible while reducing the number of scenarios [88]-[89]. Similarly, decomposition techniques would adapt the complexity of the lookahead model with the lookahead time horizon [90]. Such an approach could, for example, allow for longer time horizons to be considered by decreasing the accuracy of the uncertainty representation for the furthest time periods. Improvements could also be made to the approximations of the power-flow equations. The linear network model presented in Section 5.4.5 showed to have good scalability abilities and to reliably prevent operational issues. However, it lacks the representation of losses and cannot benefit from the flexibility to reduce the costs they induce. Augmenting this linear approximation with a gainful representation of losses may allow for more efficient policies.

7.2.2 Heuristics

Heuristic approaches can be an appealing alternative to conventional optimization algorithms in order to obtain a feasible solution within an acceptable time limit. Such approaches can be designed to benefit from the specifics of the ANM problem, while math programming solvers limit their scope to the mathematical structure of the problem. Building on top of the network

flow presented in Section 3.4.2, a two-step procedure could, for example, be developed to identify the flexibility needs first, and then to procure adequate flexibility services.

7.2.3 Stochastic modeling

Different approaches could be explored to improve the modeling of stochastic processes. Data transformation could be applied, for example by differencing the time series to improve the stationarity of the stochastic process to be learned. Instead of considering density functions that are conditional on immediately preceding time periods, feature extraction techniques could allow the identification of the time lags which are the most relevant. Feature compression could also be explored to consider a larger number of past time periods while keeping an acceptable computational cost for the learning procedure.

7.2.4 Online learning procedure

We identified in Section 6.5 how critical the adequacy of the learning dataset is to obtain a proper stochastic model. When the distribution of the data in the learning set is quite different from the distribution of the process in the near future, the lookahead scenarios are not relevant. A procedure could be developed to identify, during the simulation, when such distributions diverge in order to trigger a new execution of the learning procedure on the updated historical data.

A

LEC Minimization for Microgrids

This chapter falls within the context of the optimization of the levelized energy cost (LEC) of microgrids featuring photovoltaic panels (PV) associated with both long-term (hydrogen) and short-term (batteries) storage devices. First, we propose a novel formalization of the problem of building and operating microgrids interacting with their surrounding environment. Then we show how to optimally operate a microgrid using linear programming techniques in the context where the consumption and the production are known. It appears that this optimization technique can also be used to address the problem of optimal sizing of the microgrid, for which we propose a robust approach. These contributions are illustrated in two different settings corresponding to Belgian and Spanish data.

Contents

A.1 Introduction

Economies of scale of conventional power plants have progressively led to the development of the very large and complex electrical networks that we know today. These networks transmit and distribute the power generated by these power plants to the consumers. Over recent years, a new trend opposing this centralization of power facilities has been observed, resulting from the drop in price of distributed generation, mainly solar photovoltaic (PV) panels [91]. Due to this effect, it is expected that in the future, small scale industries and residential consumers of electricity will rely more and more on local renewable energy production capacities for covering, at least partially, their need for electrical power. This leads to the creation of the so-called microgrids that are electrical systems which include loads and distributed energy resources that can be operated in parallel with the broader utility grid or as an electrical island. State-of-the-art issues and feasible solutions associated with the deployment of microgrids are discussed in [92].

Due to the fluctuating nature of renewable energy sources (RES) (mainly solar and wind energy), small businesses and residential consumers of electricity may also be tempted to combine their local power plants with storage capacities. In principle, this would, at least partially, allow themselves freedom from using the network, enabling balancing their own electricity generation with their own consumption. This would result in paying less in transmission and distribution fees which typically make up around 50% of their electricity bill. Many different technologies are available for energy storage as discussed in the literature (see e.g. [93]). On the one hand, hydrogen is often considered as a storage solution to be combined with RES [94, 95], mainly due to its high capacity potential that makes it suitable for long-term storage [96, 97]. On the other hand, batteries are often used to ensure sufficient peak power storage and peak power generation [98]. In this chapter we focus on the specific case of microgrids that are powered by PV panels combined with both hydrogen-based storage technologies (electrolysis combined with fuel cells) and batteries (such as, for instance, $LiFePO_4$ batteries). These two types of storage aim at fulfilling, at best, the demand by addressing the seasonal and daily fluctuations of solar irradiance.

One of the main problems to be addressed in the field of microgrids is how to perform optimal sizing. The main challenge when sizing microgrids comes from the need to determine and simulate their operation, i.e. the dispatch strategy, using historical data of the loads and of the RES. Broadly speaking, the research presented in this paper relates to the research that has been

done for solving planning and scheduling problems in the field of electrical power systems. In this context, various methods have been investigated, for instance model predictive control (MPC) [99] or learning-based approaches [100, 101]. One can also mention commercial solutions such as the well-known energy modeling software HOMER [102], dedicated to hybrid renewable energy systems.

In this chapter, we first propose a novel and detailed formalization of the problem of sizing and operating microgrids. Then, we show how to optimally operate a microgrid so that it minimizes a levelized energy cost (LEC) criterion in the context where the energy production and demand are known. We show that this optimization step can be achieved efficiently using linear programming. We then show that this optimization step can also be used to address the problem of optimal sizing of the microgrid, for which we propose a robust approach by considering several energy production and consumption scenarios. We run experiments using real data corresponding to the case of typical residential consumers of electricity located in Spain and in Belgium. Experimental results show that there is an important benefit in combining batteries and hydrogen-based storage, in particular when the cost for interruption (value of loss load) in the supply is high. Note that this chapter focuses on the production planning and optimal sizing of the microgrid, and that the real-time control aspects of the microgrid to maintain both angle stability and voltage quality are left out of the scope of the chapter (see e.g. [103] for more details on that subject).

Subsequently, the chapter is organized as follows. A detailed formalization of the microgrid framework is proposed in Section A.2 and several optimization schemes for minimizing the LEC are introduced in Section A.3. The simulation results for Belgium and Spain are finally reported in Section A.4 while Section A.5 provides the conclusion.

A.2 Formalization and problem statement

In this section we provide a generic model of a microgrid powered by PV panels combined with batteries and hydrogen-based storage technologies. We formalize its constitutive elements as well as its dynamics within the surrounding environment. For the sake of clarity, we first define the space of exogenous variables and then gradually build the state and action spaces of the system. The components of these two latter spaces will be related to either the notion of *infrastructure* or the notion of *operation* of the microgrid. We then characterize

the problem of sizing and control that we want to address using an optimality criterion, which leads to the formalization of an optimal sequential decision-making problem. The evolution of the system is described as a discrete-time process over a finite time-horizon of length T. We denote by $\mathcal{T}$ the set $\{1, ..., T\}$ of time periods and by Δt the duration of a time step. We use subscript t to reference exogenous variables, state and actions at time step t. Finally we introduce the notion of LEC and discuss how it can be used as an optimality criterion.

A.2.1 Exogenous variables

We start with a definition of the microgrid's environment, i.e. the space of exogenous variables that affect the microgrid but on which the latter has no control. Assuming that there exists, respectively, J, L, and M different photovoltaic, battery, and hydrogen storage technologies, and denoting the environment space by $\mathcal{E}$, we can define the time-varying environment vector $\mathbf{E}_t$ as:

$$\mathbf{E}_t = (c_t, i_t, \mathbf{e}^{PV}_{1,t}, ..., \mathbf{e}^{PV}_{J,t}, \mathbf{e}^{B}_{1,t}, ..., \mathbf{e}^{B}_{L,t}, \mathbf{e}^{H_2}_{1,t}, ..., \mathbf{e}^{H_2}_{M,t}, \boldsymbol{\mu}_t) \in \mathcal{E},\ \forall t \in \mathcal{T} \quad \text{(A.1)}$$
$$\text{and with } \mathcal{E} = \mathbb{R}^{+^2} \times \prod_{j=1}^{J} \mathcal{E}^{PV}_j \times \prod_{l=1}^{L} \mathcal{E}^{B}_l \times \prod_{m=1}^{M} \mathcal{E}^{H_2}_m \times \mathcal{I}\,,$$

where:

- c_t [W] $\in \mathbb{R}^+$ is the electricity demand within the microgrid;
- i_t [W/m^2 or W/W$_p$] $\in \mathbb{R}^+$ denotes the solar irradiance incident to the PV panels;
- $\mathbf{e}^{PV}_{j,t} \in \mathcal{E}^{PV}_j$, $\forall j \in \{1, ..., J\}$, models a photovoltaic technology in terms of cost $c^{PV}_{j,t}$ [€/m^2], lifetime $L^{PV}_{j,t}$ [s] and efficiency $\eta^{PV}_{j,t}$ to convert solar irradiance to electrical power:

$$\mathbf{e}^{PV}_{j,t} = (c^{PV}_{j,t}, L^{PV}_{j,t}, \eta^{PV}_{j,t}) \in \mathcal{E}^{PV}_j, \quad \text{(A.2)}$$
$$\forall j \in \{1, ..., J\} \text{ and with } \mathcal{E}^{PV}_j = \mathbb{R}^{+^2} \times\,]0, 1]\,;$$

- $\mathbf{e}^{B}_{l,t} \in \mathcal{E}^{B}_l$, $\forall l \in \{1, ..., L\}$, represents a battery technology in terms of cost $c^{B}_{l,t}$ [€/Wh], lifetime L^{B}_l [s], cycle durability $D^{B}_{l,t}$, power limit for charge and discharge $P^{B}_{l,t}$ [W], discharge efficiency $\zeta^{B}_{l,t}$, and charge retention rate

$r^B_{l,t}$ [s^{-1}]:

$$\mathbf{e}^B_{l,t} = (c^B_{l,t}, L^B_{l,t}, P^B_{l,t}, \eta^B_{l,t}, \zeta^B_{l,t}, r^B_{l,t}) \in \mathcal{E}^B_l,\ \forall l \in \{1, ..., L\} \quad \text{and with } \mathcal{E}^B_l = \mathbb{R}^{+3} \times\ ]0, 1]^3\,; \tag{A.3}$$

- $\mathbf{e}^{H_2}_{m,t} \in \mathcal{E}^{H_2}_m$, $\forall m \in \{1, ..., M\}$, denotes a hydrogen storage technology in terms of cost $c^{H_2}_{m,t}$ [€/W_p], lifetime $L^{H_2}_{m,t}$ [s], maximum capacity $R^{H_2}_{m,t}$ [W], electrolysis efficiency $\eta^{H_2}_{m,t}$ (i.e. when storing energy), fuel cells efficiency $\zeta^{H_2}_{m,t}$ (i.e. when delivering energy), and charge retention rate $r^{H_2}_{m,t}$ [s^{-1}]:

$$\mathbf{e}^{H_2}_{m,t} = (c^{H_2}_{m,t}, L^{H_2}_{m,t}, R^{H_2}_{m,t}, \eta^{H_2}_{m,t}, \zeta^{H_2}_{m,t}, r^{H_2}_{m,t}) \in \mathcal{E}^{H_2}_m,\ \forall m \in \{1, ..., M\} \quad \text{and with } \mathcal{E}^{H_2}_m = \mathbb{R}^{+3} \times\ ]0, 1]^3\ . \tag{A.4}$$

Finally, the components denoted by $\boldsymbol{\mu}_t \in \mathcal{I}$ represent the model of interaction. By model of interaction we mean all the information that is required to manage and evaluate the costs (or benefits) related to electricity exchanges between the microgrid and the rest of the system. We assume that $\boldsymbol{\mu}_t$ is composed of two components k and β:

$$\boldsymbol{\mu}_t = (k, \beta) \in \mathcal{I},\ \forall\ t\ \in\ \mathcal{T} \text{ and with } \mathcal{I} = \mathbb{R}^{+2}\,. \tag{A.5}$$

The variable β characterizes the price per kWh at which it is possible to sell energy to the grid (it is set to 0 in the case of an off-grid microgrid). The variable k refers to the cost endured per kWh that is not supplied within the microgrid. In a connected microgrid, k corresponds to the price at which electricity can be bought from outside the microgrid. In the case of an off-grid microgrid, the variable k characterizes the penalty associated with a failure of the microgrid to fulfill the demand. This penalty is known as the value of loss load and corresponds to the amount that consumers of electricity would be willing to pay to avoid a disruption to their electricity supply.

A.2.2 State space

Let $\mathbf{s}_t \in \mathcal{S}$ denote a time varying vector characterizing the microgrid's state at time $t \in \mathcal{T}$:

$$\mathbf{s}_t = (\mathbf{s}^{(s)}_t, \mathbf{s}^{(o)}_t) \in \mathcal{S},\ \forall t \in \mathcal{T} \text{ and with } \mathcal{S} = \mathcal{S}^{(s)} \times \mathcal{S}^{(o)}\ , \tag{A.6}$$

where $\mathbf{s}_t^{(s)} \in \mathcal{S}^{(s)}$ and $\mathbf{s}_t^{(o)} \in \mathcal{S}^{(o)}$ respectively represent the state information related to the infrastructure and to the operation of the microgrid.

A.2.2.1 Infrastructure state

The infrastructure state vector $\mathbf{s}_t^{(s)} \in \mathcal{S}^{(s)}$ gathers all the information about the physical and electrical properties of the devices that constitute the microgrid. Its components can only change because of investment decisions or due to aging of the devices. In particular, we define this vector as:

$$\begin{aligned}\mathbf{s}_t^{(s)} = (&x_t^{PV}, x_t^B, x_t^{H_2}, L_t^{PV}, L_t^B, L_t^{H_2}, P_t^B, R_t^{H_2},\\ &\eta_t^{PV}, \eta_t^B, \eta_t^{H_2}, \zeta_t^B, \zeta_t^{H_2}, r_t^B, r_t^{H_2}) \in \mathcal{S}^{(s)} ,\\ &\forall t \in \mathcal{T} \text{ and with } \mathcal{S}^{(s)} = \mathbb{R}^{+8} \times\,]0,1]^7 ,\end{aligned} \tag{A.7}$$

where x_t^{PV} [m^2], x_t^B [Wh], and $x_t^{H_2}$ [W$_p$] denote, respectively, the sizing of the PV panels, battery and hydrogen storage. The other components have the same meaning than the exogenous variables using a similar symbol, with the difference here that they are specific to the devices that are present at time $t \in \mathcal{T}$ in the microgrid. Note that by using such a representation, we consider that, for each device type, a single device can operate in the microgrid. In other words, an investment decision for a device type substitutes any prior investment.

A.2.2.2 Operation state

For the devices with storage capacities, i.e. battery and hydrogen storage, the information provided by the environment vector $\mathbf{E}_t$ and by the infrastructure state vector $\mathbf{s}_t^{(s)}$ is not sufficient to determine the set of their feasible power injections or demands. Additional information that corresponds to the amount of energy stored in these devices for each time period is required. For this reason we introduce the operation state vector $\mathbf{s}_t^{(o)}$:

$$\mathbf{s}_t^{(o)} = (s_t^B, s_t^{H_2}) \in \mathcal{S}^{(o)},\ \forall t \in \mathcal{T} \text{ and with } \mathcal{S}^{(o)} = \mathbb{R}^{+2} , \tag{A.8}$$

where s_t^B [Wh] is the level of charge of the battery and with s_t^B [Wh] the level of charge of the hydrogen storage.

A.2.3 Action space

As for the state space, each component of the action vector $\mathbf{a}_t \in \mathcal{A}$ can be related to either sizing or control, the former affecting the infrastructure of the microgrid while the latter affects its operation. We define the action vector as:

$$\mathbf{a}_t = (\mathbf{a}_t^{(s)}, \mathbf{a}_t^{(o)}) \in \mathcal{A}_t, \ \forall t \in \mathcal{T} \text{ and with } \mathcal{A} = \mathcal{A}^{(s)} \times \mathcal{A}_t^{(o)} \ , \tag{A.9}$$

where $\mathbf{a}_t^{(s)} \in \mathcal{A}^{(s)}$ relates to sizing actions and $\mathbf{a}_t^{(o)} \in \mathcal{A}_t^{(o)}$ to control actions.

A.2.3.1 Sizing actions

The sizing actions correspond to investment decisions. For each device type, it defines the sizing of the device to install in the microgrid and its technology:

$$\begin{aligned} \mathbf{a}_t^{(s)} &= (a_t^{PV}, a_t^B, a_t^{H_2}, j_t, l_t, m_t) \in \mathcal{A}^{(s)}, \ \forall t \in \mathcal{T} \\ \text{and with } \mathcal{A}^{(s)} &= {\mathbb{R}^+}^3 \times \{1, ..., J\} \times \{1, ..., L\} \times \{1, ..., M\} \ , \end{aligned} \tag{A.10}$$

where a_t^{PV} [m^2], a_t^B [Wh], and $a_t^{H_2}$ [Wp] denote, respectively, the new sizing at time $t+1 \in \mathcal{T}$ of the PV panels, battery and hydrogen storage. Discrete variables j_t, l_t, and m_t correspond to indices that indicate the selected technology from the environment vector for PV panels, battery, and hydrogen storage, respectively. When a sizing variable (i.e. a_t^{PV}, a_t^B, or $a_t^{H_2}$) is equal to zero, it means that there is no new installation for the corresponding device type and that the present device, if it exists, remains in operation.

A.2.3.2 Operational planning

A microgrid featuring PV, battery and storage using H_2 has two control variables that correspond to the power exchanges between the battery, the hydrogen storage, and the rest of the system:

$$\mathbf{a}_t^{(o)} = (p_t^B, p_t^{H_2}) \in \mathcal{A}_t^{(o)} \ , \forall t \in \mathcal{T} \ , \tag{A.11}$$

where p_t^B [W] is the power provided to the battery and where $p_t^{H_2}$ [W] is the power provided to the hydrogen storage device. These variables are positive

when the power flows from the system to the devices and negative if it flows in the other direction. Note that the set $\mathcal{A}_t^{(o)}$ of control actions is time dependent. This comes from the fact that the feasible power exchanges with these devices depend on their capacity and level of charge. We have, $\forall t \in \mathcal{T}$:

$$\mathcal{A}_t^{(o)} = \left([-\zeta_t^B s_t^B, \frac{x_t^B - s_t^B}{\eta_t^B}] \cap [-P_t^B, P_t^B] \right) \times \left([-\zeta_t^{H_2} s_t^{H_2}, \frac{R_t^{H_2} - s_t^{H_2}}{\eta_t^{H_2}}] \cap [-x_t^{H_2}, x_t^{H_2}] \right) , \tag{A.12}$$

which expresses that the bounds on the power flows of the storing devices are, at each time step $t \in \mathcal{T}$, the most constraining among the ones induced by the charge levels and the power limits.

A.2.4 Dynamics

Using the formalism proposed above, the dynamics of the microgrid follows the following discrete-time equation:

$$\mathbf{s}_{t+1} = f(\mathbf{s}_t, \mathbf{a}_t), \forall t \in \mathcal{T} \text{ and with } (\mathbf{s}_t, \mathbf{a}_t, \mathbf{s}_{t+1}) \in \mathcal{S} \times \mathcal{A}_t \times \mathcal{S} \ . \tag{A.13}$$

The dynamics specific to the infrastructure state $\mathbf{s}_t^{(s)} \in \mathcal{S}^{(s)}$ are straightforward and can be written, $\forall t \in \mathcal{T}$:

$$(x_{t+1}^{PV}, L_{t+1}^{PV}, \eta_{t+1}^{PV}) = \begin{cases} (a_t^{PV}, L_{j_t,t}^{PV}, \eta_{j_t,t}^{PV}) & \text{if } a_t^{PV} > 0, \\ (0, 0, \eta_t^{PV}) & \text{if } L_t^{PV} \leq 1, \\ (x_t^{PV}, L_t^{PV} - 1, \eta_t^{PV}) & \text{otherwise,} \end{cases} \tag{A.14}$$

$$(x_{t+1}^{B}, L_{t+1}^{B}, P_{t+1}^{B}, \eta_{t+1}^{B}, \zeta_{t+1}^{B}, r_{t+1}^{B}) = \begin{cases} (a_t^{B}, L_{l_t,t}^{B}, P_{l_t,t}^{B}, \eta_{l_t,t}^{B}, \zeta_{l_t,t}^{B}, r_{l_t,t}^{B}) & \text{if } a_t^{B} > 0, \\ (0, 0, 0, \eta_t^{B}, \zeta_t^{B}, r_t^{B}) & \text{if } L_t^{B} \leq 1, \\ (x_t^{B}, L_t^{B} - 1, P_t^{B}, \eta_t^{B}, \zeta_t^{B}, r_t^{B}) & \text{otherwise,} \end{cases} \tag{A.15}$$

$$(x_{t+1}^{H_2}, L_{t+1}^{H_2}, R_{t+1}^{H_2}, \eta_{t+1}^{H_2}, \zeta_{t+1}^{H_2}, r_{t+1}^{H_2}) = \begin{cases} (a_t^{H_2}, L_{m_t,t}^{H_2}, R_{m_t,t}^{H_2}, \eta_{m_t,t}^{H_2}, \zeta_{m_t,t}^{H_2}, r_{m_t,t}^{H_2}) & \text{if } a_t^{H_2} > 0, \\ (0, 0, 0, \eta_t^{H_2}, \zeta_t^{H_2}, r_t^{H_2}) & \text{if } L_t^{H_2} \leq 1, \\ (x_t^{H_2}, L_t^{H_2} - 1, R_t^{H_2}, \eta_t^{H_2}, \zeta_t^{H_2}, r_t^{H_2}) & \text{otherwise,} \end{cases} \tag{A.16}$$

which describes that a device is either replaced because of a new investment or because of aging. At the end of the device's lifetime, it is discarded from the microgrid. Note that a more advanced model could include aging rules for

the other physical properties of the devices (i.e. efficiency, energy retention, capacity and power limit) but this is outside the scope of the present work.

Concerning the dynamics of the operation state $\mathbf{s}_t^{(o)} \in \mathcal{S}^{(o)}$, we have to ensure that the charge level of a storage device is reset to zero when it is replaced by a new investment. In addition, the correct efficiency factor differs depending on the direction of the power flow:

$$s_{t+1}^B = \begin{cases} 0 & \text{if } a_t^B > 0, \\ r_t^B s_t^B + \eta_t^B p_t^B \Delta t & \text{if } p_t^B \geq 0, \\ r_t^B s_t^B + \frac{p_t^B \Delta t}{\zeta_t^B} & \text{otherwise,} \end{cases} \tag{A.17}$$

$$s_{t+1}^{H_2} = \begin{cases} 0 & \text{if } a_t^{H_2} > 0, \\ r_t^{H_2} s_t^{H_2} + \eta_t^{H_2} p_t^{H_2} \Delta t & \text{if } p_t^{H_2} \geq 0, \\ r_t^{H_2} s_t^{H_2} + \frac{p_t^{H_2} \Delta t}{\zeta_t^{H_2}} & \text{otherwise.} \end{cases} \tag{A.18}$$

A.2.5 Problem statement formalization

We now rely on the introduced formalism to define three optimization problems of increasing complexity. The first one focuses on the optimal operation of a microgrid, while the two others respectively include the optimal and robust sizing of the microgrid.

A.2.5.1 Optimal operation

Let $\mathcal{G}_T$ be the set of all positive scalar functions defined over the set of T-uplets of (state, action, environment) triplets:

$$\mathcal{G}_T = \left\{ G_T : (\mathcal{S} \times \mathcal{A}_t \times \mathcal{E})^T \to \mathbb{R}^+ \right\} . \tag{A.19}$$

Problem 1 *Given a function $G_T \in \mathcal{G}_T$ and a trajectory $(E_1, \ldots, E_T)$ of T environment vectors, we formalize the problem of optimal operation of*

a microgrid in the following way:

$$\begin{aligned} \min_{\substack{a_t \in \mathcal{A}_t, \forall t \in \mathcal{T} \\ s_t \in \mathcal{S}, \forall t \in \mathcal{T} \setminus \{1\}}} \quad & G_T((s_1, a_1, E_1), \ldots, (s_T, a_T, E_T)) \\ s.t. \quad & \mathbf{s}_t = f(\mathbf{s}_{t-1}, \mathbf{a}_{t-1}), \quad \forall t \in \mathcal{T} \setminus \{1\}, \\ & (a_t^{PV}, a_t^B, a_t^{H_2}) = (0, 0, 0), \quad \forall t \in \mathcal{T}. \end{aligned}$$

This problem determines the sequence of control variables that leads to the minimization of G_T when the sizing decisions are made once for all at a prior stage $t = 0$. The initial state $\mathbf{s}_1$ of the system contains the sizing information of the microgrid and stands as a parameter of this problem.

A.2.5.2 Optimal sizing under optimal operation

Let $\mathcal{G}_0$ be the set of all positive scalar functions defined over the set of (action, environment, T-long environment trajectory) triplets:

$$\mathcal{G}_0 = \left\{ G_0 : (\mathcal{A}_t \times \mathcal{E} \times \mathcal{E}^T) \to \mathbb{R}^+ \right\}. \tag{A.20}$$

Problem 2 *Given a function $G_0 \in \mathcal{G}_0$, a function $G_T \in \mathcal{G}_T$, a trajectory $(E_1, \ldots, E_T)$ of T environment vectors, and an initial environment E_0 that describes the available technologies at the sizing step, we formalize the problem of optimal sizing of a microgrid under optimal operation in the following way:*

$$\begin{aligned} \min_{\substack{a_t \in \mathcal{A}_t, s_t \in \mathcal{S}, \\ \forall t \in \{0\} \cup \mathcal{T}}} \quad & G_0(a_0, E_0, E_1, \ldots, E_T) + G_T((s_1, a_1, E_1), \ldots, (s_T, a_T, E_T)) \\ \text{s.t.} \quad & \mathbf{s}_t = f(\mathbf{s}_{t-1}, \mathbf{a}_{t-1}), \quad \forall t \in \mathcal{T}, \\ & \mathbf{s}_0 = \mathbf{0}, \\ & (a_t^{PV}, a_t^B, a_t^{H_2}) = (0, 0, 0), \quad \forall t \in \mathcal{T}, \end{aligned}$$

with $\mathbf{s}_0$ being the null vector to model that we start from an empty microgrid.

This problem determines an initial sizing decision $\mathbf{a}_0$ such that, together with the sequence of control variables over $\{1, \ldots, T\}$, it leads to the minimization of $G_0 + G_T$.

A.2.5.3 Robust sizing under optimal operation

Let $\mathbf{E}$ be a set of environment trajectories:

$$\begin{aligned}\mathbf{E} &= \{(E_t^1)_{t=1...T}, ..., (E_t^N)_{t=1...T}\}\,, \\ \text{with } E_t^i &\in \mathcal{E},\ \forall (t,i) \in \mathcal{T} \times \{1,\dots,N\}\,.\end{aligned} \tag{A.21}$$

Problem 3 *Given a function $G_0 \in \mathcal{G}_0$, a function $G_T \in \mathcal{G}_T$, an initial environment E_0, and a set $\mathbf{E}$ of trajectories of T environment vectors that describes the potential scenarios of operation that the microgrid could face, we formalize the problem of robust sizing of a microgrid under optimal operation in the following way:*

$$\begin{aligned}\min_{a_0 \in \mathcal{A}_0} \max_{i \in \{1,\dots,N\}} \min_{\substack{a_{i,t} \in \mathcal{A}_{i,t}, s_{i,t} \in \mathcal{S}, \\ \forall t \in \mathcal{T}}} \quad & G_0(a_0, E_0, E_1^i, \dots, E_T^i) \\ & + G_T((s_{i,1}, a_{i,1}, E_1^i), \dots, (s_{i,T}, a_{i,T}, E_T^i)) \\ \text{s.t.} \quad & \mathbf{s}_{i,t} = f(\mathbf{s}_{i,t-1}, \mathbf{a}_{i,t-1})\,, \quad \forall t \in \mathcal{T}\backslash\{1\}\,, \\ & \mathbf{s}_{i,1} = f(\mathbf{s}_0, \mathbf{a}_0)\,, \\ & \mathbf{s}_0 = \mathbf{0}\,, \\ & (a_{i,t}^{PV}, a_{i,t}^{B}, a_{i,t}^{H_2}) = (0,0,0), \quad \forall t \in \mathcal{T}\,.\end{aligned}$$

This robust optimization considers a microgrid under optimal operation and determines the sizing so that, in the worst case scenario, it minimizes the objective function. The innermost min is for the optimal operation, the max is for the worst environment trajectory and the outermost min is the minimization over the investment decisions. The outermost min-max succession is classic in robust optimizations (see e.g. [104]).

A.2.6 The specific case of the Levelized Energy Cost

In this section, we introduce the $r-$discounted levelized energy cost (LEC), denoted LEC_r, which is an economic assessment of the cost that covers all the expenses over the lifetime of the microgrid (i.e. initial investment, operation, maintenance and cost of capital). We then show how to choose functions $G_0 \in \mathcal{G}_0$ and $G_T \in \mathcal{G}_T$ such that Problems 1, 2, and 3 result in the optimization of this economic assessment. Focusing on the decision processes that consist

only with an initial investment (i.e. a single sizing decision taking place at $t = 1$) for the microgrid, followed by the control of its operation, we can write the expression for LEC_r as

$$LEC_r = \frac{I_0 + \sum_{y=1}^{n} \frac{M_y}{(1+r)^y}}{\sum_{y=1}^{n} \frac{\varepsilon_y}{(1+r)^y}}, \tag{A.22}$$

where

- n denotes the lifetime of the system in years;
- I_0 corresponds to the initial investment expenditures;
- M_y represents the operational expenses in the year y;
- ε_y is electricity consumption in the year y;
- r denotes the discount rate which may refer to the interest rate or to the discounted cash flow.

Note that, in the more common context of an electrical generation facility, the LEC_r can be interpreted as the price at which the electricity generated must be sold to break even over the lifetime of the project. For this reason, it is often used to compare the costs of different electrical generation technologies. When applied to the microgrid case, it can also be interpreted as the retail price at which the electricity from the grid must be bought in order to face the same costs when supplying a sequence $(\varepsilon_1, \ldots, \varepsilon_n)$ of yearly consumptions.

The initial investment expenditures I_0 and the yearly consumptions ε_y are simple to express as a function of the initial sizing decision $\mathbf{a}_0$ and environment vector $\mathbf{E}_0$ for the former, and of the environment trajectory $(E_1, \ldots, E_T)$ for the latter. Let $\tau_y \subset \mathcal{T}$ denotes, $\forall y \in \{1, \ldots, n\}$, the set of time steps t belonging to year y, we have:

$$I_0 = a_0^{PV} c_0^{PV} + a_0^{B} c_0^{B} + a_0^{H_2} c_0^{H_2} \tag{A.23}$$

$$\varepsilon_y = \sum_{t \in \tau_y} c_t \ \Delta t, \ \forall y \in \{1, \ldots, n\}. \tag{A.24}$$

From these two quantities, we can define the function $G_0 \in \mathcal{G}_0$ that implements the LEC case as:

$$\begin{aligned} G_0(a_0, E_0, E_1, \ldots, E_T) &= \frac{I_0}{\sum_{y=1}^{n} \frac{\varepsilon_y}{(1+r)^y}} \\ &= \frac{a_0^{PV} c_0^{PV} + a_0^{B} c_0^{B} + a_0^{H_2} c_0^{H_2}}{\sum_{y=1}^{n} \frac{\sum_{t \in \tau_y} c_t \Delta t}{(1+r)^y}}, \end{aligned} \tag{A.25}$$

while the remaining term of LEC_r defines $G_T \in \mathcal{G}_T$:

$$G_T((s_1, a_1, E_1), \ldots, (s_T, a_T, E_T)) = \frac{\sum_{y=1}^{n} \frac{M_y}{(1+r)^y}}{\sum_{y=1}^{n} \frac{\varepsilon_y}{(1+r)^y}} \,. \tag{A.26}$$

The last quantities to specify are the yearly operational expenses M_y, which correspond to the opposite of the sum over the year $y \in \mathcal{Y}$ of the revenues ρ_t observed at each time step $t \in \tau_y$ when operating the microgrid:

$$M_y = -\sum_{t \in \tau_y} \rho_t \,. \tag{A.27}$$

These revenues are more complex to determine than the investment expenditures and depend, among other elements, on the model of interaction $\boldsymbol{\mu}_t$ at the time of the operation.

A.2.6.1 Operational revenues

The instantaneous operational revenues ρ_t at time step $t \in \mathcal{T}$ correspond to the reward function of the system. This is a function of the electricity demand c_t, of the solar irradiance i_t, of the model of interaction $\boldsymbol{\mu}_t = (k, \beta)$, and of the control actions $\mathbf{a}_t^{(o)}$:

$$\rho_t : (c_t, i_t, \boldsymbol{\mu}_t, \mathbf{a}_t^{(o)}) \to \mathbb{R} \,.$$

We now introduce three quantities that are prerequisites to the definition of the reward function:

- ϕ_t [kW] $\in \mathbb{R}^+$ is the electricity generated locally by the photovoltaic installation, we have:

$$\phi_t = \eta_t^{PV} x_t^{PV} i_t \,; \tag{A.28}$$

- d_t [kW] $\in \mathbb{R}$ denotes the net electricity demand, which is the difference between the local consumption and the local production of electricity:

$$d_t = c_t - \phi_t \,; \tag{A.29}$$

- δ_t [kW] $\in \mathbb{R}$ represents the power balance within the microgrid, taking into account the contributions of the demand and of the storage devices:

$$\delta_t = -p_t^B - p_t^{H_2} - d_t \,. \tag{A.30}$$

These quantities are illustrated in a diagram of the system in Figure A.1, which allows for a more intuitive understanding of the power flows within the microgrid.

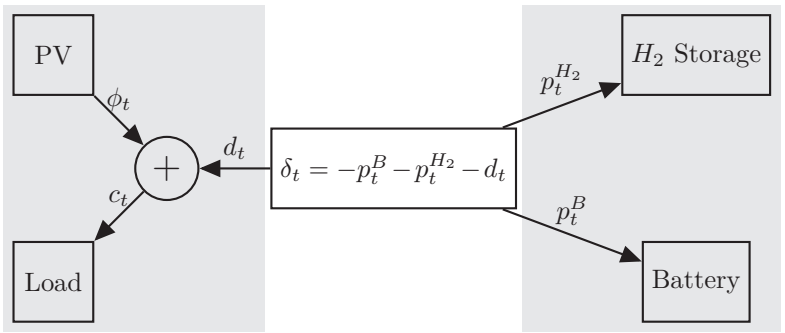

Figure A.1: Schema of the microgrid featuring PV panels associated with a battery and a hydrogen storage device.

At each time step $t \in \mathcal{T}$, a positive power balance δ_t reflects a surplus of production within the microgrid, while it is negative when the power demand is not met. As the law of conservation of energy requires that the net power within the microgrid must be null, compensation measures are required when δ_t differs from zero. In the case of a connected microgrid, this corresponds to a power exchange with the grid. In the case of an off-grid system, a production curtailment or a load shedding is required. The instantaneous operational revenues we consider correspond to the financial impact of a surplus or lack of production. The reward function ρ_t is a linear function of the power balance δ_t and, because the price β at which the energy surplus can be sold to the grid usually differs from the retail price k to buy electricity from the grid, the definition of the reward function at time step $t \in \mathcal{T}$ depends of the sign of δ_t:

$$\rho_t = \begin{cases} \beta\ \delta_t \Delta t & \text{if } \delta_t \geq 0\,, \\ k\ \delta_t \Delta t & \text{otherwise.} \end{cases} \tag{A.31}$$

Using Equations A.28, A.29, and A.30, the reward function can be expressed as a function of the system variables:

$$\rho_t = \begin{cases} \beta\ (-p_t^B - p_t^{H_2} - c_t + \eta_t^{PV} x_t^{PV} i_t)\ \Delta t & \text{if } -p_t^B - p_t^{H_2} - c_t + \eta_t^{PV} x_t^{PV} i_t \geq 0\,, \\ k\ (-p_t^B - p_t^{H_2} - c_t + \eta_t^{PV} x_t^{PV} i_t)\ \Delta t & \text{otherwise.} \end{cases} \tag{A.32}$$

A.3 Optimisation

In this section, we detail how to implement the LEC version of Problems 1, 2, and 3, to obtain an optimal solution using mathematical programming techniques. Even though the formalization of the problem includes non-linear relations (e.g. Equations A.17, A.18, and A.32), we show how to obtain a linear program by using auxiliary variables. The presented approach assumes that the following conditions are met:

- a single candidate technology is considered for each device type (i.e. $J = L = M = 1$);
- the lifetime of the devices is at least as long as the considered time-horizon (i.e. $L^{PV}, L^{B}, L^{H_2} \geq T$) and the aging of the devices can thus be ignored;
- the whole trajectory $E_1, \ldots, E_T$ of environment vectors is known at the time of operation (i.e. when minimizing G_T).

A.3.1 Optimal operation over a known trajectory

We first consider the implementation as a linear program of Problem 1 with G_T defined by Equation A.26. The output of this program is the optimal sequence of control actions $\mathbf{a}_t^{(o)} = (p_t^{H_2}, p_t^{B})$ and the corresponding minimal value of G_T over the considered time-horizon T. Before writing the optimization model, we introduce, $\forall t \in \mathcal{T}$, the following auxiliary variables:

$$p_t^{B,+}, p_t^{B,-}, p_t^{H_2,+}, p_t^{H_2,-}, \delta_t^{+}, \delta_t^{-} \in \mathbb{R}^{+}, \text{ such that } \begin{cases} p_t^{B} = p_t^{B,+} - p_t^{B,-} \\ p_t^{H_2} = p_t^{B,+} - p_t^{B,-} \\ \delta_t = \delta_t^{+} - \delta_t^{-} \end{cases},$$

which allow the use of the adequate efficiency factor (i.e. η or ξ) and price (i.e. k or β) depending on the direction of the power flows. The overall linear program $\mathcal{M}_{\text{op}}$, having as parameters the time-horizon T, the time step Δt, the number of years n spanned by the time-horizon, the sets $\tau_1, \ldots, \tau_n$ mapping years to time steps, the discount rate r, a trajectory $\mathbf{E}_1, \ldots, \mathbf{E}_T$ of the exogenous variables, and the time-invariant sizing state

$\mathbf{s}^{(s)} = (x^{PV},x^{B},x^{H_2},P^{B},R^{H_2},\eta^{PV},\eta^{B},\eta^{H_2},\zeta^{B},\zeta^{H_2},r^{B},r^{H_2})$ of the devices, can be written as:

$$\mathcal{M}_{\text{op}}\big(T,\Delta t,n,\tau_1,\dots,\tau_n,r,\mathbf{E}_1,\dots,\mathbf{E}_T,\mathbf{s}^{(s)}\big) \tag{A.33a}$$

$$= \min \quad \frac{\sum_{y=1}^{n} \frac{M_y}{(1+r)^y}}{\sum_{y=1}^{n} \frac{\sum_{t\in\tau_y} c_t \Delta t}{(1+r)^y}} \tag{A.33b}$$

$$\text{s.t.} \quad \forall y \in \{1,\dots,n\}: \tag{A.33c}$$

$$M_y = \sum_{t\in\tau_y} \left(k\,\delta_t^- - \beta\,\delta_t^+\right)\Delta t\,, \tag{A.33d}$$

$$\forall t \in \{1,\dots,T\}: \tag{A.33e}$$

$$0 \le s_t^B \le x^B\,, \tag{A.33f}$$

$$0 \le s_t^{H_2} \le R^{H_2}\,, \tag{A.33g}$$

$$-P^B \le p_t^B \le P^B\,, \tag{A.33h}$$

$$-x^{H_2} \le p_t^{H_2} \le x^{H_2}\,, \tag{A.33i}$$

$$\delta_t = -p_t^B - p_t^{H_2} - c_t + \eta^{PV} x^{PV} i_t\,, \tag{A.33j}$$

$$p_t^B = p_t^{B,+} - p_t^{B,-}\,, \tag{A.33k}$$

$$p_t^{H_2} = p_t^{B,+} - p_t^{B,-}\,, \tag{A.33l}$$

$$\delta_t = \delta_t^+ - \delta_t^-\,, \tag{A.33m}$$

$$p_t^{B,+}, p_t^{B,-}, p_t^{H_2,+}, p_t^{H_2,-}, \delta_t^+, \delta_t^- \ge 0\,, \tag{A.33n}$$

$$\forall t \in \{2,\dots,T\}: \tag{A.33o}$$

$$s_t^B = r^B s_{t-1}^B + \eta^B p_{t-1}^{B,+} - \tfrac{p_{t-1}^{B,-}}{\zeta^B}\,, \tag{A.33p}$$

$$s_t^{H_2} = r^{H_2} s_{t-1}^{H_2} + \eta^B p_{t-1}^{H_2,+} - \tfrac{p_{t-1}^{H_2,-}}{\zeta^{H_2}}\,, \tag{A.33q}$$

$$-\zeta^B s_T^B \le p_T^B \le \tfrac{x^B - s_T^B}{\eta^B}\,, \tag{A.33r}$$

$$-\zeta^{H_2} s_T^{H_2} \le p_T^{H_2} \le \tfrac{R^{H_2} - s_T^{H_2}}{\eta^{H_2}}\,. \tag{A.33s}$$

The physical limits of the storage devices are modeled by Constraints A.33f-A.33i, while the transition laws of their state correspond to Constraints A.33p and A.33q. Because of the absence of time step $T+1$, there is no guarantee that the charge levels that immediately follow the time-horizon are positive, which is why Constraints A.33r and A.33s ensure that the last action $\mathbf{a}_T^{(o)}$ is compatible with the last charge level of the devices. Finally, Constraints A.33j and A.33d respectively denote the power balance within the microgrid and the cost it induces on a yearly scale.

A.3.2 Optimal sizing under optimal operation

In Problem 2, the initial sizing of the microgrid becomes an output of the optimization model and the function G_0, here defined by Equation A.25, integrates the objective function. We denote this new problem by $\mathcal{M}_{\text{size}}$, which is still a linear program:

$$\mathcal{M}_{\text{size}}(T,\Delta t,n,\tau_1,...,\tau_n,r,\mathbf{E}_0,\mathbf{E}_1,...,\mathbf{E}_T) \tag{A.34a}$$

$$= \min \quad \frac{I_0 + \sum_{y=1}^{n} \frac{M_y}{(1+r)^y}}{\sum_{y=1}^{n} \frac{\sum_{t\in\tau_y} c_t \Delta t}{(1+r)^y}} \tag{A.34b}$$

$$\text{s.t.} \quad I_0 = a_0^{PV} c_0^{PV} + a_0^B c_0^B + a_0^{H_2} c_0^{H_2}\,, \tag{A.34c}$$

$$(x^B, x^{H_2}, x^{PV}) = (a_0^B, a_0^{H_2}, a_0^{PV})\,, \tag{A.34d}$$

$$A.33c - A.33s\,. \tag{A.34e}$$

This new model includes all the constraints from $\mathcal{M}_{\text{op}}$, as well as the definition of the sizing of the devices from the initial sizing decisions, i.e. Constraint A.34d, and the expression of the initial investment as a function of these sizing decisions, i.e. Constraint A.34c. Note that the value of physical properties of the devices other then variables x^B, x^{H_2}, x^{PV} is provided by the initial environment vector $\mathbf{E}_0$, which also provides the cost of the available technology for every device type.

A.3.3 Robust sizing under optimal operation

The extension of linear program $\mathcal{M}_{\text{size}}$ to an optimization model that integrates a set $\mathbf{E} = \{(E_t^1)_{t=1...T}, ..., (E_t^N)_{t=1...T}\}$ of candidate trajectories of the environment vectors, i.e. to the implementation of Problem 3, is straightforward and requires two additional levels of optimization:

$$\mathcal{M}_{\text{rob}}(T,\Delta t,n,\tau_1,...,\tau_n,r,\mathbf{E}_0,\mathbf{E})$$

$$= \min_{a_0^B, a_0^{H_2}, a_0^{PV}} \max_{i\in 1,...,N} \mathcal{M}_{\text{size}}(T,\Delta t,n,\tau_1,...,\tau_n,r,\mathbf{E}_0,\mathbf{E}_1^{(i)},...,\mathbf{E}_T^{(i)})\,. \tag{A.35}$$

This mathematical program cannot be solved using only linear programming techniques. In particular, the numerical results reported further in this chap-

ter relied on an exhaustive search approach to address the outer min max, considering a discretized version of sizing variables.

A.4 Simulations

This section presents case studies of the proposed operation and sizing problems of a microgrid. We first detail the considered technologies, specify the corresponding parameter values, and showcase the optimal operation of a fixed-size microgrid. The optimal sizing approaches are then run using realistic price assumptions and using historical measures of residential demand and of solar irradiance with $\Delta t = 1h$. By comparing the solutions for irradiance data of both Belgium and Spain, we observe that they depend heavily on this exogenous variable. Finally, we compare the obtained LEC values with the current retail price of electricity and stress the precautions to be taken when interpreting the results.

A.4.1 Technologies

In this subsection, we describe the parameters that we consider for the PV panels, the battery and the hydrogen storage device. The physical parameters are selected to fit, at best, the state-of-the-art manufacturing technologies, and the costs that we specify are for self-sufficient devices, i.e. including the required converters or inverters to enable their correct operation.

PV panels. The electricity is generated by converting sunlight into direct current (DC) electricity using materials that exhibit the photovoltaic effect. Driven by advances in technology as well as economies of manufacturing scale, the cost of PV panels has steadily declined and is about to reach a price of 1€/W$_p$ with inverters and balance of systems included [105]. The parameters that are taken into account in the simulations can be found in Table A.1.

Parameter	Value
c^{PV}	1€/W$_p$
η^{PV}	18%
L^{PV}	20 years

Table A.1: Characteristics used for the PV panels.

Battery The purpose of the battery is to act as a short-term storage device; it must therefore have good charging and discharging efficiencies as well as enough specific power to handle all the short-term fluctuations. The charge retention rate and the energy density are not major concerns for this device. A battery's characteristics may vary due to many factors, including internal chemistry, current drain and temperature, resulting in a wide range of available performance characteristics. Compared to lead-acid batteries, $LiFePO_4$ batteries are more expensive but offer a better capacity, a longer lifetime and a better power density [106]. We consider this latter technology and Table A.2 summarizes the parameters that we deem to be representative. $LiFePO_4$ batteries are assumed to have a power density that is sufficient to accommodate the instantaneous power supply of the microgrid. It is also assumed to have a charging efficiency (η^c) and discharging efficiency (ζ_0^B) of 90% for a round trip efficiency of 81%. Finally, we consider a cost of 500 €per usable kWh of storage capacity (c^B).

Parameter	Value
c^B	500 €/kWh
η_0^B	90%
ζ_0^B	90%
P^B	$>$ 10kW
r^B	99%/month
L^B	20 years

Table A.2: Data used for the $LiFePO_4$battery.

Hydrogen storage device The long-term storage device must store a large quantity of energy at a low cost while its specific power is less critical than that for the battery. In this chapter we will consider a hydrogen-based storage technology composed of three main parts: (i) an electrolyzer that transforms water into hydrogen using electricity (ii) a tank where the hydrogen is stored (iii) a fuel cell where the hydrogen is transformed into electricity (note that a (combined heat and) power engine could be used instead). This hydrogen storage device is such that the maximum input power of the fuel cell before losses is equal to the maximum output power of the electrolyzer after losses. The considered parameters are presented in Table A.3.

A.4.2 Optimal operation

An example of output of the optimal operation program $\mathcal{M}_{\text{op}}$ in Figure A.2b illustrates well the role of each storage device. The figure sketches the evolution

Parameter	Value
c^{H_2}	14 €/W$_p$
$\eta_0^{H_2}$	65%
$\zeta_0^{H_2}$	65%
r^{H_2}	99%/month
L^{H_2}	20 years
R^{H_2}	∞

Table A.3: Data used for the Hydrogen storage device.

of the charge levels of the battery and of the hydrogen storage device when facing the net demand defined in Figure A.2a. In this example, the battery has a capacity of 3kWh and the hydrogen storage device has a power limit of 1kW. The role of each storage device is clear as we observe that the battery handles the short fluctuations, while the hydrogen device accumulates the excesses of production on a longer time-scale. Overall, since the production is higher than the consumption by a significant margin, the optimization problem is not constrained and hydrogen is left in the tank at the end of the simulation.

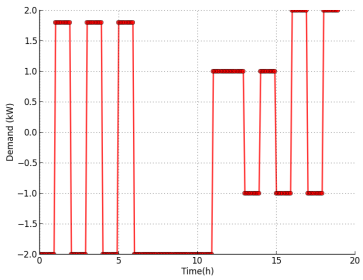

(a) Net demand (negative demand represents a production higher than the consumption)

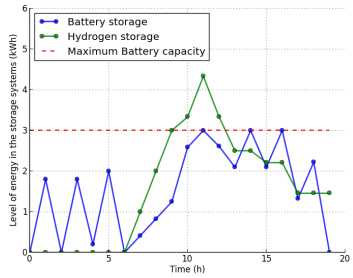

(b) Optimal operation of the storage devices

Figure A.2: Left graphic shows the evolution of the charge levels within a microgrid that faces the given net demand of right graphic.

A.4.3 Production and consumption profiles

In this subsection, we describe the PV production profiles and the consumption profiles that will be used in the remaining simulations.

A.4.3.1 PV production

Solar irradiance varies throughout the year depending on the seasons, and it also varies throughout the day depending on the weather and the position of the sun in the sky relative to the PV panels. Therefore, the production profile varies strongly as a function of the geographical area, mainly as a function of the latitude of the location. The two cases considered in this chapter are a residential consumer of electricity in the south of Spain and in Belgium. The main distinction between these profiles is the difference between summer and winter PV production. In particular, production in the south of Spain varies with a factor 1:2 between winter and summer (see Figure A.3) and changes to a factor of about 1:5 in Belgium or in the Netherlands (see Figure A.4).

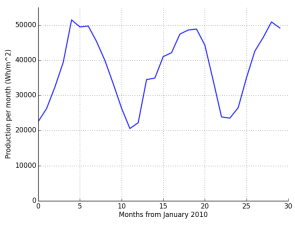

Total energy produced per month

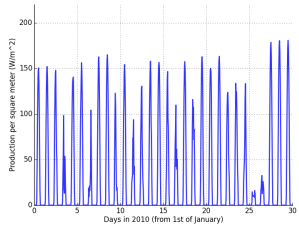

Example of production in winter

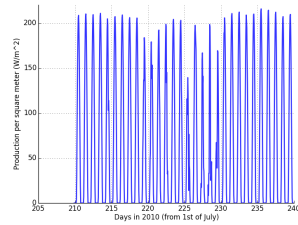

Example of production in summer

Figure A.3: Simulated production of PV panels in the South of Spain (Data from Solargis [107] for the solar platform of Almeria in Spain).

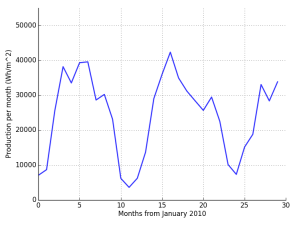

Total energy produced per month

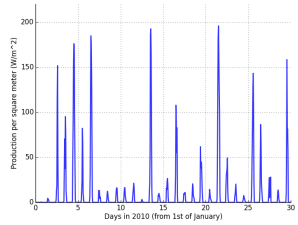

Example of production in winter

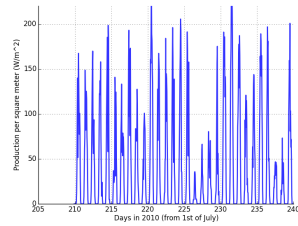

Example of production in summer

Figure A.4: Measurements of PV panels production for a residential customer located in Belgium.

A.4.3.2 Consumption

A simple residential consumption profile is considered with a daily consumption of 18kWh. The profile can be seen on Figure A.5. This profile is a good substitute of any residential consumption profile with the same average consumption per day. Additional precautions should be taken in the case of high consumption peaks to ensure that the battery will be able to handle large power outputs. Note that in a more realistic case, we may have higher consumption during winter, which may substantially affect the sizing and operation solutions.

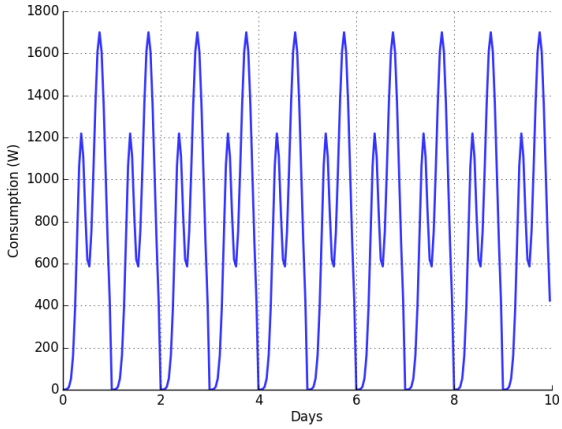

Figure A.5: Representative residential consumption profile.

A.4.4 Optimal sizing and robust sizing

For the optimal sizing under optimal operation of the microgrid, as defined by Problem 2, we use a unique scenario built from the data described in Section A.4.3 for the consumption and production profiles. Since the available data are shorter than the time-horizon, we repeat them so as to obtain a twenty-year-long time-horizon. In the following we make the hypothesis that $\beta = 0$ €/kWh.

For the robust optimization of the sizing, we refer to the Problem 3. This approach requires the selection of a set of different environment trajectories

and, for computational purposes, to discretize the sizing states. The three different scenarios considered are the following:

- The production is 10% lower and the consumption is 10% higher than the representative residential production/consumption profile.
- The production and the consumption are conform to the representative residential production/consumption profile (scenario used in the non-robust optimisation)
- The production is 10% higher and the consumption is 10% lower than the representative residential production/consumption profile.

To build the discretized sizing states we start by solving Problem 2 on the mean scenario. For our simulations we then select all possible variations compared to the sizing of each variable x^B, x^{H_2} and x^{PV} by +0%, +10% and +20%. This leaves us with 27 possible sizings that are used to build the discretized sizing space. Equation A.35 is solved by performing an exhaustive search over this set of potential sizings so as to obtain the robust LEC.

A.4.4.1 The Spanish case

We first considered a residential consumer of electricity located in Spain. For different values of costs k endured per kWh not supplied within the microgrid, we performed the optimal sizing and the robust-type optimization schemes described above. We reported the obtained LEC in Figure A.6. We observed the following : (i) for a retail price of 0.2€/kWh, the residential consumer of electricity benefits from a LEC of slightly more than 0.10€/kWh; (ii) in the fully off-grid case, the microgrid is still more profitable than buying electricity at all times from the utility grid for all configurations as long as k is lower than approximately 3€/kWh (i.e. with a value of loss load smaller than 3 €/kWh, it is always preferable to go fully off-grid than buying all the electricity from the grid); (iii) due to the relatively low inter-seasonal fluctuations (compared to Belgium for instance (see later)) investing in a hydrogen storage system is not actually profitable for low values of k.

A.4.4.2 The Belgian case

We then considered a residential consumer of electricity located in Belgium and we reported the obtained LEC for different values of k. As can be seen

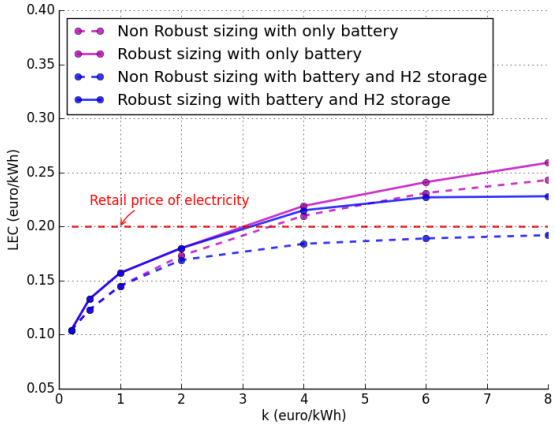

Figure A.6: LEC ($r = 2\%$) in Spain over 20 years for different investment strategy as a function of the cost endured per kWh not supplied within the microgrid.

from Figure A.7, a residential consumer of electricity in Belgium has incentives to invest in his own microgrid system (at least PV panels) since the obtained LEC while operating in parallel with the main utility grid at a retail price of 0.2€/kWh gives the residential consumer of electricity a lower electricity price than buying it from the grid at all times. With the current state of the technology however, it is not yet profitable for a residential consumer of electricity in Belgium to go fully off-grid since they would then suffer from a higher overall cost. Contrary to the results observed for Spain, in Belgium there is an important potential gain in combining both short-term and long-term energy storage devices. This is due to the critical inter-seasonal fluctuations of PV electrical production in Belgium.

We also investigate how the LEC evolves as a function of the price decrease of the elements in the microgrid. Figure A.8 shows the reported LEC as a function of a uniform price decrease of the elements of the microgrid while assuming a value of loss load of 0.2€/kWh and a robust sizing. It is shown that when the prices of constitutive elements of the microgrid are less than half of those given in A.1, A.2, and A.3, the business case for a fully off-grid microgrid in Belgium may actually become cost-effective.

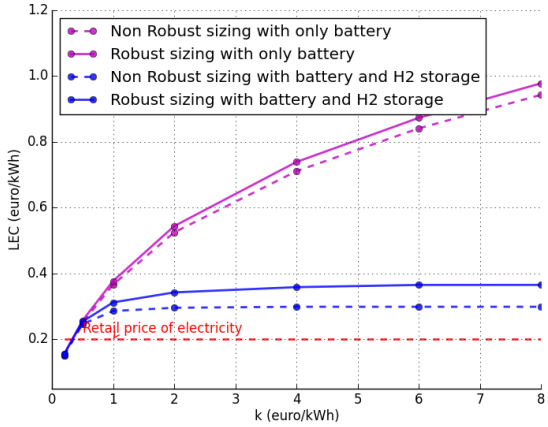

Figure A.7: LEC (r=2%) in Belgium over 20 years for different investment strategy as a function of the cost endured per kWh not supplied within the microgrid.

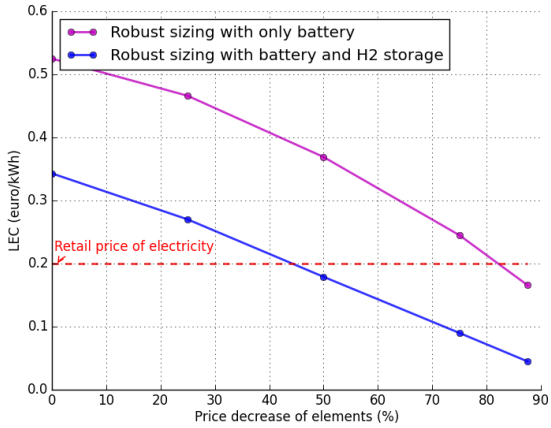

Figure A.8: LEC (r=2%) in Belgium over 20 years for a value of loss load of 2€/kWh as a function of a uniform price decrease for all the constitutive elements of the microgrid.

A.5 Conclusion

This chapter has proposed a novel formulation of electrical microgrids featuring PV, long-term (hydrogen) and short-term (batteries) storage devices. Using linear programming we managed to set up an algorithm for optimally sizing

and operating microgrids under some (potentially robust) hypotheses on the surrounding environment. The approach has been illustrated in the context of Belgium and Spain, for which we evaluate the values of the LEC and compare it with the cost of electricity from traditional electricity networks.

Future works will include relaxing the assumption that the future is deterministically known when computing the optimal operation. In particular, we plan to investigate how to incorporate stochastic weather forecasts in the optimization of the microgrid operation.

Bibliography

[1] D. Fouquet and T. B. Johansson. European renewable energy policy at crossroads – Focus on electricity support mechanisms. *Energy Policy*, 36(11):4079–4092, 2008.

[2] B. Cornélusse, D. Vangulick, M. Glavic, and D. Ernst. Global capacity announcement of electrical distribution systems: A pragmatic approach. *Sustainable Energy, Grids and Networks*, 4:43–53, 2015.

[3] D. T. Wang, L. F. Ochoa, and G. P. Harrison. Dg impact on investment deferral: Network planning and security of supply. *Power Systems, IEEE Transactions on*, 25(2):1134–1141, 2010.

[4] J. A. P. Lopes, N. Hatziargyriou, J. Mutale, P. Djapic, and N. Jenkins. Integrating distributed generation into electric power systems: A review of drivers, challenges and opportunities. *Electric Power Systems Research*, 77(9):1189–1203, 2007.

[5] S. N. Liew and G. Strbac. Maximising penetration of wind generation in existing distribution networks. *IEE Proceedings: Generation, Transmission and Distribution*, 149(3):256–262, 2002.

[6] L. F. Ochoa, C. J. Dent, and G. P. Harrison. Distribution network capacity assessment: Variable DG and active networks. *IEEE Transactions on Power Systems*, 25(1):87–95, 2010.

[7] M. J. Dolan, E. M. Davidson, I. Kockar, G. W. Ault, and S. D. J. McArthur. Distribution power flow management utilizing an online optimal power flow technique. *IEEE Transactions on Power Systems*, 27(2):790–799, 2012.

[8] Q. Gemine, E. Karangelos, D. Ernst, and B. Cornelusse. Active network management: Planning under uncertainty for exploiting load modulation. In *Bulk Power System Dynamics and Control - IX Optimization, Security and Control of the Emerging Power Grid (IREP), IREP Symposium*, 2013.

[9] S. Gill, I. Kockar, and G. Ault. Dynamic optimal power flow for active distribution networks. *Power Systems, IEEE Transactions on*, 29(1):121–131, 2014.

[10] L. H. Macedo, J. F. Franco, M. J. Rider, and R. Romero. Optimal operation of distribution networks considering energy storage devices. *Smart Grid, IEEE Transactions on*, 6(6):2825–2836, 2015.

[11] F. Olivier, P. Aristidou, D. Ernst, and T. Van Cutsem. Active management of low-voltage networks for mitigating overvoltages due to photovoltaic units. *Smart Grid, IEEE Transactions on*, 7(2):926–936, 2015.

[12] F. Capitanescu, J. L. Martinez Ramos, P. Panciatici, D. Kirschen, A. Marano Marcolini, L. Platbrood, and L. Wehenkel. State-of-the-art, challenges, and future trends in security constrained optimal power flow. *Electric Power Systems Research*, 81(8):1731–1741, 2011.

[13] L. F. Ochoa and G. P. Harrison. Minimizing energy losses: Optimal accommodation and smart operation of renewable distributed generation. *IEEE Transactions on Power Systems*, 26(1):198–205, 2011.

[14] L. F. Ochoa and G. P. Harrison. Using AC optimal power flow for DG planning and optimisation. In *IEEE PES General Meeting*, 2010.

[15] H. Klinge Jacobsen and S. T. Schröder. Curtailment of renewable generation: Economic optimality and incentives. *Energy Policy*, 49(C):663–675, 2012.

[16] S. W. Wallace and S.-E. Fleten. Stochastic programming models in energy. *Handbooks in operations research and management science*, 10:637–677, 2003.

[17] A. Shapiro, D. Dentcheva, and A. Ruszczyński. *Lectures on Stochastic Programming: Modeling and Theory*. SIAM, 2009.

[18] T. Achterberg. SCIP: solving constraint integer programs. *Mathematical Programming Computation*, 1(1):1–41, January 2009.

[19] A. Wächter and L. Biegler. On the implementation of a primal-dual interior point filter line search algorithm for large-scale nonlinear programming. *Mathematical Programming*, 106(1):25—-57, 2006.

[20] R. Byrd, J. Nocedal, and R. Waltz. Knitro: an integrated package for nonlinear optimization. *Large-scale nonlinear optimization*, pages 1–25, 2006.

[21] S. Mathieu, D. Ernst, and Q. Louveaux. An efficient algorithm for the provision of a day-ahead modulation service by a load aggregator. In *IEEE PES ISGT Europe 2013*, pages 1–5. IEEE, 2013.

[22] J. Lavaei and S. H. Low. Zero Duality Gap in Optimal Power Flow Problem. *IEEE Transactions on Power Systems*, 27(1):92–107, February 2012.

[23] D. Phan. Lagrangian duality and branch-and-bound algorithms for optimal power flow. *Operations Research*, 60(2):275–285, May 2012.

[24] B. Cornélusse. *Supervised Learning for Sequential and Uncertain Decision Making Problems - Application to Short-Term Electric Power Generation Scheduling.* PhD thesis, Université de Liège, 2010.

[25] B. Defourny, D. Ernst, and L. Wehenkel. Multistage stochastic programming: A scenario tree based approach to planning under uncertainty. *Decision theory models for applications in artificial intelligence: concepts and solutions, Sucar LE, Morales EF, Hoey J (eds). Information Science Publishing: Hershey, Pennsylvania, USA*, 2011.

[26] M. Aguado, R. Bourgeois, J. Y. Bourmaud, J. Casteren, M. Ceratto, M. Jäkel, B. Malfliet, C. Mestda, P. Noury, M. Pool, et al. Flow-based market coupling in the central western european region–on the eve of implementation. *CIGRE, C5-204*, 2012.

[27] F. Capitanescu, M. Glavic, D. Ernst, and L. Wehenkel. Interior-point based algorithms for the solution of optimal power flow problems. *Electric Power Systems Research*, 77(5–6):508–517, 2007.

[28] S. Bose, D. F. Gayme, K. M. Chandy, and S. H. Low. Quadratically constrained quadratic programs on acyclic graphs with application to power flow. *ArXiv e-prints*, 2012.

[29] L. Gan, N. Li, U. Topcu, and S. Low. On the exactness of convex relaxation for optimal power flow in tree networks. In *Proceedings of the IEEE 51st Annual Conference on Decision and Control (CDC)*, pages 465–471, 2012.

[30] A. Gopalakrishnan, A. U. Raghunathan, D. Nikovski, and L. T. Biegler. Global optimization of optimal power flow using a branch & bound algorithm. In *Communication, Control, and Computing (Allerton), 50th Annual Allerton Conference on*, pages 609–616, 2012.

[31] D. Gayme and U. Topcu. Optimal power flow with distributed energy storage dynamics. In *American Control Conference (ACC)*, pages 1536–1542, 2011.

[32] A. Gopalakrishnan, A. U. Raghunathan, D. Nikovski, and L. T. Biegler. Global optimization of multi-period optimal power flow. In *American Control Conference (ACC)*, pages 1157–1164, 2013.

[33] N. Alguacil and A. J. Conejo. Multiperiod optimal power flow using benders decomposition. *Power Systems, IEEE Transactions on*, 15(1):196–201, 2000.

[34] S. Boyd, L. Xiao, and A. Mutapcic. Subgradient methods. *lecture notes, Stanford University*, 2003.

[35] S. Feltenmark and K. C. Kiwiel. Dual applications of proximal bundle methods, including lagrangian relaxation of nonconvex problems. *SIAM Journal on Optimization*, 10(3):697–721, 2000.

[36] H. D. Sherali and W. P. Adams. *A reformulation-linearization technique for solving discrete and continuous nonconvex problems*, volume 31 of *Nonconvex Optimization and Its Applications*. Springer, 1998.

[37] J. P. Ruiz and I. E. Grossmann. Using redundancy to strengthen the relaxation for the global optimization of MINLP problems. *Computers & Chemical Engineering*, 35(12):2729–2740, 2011.

[38] K. M. Anstreicher. On convex relaxations for quadratically constrained quadratic programming. *Mathematical programming*, 136(2):233–251, 2012.

[39] C. Helmberg. The conicbundle library for convex optimization, 2009.

[40] E. D. Andersen, C. Roos, and T. Terlaky. On implementing a primal-dual interior-point method for conic quadratic optimization. *Mathematical Programming*, 95(2):249–277, 2003.

[41] G. Guennebaud, B. Jacob, et al. Eigen v3. http://eigen.tuxfamily.org, 2010.

[42] A. J. Wood and B. F. Wollenberg. *Power generation, operation, and control*. John Wiley & Sons, 2012.

[43] R. D. Zimmerman, C. E. Murillo-Sánchez, and R. J. Thomas. Matpower: Steady-state operations, planning, and analysis tools for power systems research and education. *Power Systems, IEEE Transactions on*, 26(1):12–19, 2011.

[44] R. Christie. Power systems test case archive. *Electrical Engineering dept., University of Washington*, 2000.

[45] E. L. Lawler and D. E. Wood. Branch-and-bound methods: A survey. *Operations research*, 14(4):699–719, 1966.

[46] P. Panciatici, G. Bareux, and L. Wehenkel. Operating in the fog: Security management under uncertainty. *Power and Energy Magazine, IEEE*, 10(5):40–49, 2012.

[47] H. Farhangi. A road map to integration: Perspectives on smart grid development. *Power and Energy Magazine, IEEE*, 12(3):52–66, 2014.

[48] P. Auer, N. Cesa-Bianchi, and P. Fischer. Finite-time analysis of the multiarmed bandit problem. *Machine learning*, 47(2-3):235–256, 2002.

[49] P. Pinson, C. Chevallier, and G. N. Kariniotakis. Trading wind generation from short-term probabilistic forecasts of wind power. *Power Systems, IEEE Transactions on*, 22(3):1148–1156, 2007.

[50] A. M. Foley, P. G. Leahy, A. Marvuglia, and E. J. McKeogh. Current methods and advances in forecasting of wind power generation. *Renewable Energy*, 37(1):1–8, 2012.

[51] P. Chen, T. Pedersen, B. Bak-Jensen, and Z. Chen. Arima-based time series model of stochastic wind power generation. *Power Systems, IEEE Transactions on*, 25(2):667–676, 2010.

[52] P. Bacher, H. Madsen, and H. A. Nielsen. Online short-term solar power forecasting. *Solar Energy*, 83(10):1772–1783, 2009.

[53] G. Valverde, J. Q. Tortós, and V. Terzija. Comparison of gaussian mixture reductions for probabilistic studies in power systems. In *Power and Energy Society General Meeting, 2012 IEEE*, pages 1–7. IEEE, 2012.

[54] R. Singh, B. C. Pal, R. Jabr, et al. Statistical representation of distribution system loads using gaussian mixture model. *Power Systems, IEEE Transactions on*, 25(1):29–37, 2010.

[55] N. Abdel-Karim and M. Ilic. Modeling uncertain load and wind power in the electric energy systems. In *Power and Energy Society General Meeting, 2012 IEEE*, pages 1–8. IEEE, 2012.

[56] E. Eirola and A. Lendasse. Gaussian mixture models for time series modelling, forecasting, and interpolation. In *Advances in Intelligent Data Analysis XII*, pages 162–173. Springer, 2013.

[57] G. W. Brier. Verification of forecasts expressed in terms of probability. *Monthly weather review*, 78(1):1–3, 1950.

[58] C. M. Bishop. *Pattern recognition and machine learning*. springer, 2006.

[59] R. Redner and H. Walker. Mixture densities, maximum likelihood and the EM algorithm. *SIAM Review*, 26(2):pp. 195–239, 1984.

[60] F. Pedregosa, G. Varoquaux, A. Gramfort, V. Michel, B. Thirion, O. Grisel, M. Blondel, P. Prettenhofer, R. Weiss, V. Dubourg, et al. Scikit-learn: Machine learning in python. *The Journal of Machine Learning Research*, 12:2825–2830, 2011.

[61] H. Dommel and W. Tinney. Optimal power flow solutions. *IEEE transactions on Power Apparatus and Systems*, PAS-87(10):1866–1876, 1968.

[62] R. A. Jabr. Radial distribution load flow using conic programming. *Power Systems, IEEE Transactions on*, 21(3):1458–1459, 2006.

[63] S. Bolognani and S. Zampieri. On the existence and linear approximation of the power flow solution in power distribution networks. *Power Systems, IEEE Transactions on*, 31(1):163–172, 2016.

[64] Q. Gemine, D. Ernst, Q. Louveaux, and B. Cornélusse. Relaxations for multi-period optimal power flow problems with discrete decision variables. In *Proceedings of the 18th Power Systems Computation Conference (PSCC-14)*, page 7, 2014.

[65] G. Andersson. Modelling and analysis of electric power systems. *EEH-Power Systems Laboratory, Swiss Federal Institute of Technology (ETH), Zürich, Switzerland*, 2004.

[66] A. Monticelli. *State estimation in electric power systems: a generalized approach*, volume 507. Springer Science & Business Media, 1999.

[67] S. Engelhardt, I. Erlich, C. Feltes, J. Kretschmann, and F. Shewarega. Reactive power capability of wind turbines based on doubly fed induction generators. *Energy Conversion, IEEE Transactions on*, 26(1):364–372, 2011.

[68] H. Soleimani Bidgoli, M. Glavic, and T. Van Cutsem. Receding-horizon control of distributed generation to correct voltage or thermal violations and track desired schedules. In *Proceedings of the 19th Power Systems Computation Conference (PSCC 2016)*, 2016.

[69] W. Powell. A Unified Framework for Optimization under Uncertainty. Informs TutORials in Operations Research, 2016.

[70] R. Bellman. *Dynamic Programming*. Princeton University Press, 1957.

[71] D. Bertsekas and S. Shreve. *Stochastic Optimal Control: The Discrete Time Case*. Academic Press New York, 1978.

[72] J. Fortuny-Amat and B. McCarl. A representation and economic interpretation of a two-level programming problem. *Journal of the operational Research Society*, pages 783–792, 1981.

[73] F. Capitanescu, L. F. Ochoa, H. Margossian, and N. D. Hatzargyriou. Assessing the potential of network reconfiguration to improve distributed generation hosting capacity in active distribution systems. *IEEE Trans. Power Syst.*, 1:346–356, 2015.

[74] SEDG Centre. UK generic distribution system (UKGDS) project. `http://www.sedg.ac.uk/`, 2010.

[75] J.-M. Marin, P. Pudlo, C. Robert, and R. Ryder. Approximate bayesian computational methods. *Statistics and Computing*, 22(6):1167–1180, 2012.

[76] A. Grelaud, C. Robert, J.-M. Marin, F. Rodolphe, and J.-F. Taly. ABC likelihood-free methods for model choice in gibbs random fields. *Bayesian Analysis*, 4(2):317–335, 06 2009.

[77] Q. Gemine, B. Cornélusse, M. Glavic, R. Fonteneau, and D. Ernst. A gaussian mixture approach to model stochastic processes in power systems. In *Proceedings of the 19th Power Systems Computation Conference (PSCC'16)*, 2016.

[78] E. Jones, T. Oliphant, and P. Peterson. SciPy: Open source scientific tools for Python, 2014.

[79] T. Hastie, R. Tibshirani, J. Friedman, and J. Franklin. The elements of statistical learning: data mining, inference and prediction. *The Mathematical Intelligencer*, 27(2):83–85, 2005.

[80] W. Hart, C. Laird, J.-P. Watson, and D. Woodruff. *Pyomo–optimization modeling in python*, volume 67. Springer Science & Business Media, 2012.

[81] P. Bonami and J. Lee. BONMIN users manual., 2006.

[82] L. Busoniu, D. Ernst, B. De Schutter, and R. Babuska. Cross-entropy optimization of control policies with adaptive basis functions. *IEEE Transactions on Systems, Man, and Cybernetics, Part B: Cybernetics*, 41(1):196–209, 2011.

[83] D. Bertsekas and J. Tsitsiklis. *Neuro-Dynamic Programming.* Athena Scientific, Belmont, MA, 1996.

[84] L. Busoniu, R. Babuska, B. De Schutter, and D. Ernst. *Reinforcement Learning and Dynamic Programming Using Function Approximators.* CRC Press, Boca Raton, FL, 2010.

[85] W. Powell. Clearing the Jungle of Stochastic Optimization. Informs TutORials, 2014.

[86] B. Cornélusse, D. Vangulick, M. Glavic, and D. Ernst. A process to address electricity distribution sector challenges: the gredor project approach. In *Proceedings of the International Conference on Electricity Distribution, CIRED 2015*, 2015.

[87] P. Smyth. Model selection for probabilistic clustering using cross-validated likelihood. *Statistics and computing*, 10(1):63–72, 2000.

[88] J. Dupačová, N. Gröwe-Kuska, and W. Römisch. Scenario reduction in stochastic programming. *Mathematical programming*, 95(3):493–511, 2003.

[89] N. Growe-Kuska, H. Heitsch, and W. Romisch. Scenario reduction and scenario tree construction for power management problems. In *Power Tech Conference Proceedings, 2003 IEEE Bologna*, volume 3, pages 7–pp. IEEE, 2003.

[90] O. Mégel, G. Andersson, and J. L. Mathieu. Reducing the computational effort of stochastic multi-period dc optimal power flow with storage. In *2016 Power Systems Computation Conference (PSCC)*, pages 1–7. IEEE, 2016.

[91] M. Bazilian, I. Onyeji, M. Liebreich, I. MacGill, J. Chase, J. Shah, D. Gielen, D. Arent, D. Landfear, and S. Zhengrong. Re-considering the economics of photovoltaic power. *Renewable Energy*, 53:329–338, 2013.

[92] T. S. Ustun, C. Ozansoy, and A. Zayegh. Recent developments in microgrids and example cases around the world-a review. *Renewable and Sustainable Energy Reviews*, 15(8):4030–4041, 2011.

[93] H. L. Ferreira, R. Garde, G. Fulli, W. Kling, and J. P. Lopes. Characterisation of electrical energy storage technologies. *Energy*, 53:288–298, 2013.

[94] G. Krajačić, N. Duić, and M. da Graça Carvalho. H_2 RES, energy planning tool for island energy systems–the case of the island of mljet. *International journal of hydrogen energy*, 34(16):7015–7026, 2009.

[95] D. Connolly, H. Lund, B. V. Mathiesen, and M. Leahy. The first step towards a 100% renewable energy-system for Ireland. *Applied Energy*, 88(2):502–507, 2011.

[96] V. François-Lavet, R. Fonteneau, and D. Ernst. Using approximate dynamic programming for estimating the revenues of a hydrogen-based high-capacity storage device. In *IEEE Symposium on Adaptive Dynamic Programming and Reinforcement Learning (ADPRL), 2014*, pages 1–8. IEEE, 2014.

[97] N. Armaroli and V. Balzani. The hydrogen issue. *ChemSusChem*, 4(1):21–36, 2011.

[98] S. M. Schoenung. Characteristics and technologies for long-vs. short-term energy storage. *United States Department of Energy*, 2001.

[99] O. Hafez and K. Bhattacharya. Optimal planning and design of a renewable energy based supply system for microgrids. *Renewable Energy*, 45:7–15, 2012.

[100] D. Ernst, M. Glavic, and L. Wehenkel. Power systems stability control: reinforcement learning framework. *Power Systems, IEEE Transactions on*, 19(1):427–435, 2004.

[101] F.-D. Li, M. Wu, Y. He, and X. Chen. Optimal control in microgrid using multi-agent reinforcement learning. *ISA transactions*, 51(6):743–751, 2012.

[102] H. Analysis. http://homerenergy.com.

[103] F. Katiraei, M. R. Iravani, and P. Lehn. Micro-grid autonomous operation during and subsequent to islanding process. *Power Delivery, IEEE Transactions on*, 20(1):248–257, 2005.

[104] A. Ben-Tal and A. Nemirovski. Robust optimization–methodology and applications. *Mathematical Programming*, 92(3):453–480, 2002.

[105] H. Ossenbrink, T. Huld, A. Jäger Waldau, and N. Taylor. Photovoltaic electricity cost maps. Technical report, JRC, European Commission, 2013.

[106] H. A. Chih-Chiang and S. B. Zong-Wei. Charge and discharge characteristics of lead-acid battery and lifepo4 battery. In *Power Electronics Conference (IPEC), 2010 International*, pages 1478–1483. IEEE, 2010.

[107] M. Šúri, T. Cebecauer, and A. Skoczek. Solargis: solar data and online applications for pv planning and performance assessment. In *26th European photovoltaics solar energy conference*, 2011.